Exploring The Role of Indian Hedgehog in Regulating Immunogenicity in Colorectal Cancer

Stefanie Hasan
Hertford College
University of Oxford

A thesis submitted for the degree of *Master of Science by Research* to the Department of Oncology, University of Oxford

Supervised by Professor Simon Buczacki

Michaelmas 2024

1 Abstract

Colorectal cancer (CRC) remains the second-leading cause of cancer-related mortality worldwide, with patients showing varied responses to immunotherapy. Notably, immune checkpoint inhibitors (ICIs) have demonstrated remarkable efficacy in metastatic CRC patients with microsatellite instability (MSI), inducing durable responses in a significant proportion of these patients. In contrast, microsatellite stable (MSS) tumours, which comprise 80-85% of CRC cases, have exhibited limited responses to ICIs. Beyond microsatellite stability status, there is a lack of reliable biomarkers for predicting responses to ICIs, and factors influencing tumour immunogenicity in CRC remains underexplored. Leveraging multi-omic data from The Cancer Genome Atlas, our laboratory has identified Indian Hedgehog (*IHH*) expression as a potential negative regulator of tumour immunogenicity in CRC. IHH, a member of the Hedgehog family of proteins in vertebrates, is a key signalling molecule that regulates embryonic morphogenesis and adult tissue homeostasis. Despite its known role as a regulator of normal intestinal immunity, its influence on the immune microenvironment in CRC remains largely unexplored. The present thesis provides preliminary insights into the role of IHH in regulating CRC immunogenicity, revealing that IHH, secreted by CRC cells, exerts its immunomodulatory effects primarily through paracrine interactions with the surrounding tumour microenvironment. Specifically, IHH appears to facilitate immune evasion in CRC by downregulating chemokines critical for the recruitment of cytotoxic T lymphocytes (*CCL4*, *CCL5*, *CXCL10*, and *CXCL11*) in cancer-associated fibroblasts, while skewing the polarization of tumour-associated macrophages toward a more immunosuppressive, less pro-inflammatory phenotype. These findings highlight IHH as a potential modulator of tumour immune responses in CRC and offer potential avenues for targeting IHH signalling to enhance immunotherapy efficacy in CRC.

2 Declaration of Authentication

The material presented in this thesis was performed under the supervision of Professor Simon Buczacki, Nuffield Department of Surgical Sciences, University of Oxford. This work is entirely my own and any contributions made by others has been acknowledged. The work submitted does not form part of another thesis in this or any other university.

Stefanie Hasan

October 2024

3 Acknowledgements

I truly enjoyed my time engaging in cancer research as a Master's student, and much of the credit goes to the people I had the privilege of being surrounded by.

Firstly, I would like to express my deepest gratitude for my supervisor, Professor Simon Buczacki. Your guidance, support and kindness has been invaluable for my research experience. The enthusiasm you share for research inspires me, and I am genuinely grateful to have had the opportunity to work under your guidance.

I would like to extend my gratitude to all my lab members, who have shown me nothing but kindness throughout my time here. Much of this work would not have been possible without Jack, Yi, Amit, and Scott, who always took time out of their busy schedules to offer me with patient guidance and expertise whenever I needed it. As for Alex, Kirsty, James and Jasmine, your cheerful presence has brought wonderful energy to the lab, making it a truly welcoming place. I thoroughly enjoyed working alongside each of you.

Special mentions to our honorary lab member, Dr Anjali Arora, whose guidance, and support in troubleshooting my experiments have been instrumental in preventing more than a few mental breakdowns. I truly appreciate your assistance in navigating the challenges I have faced along the way.

And finally, big thanks to my mom, dad, and big sis Jac for always supporting me to pursue what I love most.

4 Table of Contents

1 Abstract 2

2 Declaration of Authentication 3

3 Acknowledgements 4

5 List of Abbreviations 7

6 Introduction 9

6.1 Introduction to Colorectal Cancer 9
6.1.1 Epidemiology 9
6.1.2 Pathogenesis 11
6.1.3 Conventional treatments 16

6.2 Cancer and the Immune System 18
6.2.1 Tumour immunosurveillance 18
6.2.2 Cancer Immunoediting 20
6.2.3 Mechanisms of immune evasion 22
6.2.4 Immunotherapy 23

6.3 Hedgehog Signalling 25
6.3.1 Hedgehog Proteins 25
6.3.2 Mechanism of HH signalling in Mammals 27
6.3.3 Hedgehog Signalling in Intestinal Homeostasis 29
6.3.4 Hedgehog Signalling in Cancer 33

7 Materials and Methods 42

7.1 Cell culture 42
7.1.1 2D cell lines 42
7.1.2 3D Organoid lines 43

7.2 CRISPR-Cas9 mediated gene editing 44
7.2.1 2D cell line 44
7.2.2 3D organoid line 45

7.3 Generation of Single Cell-Derived IHH-knockout clones 46

7.4 Gene set enrichment analysis (GSEA) 47

7.5 Macrophage Polarisation Assay 47

7.6 Processing and Analysis of RNA-sequencing data 48

7.7 Profiling IHH-induced Immune-Related Genes Using an RT2 Profiler PCR Array 49

7.8 Sanger sequencing 50

7.9 Sample Preparation for RNA-sequencing 51

7.10 SiRNA knockdown of IHH 51

7.11 Western Blotting 52
7.11.1 Protein Extraction and Quantification 52
7.11.2 SDS-PAGE 52
7.11.3 Immunoblotting 53

7.12 Quantitative Reverse Transcription Polymerase Chain Reaction (qRT-PCR) 53
7.12.1 TaqMan 54
7.12.2 SYBR Green 54

7.13 Statistical analyses 55
8 Results 56
8.1 In Silico Analysis: Identifying IHH Expression as a Potential Regulator of CRC Immunogenicity 56
8.2 Exploring the Potential Immunosuppressive Mechanisms of IHH in CRC 61
8.2.1 Autocrine Effects on Cancer Cells 63
8.2.2 Paracrine Signalling to Macrophages 81
8.2.3 Paracrine Signalling to Fibroblasts 94
9 Concluding Remarks 99
10 Appendix 102
11 References 113

5 List of Abbreviations

APC	Adenomatous Polyposis Coli
ASR	Age-Standardised Incidence Rates
BMP	Bone Morphogenetic Protein
CAF	Cancer-Associated Fibroblast
CCL	C-C Motif Chemokine Ligand
CIMP	CpG Island Methylator Phenotype
CD274	Cluster of differentiation 274
CK1	Casein Kinase 1
CRC	Colorectal Cancer
CTL	Cytotoxic T Lymphocyte
CTLA-4	Cytotoxic T Lymphocyte-Associated Protein 4
DHH	Desert Hedgehog
DISP1	Dispatched-1
EMT	Epithelial-to-Mesenchymal Transition
ER	Endoplasmic Reticulum
FDR	False Discovery Rate
FOXP3	Forkhead Box Protein P3
GLI	Glioma-Associated Oncogene
GSEA	Gene Set Enrichment Analysis
GSK3β	Glycogen Synthase Kinase-3β
HH	Hedgehog
IBD	Inflammatory Bowel Disease
ICB	Immune Checkpoint Blockade
ICI	Immune Checkpoint Inhibitors
IFN	Interferon
IHC	Immunohistochemistry
IHH	Indian Hedgehog
IL	Interleukin
LPS	Lipopolysaccharide
MAPK	Mitogen-activated Protein Kinase
MDSC	Myeloid-Derived Suppressor Cell
MHC	Major Histocompatibility Complex

MHC-I	Major Histocompatibility Complex Class I
MMR	Mismatch Repair
MSI	Microsatellite Instability
MSI-H	High Microsatellite Instability
MSI-L	Low Microsatellite Instability
MSigDB	Molecular Signatures Database
NES	Normalised Enrichment Score
PCR	Polymerase Chain Reaction
PD-1	Programmed Cell Death Protein 1
PD-L1	Programmed Cell Death Ligand 1
PI3K	Phosphoinositide 3-Kinase
PKA	Protein Kinase A
PMA	Phorbol 12-Myristate 13-Acetate
PRI	Potential Regulatory of Immunogenicity
PTCH1	Patched Homolog 1
SCUBE2	Signal Peptide-CUB-EGF-Like Domain-Containing Protein 2
SHH	Sonic Hedgehog
SMO	Smoothened
SpCas9	Streptococcus Pyogenes-Derived Cas9
TAM	Tumour-Associated Macrophage
TCGA	The Cancer Genome Atlas
TCR	T-Cell Receptor
TGF-β	Transforming Growth Factor Beta
TLR	Toll-Like Receptor
TME	Tumour Microenvironment
TNF	Tumour Necrosis Factor
TRAIL	Tumour Necrosis Factor-Related Apoptosis-Inducing Ligand
Treg	Regulatory T Cells
qRT-PCR	Quantitative Reverse Transcription Polymerase Chain Reaction

6 Introduction

6.1 Introduction to Colorectal Cancer

6.1.1 Epidemiology

Colorectal cancer (CRC) remains one of the most prevalent and fatal malignancies worldwide, exhibiting pronounced geographic and demographic variations in incidence and mortality rates. Globally, it is the third most common cancer and the second leading cause of cancer-related mortalities, with an estimated 1.9 million new cases and over 900,000 deaths in 2022 (1, 2). The high burden of this disease necessitates ongoing efforts in prevention, early detection, and treatment.

CRC incidences show pronounced geographic variation, with notably higher incidences in economically developed countries such as the United States, Australia and many European nations compared to less-developed regions such as Africa and Latin America (Figure 1). This disparity likely reflects differences in lifestyle, environmental exposures, and healthcare accessibility. The high incidence of CRC in developed countries is largely influenced by Western lifestyles and dietary patterns, which are characterised by sedentary habits and diets featuring high consumption of red and processed meats, low intake of dietary fibre, and elevated levels of saturated fats and sugar. These factors collectively contribute to an increased risk of developing CRC. Conversely, developing countries are experiencing rapidly rising CRC rates as they undergo economic development and increasingly adopt Westernised diets and lifestyles. Despite high CRC incidences in developed nations, the implementation of screening programmes has significantly impacted CRC outcomes, contributing to a steady decline in CRC-associated mortality in countries such as the United States,

Japan, and Austria. In these countries, widespread adoption of screening techniques such as colonoscopy and faecal blood tests have led to earlier detection of CRC, leading to improved prognosis and reduced mortality rates (1).

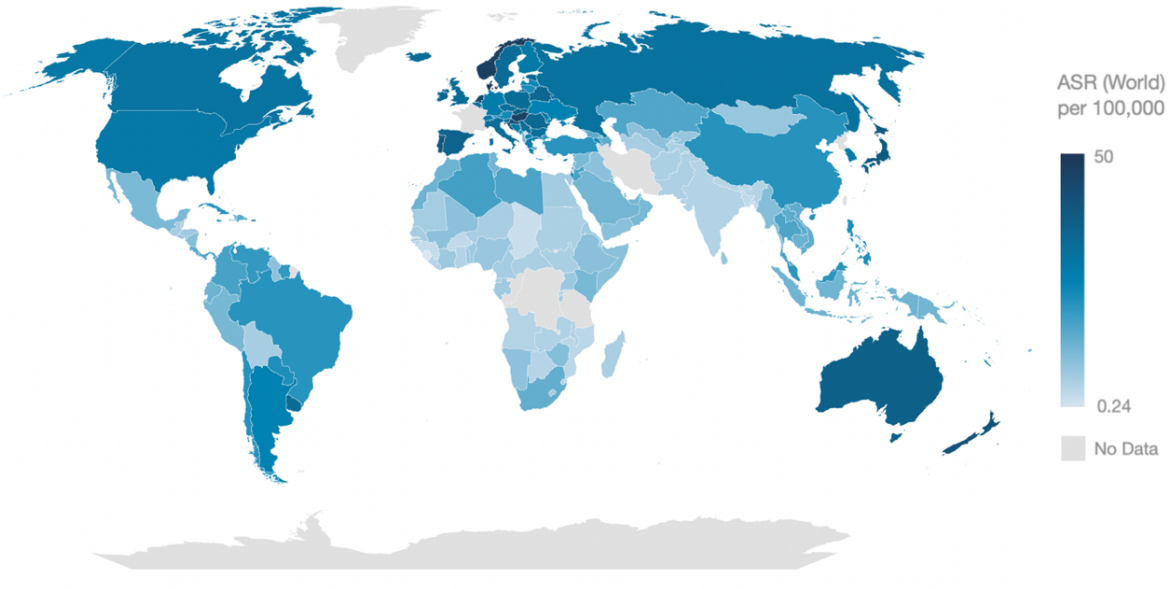

Figure 1. Estimated Age-Standardised Incidence Rates for Colorectal Cancer in 2022. A global map depicting the estimated age-standardised incidence rates of CRC per 100,000 population across different countries in 2022. The ASR(world) is adjusted to the World Standard Population to account for variations in age distribution across different countries, allowing fair comparisons of CRC incidence globally. Data source: Global Cancer Observatory 2022 (3).

In addition to geographic differences, CRC incidences varies by age and gender. The incidence of CRC escalates rapidly with age, with an estimated 90% of CRC diagnoses occurring in individuals aged 50 and older (2). However, recent trends reveal a concerning rise in CRC cases among younger populations in developed countries (1). This shift may be associated with changing dietary habits, a sedentary lifestyle, increased obesity rates, and other environmental factors. Furthermore, a notable gender disparity in CRC incidence persists, with higher age-standardized

incidence rates seen in men (21.9 per 100,000 individuals) compared to women (15.2 per 100,000 individuals) in 2022 (2). This disparity may be related to differences in lifestyle factors and biological variations between genders.

Epidemiological trends in CRC are continually evolving, driven by changes in lifestyle, dietary habits, and healthcare accessibility. Rising incidence rates, particularly among younger individuals and in regions experiencing economic and dietary transitions, highlights the critical need for ongoing advancements in prevention, diagnosis, and treatment to effectively mitigate the burden of this disease.

6.1.2 Pathogenesis

CRC is a multifactorial disease characterised by the malignant transformation of colonic and rectal epithelial cells. The pathogenesis of CRC involves a complex interplay between genetic, environmental, and lifestyle factors that disrupt normal cellular processes and promote tumour development (Figure 2) (4, 5). CRC can be broadly categorised into sporadic, hereditary, and familial cases. Approximately 75% of CRC cases are classified as sporadic, occurring without a clear hereditary or familial link. These cases are not linked to specific inherited genetic mutations but instead arise due to a combination of environmental, lifestyle, and random genetic factors. Meanwhile, familial CRC accounts for around 25% of cases, emerging in families with a higher-than-expected incidence of the disease, but without specific identifiable genetic mutations. Only 5-10% of cases are hereditary, which are associated with genetic syndromes such as Lynch Syndrome or Familial Adenomatous Polyposis, which involve inherited mutations that significantly elevate cancer risk and often lead

to earlier onset (6). CRC can arise through one of two main biological pathways: the adenoma-carcinoma sequence or the serrated pathway (7).

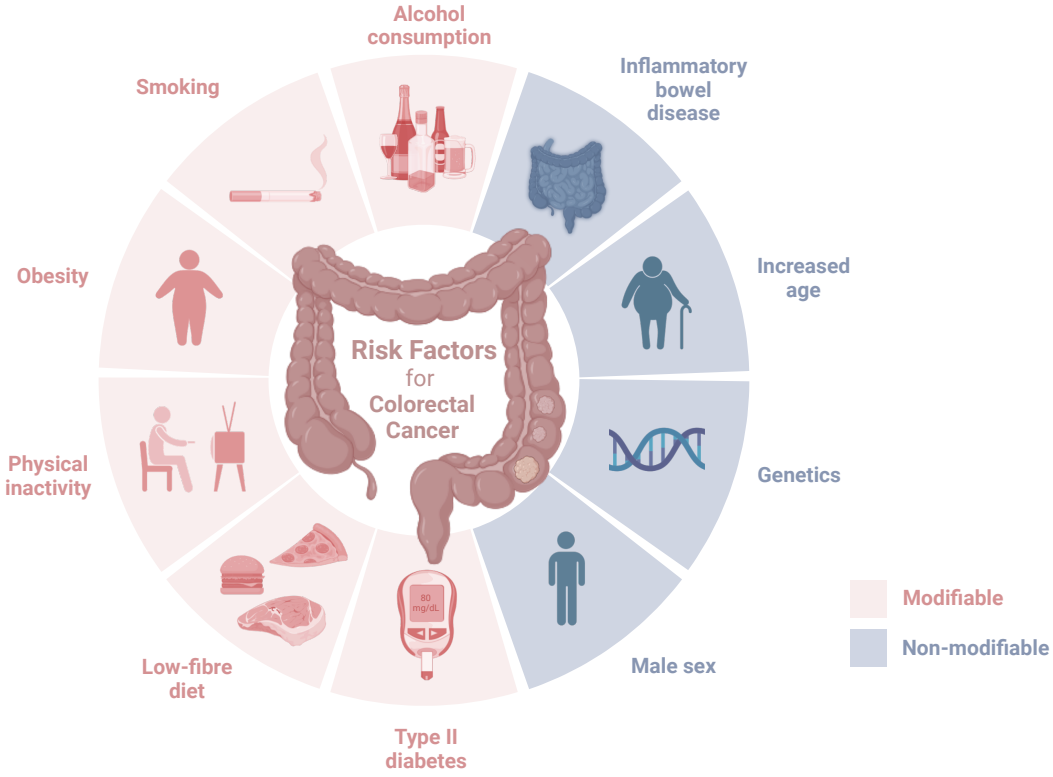

Figure 2. Risk factors for Colorectal Cancer. Both modifiable (red) and non-modifiable (blue) factors contribute to the development of colorectal cancer.

6.1.2.1 Adenoma-Carcinoma Sequence

The most well-characterised pathway in CRC development is the adenoma-carcinoma sequence, initially proposed by Fearon and Vogelstein (Figure 3) (8). It is widely accepted that the majority of colorectal carcinomas arise from pre-existing adenomatous polyps (adenomas), which includes tubular, tubulovillous, and villous adenomas. The adenoma-carcinoma sequence describes the process by which benign adenomatous polyps in the colon or rectum gradually progresses into malignant carcinomas, which is driven by the sequential accumulation of genetic mutations (5). The adenoma-carcinoma sequence begins with the mutation of the adenomatous polyposis coli (*APC*) gene, a key tumour suppressor. The *APC* gene

plays a crucial role in regulating the Wnt signalling pathway, which controls cell growth and differentiation. Mutations in *APC* lead to the accumulation of β-catenin in the cell nucleus, where it activates genes that drive uncontrolled cell proliferation (9). This initial genetic alteration results in the formation of a benign lesion known as an adenoma. As adenomas continue to grow, additional genetic mutations accumulate, including in the *KRAS* oncogene, and the tumour suppressor genes *SMAD4* and *TP53*, which promote further dysplasia and progression towards malignancy. Activating mutations in *KRAS* leads to the activation of downstream signalling pathways such as the MAPK/ERK and PI3K/AKT pathway, which further promotes cell proliferation and survival (10). Meanwhile, the loss of SMAD4 and p53 function disrupts critical growth control and apoptotic mechanisms, promoting genetic instability and uncontrolled cellular proliferation, ultimately culminating in the transition from adenoma to carcinoma (11, 12).

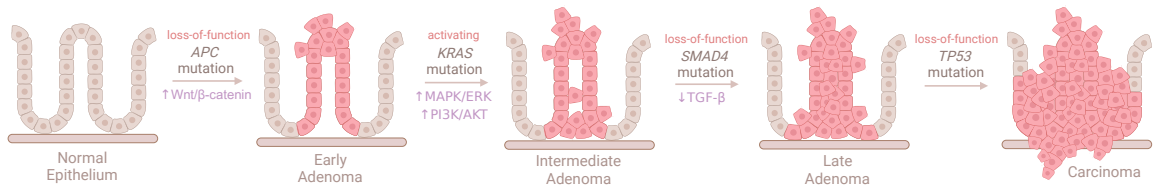

Figure 3. The Adenoma-Carcinoma Sequence in Colorectal Cancer (CRC) Development. The adenoma-carcinoma sequence is a well-established model of CRC development, which describes the stepwise progression of normal colonic epithelium through benign adenomas to malignant carcinomas. This process is driven by the stepwise accumulation of key genetic mutations in *APC*, *KRAS*, *SMAD4* and *TP53*. The adenoma-carcinoma sequence initiates with a loss of function mutation in the *APC* gene, a regulator of the Wnt signaling pathway, leading to abnormal cell proliferation and the formation of early adenomas. As the adenoma grows, activating mutations in the *KRAS* oncogene, a regulator of the MAPK/ERK and PI3K/AKT pathway, further promotes cell proliferation and survival, progressing the lesion to an intermediate adenoma. The transition from an intermediate to a late adenoma is associated with mutations in *SMAD4*, a regulator of the transforming growth factor beta (TGF-β) signalling pathway, impairing cell cycle regulation and apoptosis, which promotes further dysplasia. Finally, progression to carcinoma occurs with the loss of function in the *TP53* gene, a critical

tumour suppressor involved in DNA damage repair and apoptosis, allowing cells with significant DNA damage to survive and proliferate. The sequential accumulation of these genetic alterations underscores the multi-step process of colorectal carcinogenesis, with each genetic alteration conferring selective growth advantages that facilitate the progression from benign adenomas to malignant carcinomas.

6.1.2.2 Serrated Pathway

While it was initially thought that adenomas were the only benign lesions capable of progressing to CRC, it is now recognised that up to 30% of CRCs arise from serrated polyps. These polyps exhibit a characteristic serrated or saw-toothed histological appearance and are classically divided into three types: hyperplastic polyps, sessile serrated adenomas/polyps and traditional serrated adenomas (13).

The molecular mechanisms underlying the serrated pathway are distinct from those observed in the conventional adenoma-carcinoma sequence. Unlike the adenoma-carcinoma pathway, the serrated pathway rarely exhibits mutations in the *APC* gene (13). Instead, Wnt signalling can be activated via alternative mechanisms, such as via inactivating mutations in *RNF43* (14).

Two key molecular features facilitate CRC development in the serrated pathway: the activating *BRAF V600E* mutation and the CpG island methylator phenotype (CIMP) (13). The *BRAF V600E* mutation leads to the aberrant activation of MAPK/ERK signalling pathway, promoting uncontrolled cellular proliferation and survival (15). In parallel, the CIMP is characterized by widespread hypermethylation of CpG islands in gene promoter regions, resulting in the silencing of critical tumour suppressor genes (16). This epigenetic alteration not only facilitates the progression of serrated lesions to CRC, but also contributes to the development of microsatellite

instability (MSI) in associated CRCs through the silencing of *MLH1* (see section 6.1.2.3) (17).

6.1.2.3 Microsatellite Instability (MSI)

MSI is a key molecular characteristic observed in 15-20% of CRCs, and is closely associated with Lynch syndrome, a hereditary condition which significantly elevates the risk of CRC development. MSI arises from the dysfunction in the DNA mismatch repair (MMR) system, which is responsible for correcting errors that occur during DNA replication. This dysfunction in the MMR system arises due to epigenetic silencing or mutations in one or more key MMR genes: *MLH1*, *MSH2*, *MSH6*, and *PMS2*. MMR-deficiency results in an accumulation of mutations in the genome, particularly in microsatellite regions, which are short, repetitive sequences of DNA (18, 19).

MSI is notably prevalent in serrated CRCs, particularly those that arise from sessile serrated adenomas (20). The CpG island methylator phenotype (CIMP) associated with serrated CRCs promote MSI through the hypermethylation of the *MLH1* gene promoter (17). This hypermethylation event is recognised as the major cause of MSI in sporadic cancers, resulting in deficient MMR activity (21). In contrast to serrated CRCs, CRCs that arise from adenomas rarely exhibit MSI, except in the context of Lynch Syndrome. In patients with Lynch Syndrome, inherited mutations in one of the key MMR genes generally give rise to MSI CRCs emerging through an accelerated adenoma-carcinoma pathway (22).

At present, MSI or MMR-deficiency is primarily diagnosed using immunohistochemistry (IHC) or polymerase chain reaction (PCR). The IHC approach analyses the expression of MMR proteins, specifically MLH1, MSH2, MSH6, and PMS2, in tumour tissue, with absent expression of one or more of these proteins indicating MMR-deficiency. Alternatively, in the PCR approach, five specific microsatellite loci are amplified and analysed for length variations between tumour and normal tissue samples, where differences in microsatellite lengths indicate the presence of MSI. Tumours exhibiting instability in two or more microsatellite markers are classified as MSI-high (MSI-H), characterised by a high level of genomic instability due to deficient mismatch repair (MMR) activity. Meanwhile, tumours displaying instability in only one marker are denoted MSI-low (MSI-L), which exhibit a lower degree of genetic instability and are generally not associated with MMR deficiency. Tumours with no detectable instability in any of the microsatellite markers are classified as microsatellite stable (MSS) (23). However, in clinical research, MSI-L and MSS statuses are generally classified as one group due to their similar biological characteristics and clinical implications (24).

6.1.3 Conventional treatments

The treatment of CRC typically involves a multidisciplinary approach combining surgery, chemotherapy, radiotherapy, and targeted therapies. Each treatment approach is tailored to the stage and location of the cancer, aiming to optimise outcomes and improve quality of life.

Surgery remains the mainstay curative treatment for patients with non-metastasised CRC. The primary objective of surgical resection is to excise the

cancerous tumour along with a margin of surrounding healthy tissue accompanied by removal of the draining lymph nodes for staging purposes (5). Surgery alone is highly effective in the treatment of early-stage disease where the cancer has not yet spread to regional lymph nodes (Stage I-II). With surgical intervention, the 5-year survival rate is around 90% and 85% in stage I and II patients respectively, reflecting a high likelihood of long-term remission and minimal risk of local recurrence (25). For Stage III CRC, where the cancer has spread to regional lymph nodes, surgical resection remains a vital component of treatment but is often complemented with adjuvant chemotherapy to address residual microscopic disease. Following surgical resection, adjuvant fluoropyrimidine-based chemotherapy is recommended as standard clinical practice for patients (26). This recommendation is supported by evidence from a clinical trial led by Moertel *et* al, demonstrating that adjuvant therapy involving the chemotherapeutic agent 5-fluorouracil reduced cancer recurrence and increased overall survival in stage III CRC patients (27).

For Stage IV CRC, characterized by metastasis to distant organs, chemotherapy serves as the cornerstone of treatment. At this advanced stage, the primary objective of therapy shifts from curative intent to controlling disease progression and managing symptoms. Given that Stage IV CRC involves the spread of cancer beyond the primary site to distant organs, most frequently the liver and lungs, a systemic approach is necessary to address cancer cells throughout the body. Chemotherapy plays a crucial role in this context by targeting rapidly dividing cancer cells across the body to inhibit their growth. Chemotherapy regimens for Stage IV CRC typically involve a two-drug regimen consisting of 5-Fluorouracil (5-FU) and either oxaliplatin (FOLFOX) or irinotecan (FOLFIRI). Depending on the tumour's molecular characteristics, these

regimens may be further complemented with targeted therapies such as bevacizumab or cetuximab (28). With current therapies, the 5-year survival rate for patients with stage IV CRC is only around 10% (25). Given that over 20% of CRC cases are diagnosed at stage IV, this underscores the importance of continued research and development of more effective treatment options, particularly for late-stage disease (29).

6.2 Cancer and the Immune System

6.2.1 Tumour immunosurveillance

Tumour immunosurveillance, a concept initially proposed by Paul Ehrlich and later expanded by Burnet and Thomas, refers to the process by which the immune system identifies and eliminates malignantly transformed cells to prevent the development and progression of cancer (30). This hypothesis is strongly supported by evidence from murine studies which demonstrated that immunodeficient mice exhibited an increased susceptibility to developing spontaneous and chemically-induced tumours, highlighting the critical role of a competent immune system in suppressing cancer development (31-34). Tumour immunosurveillance is mediated through the coordinated action of the innate and adaptive immune systems, with cytotoxic T lymphocytes (CTLs) from the adaptive immune system and natural killer (NK) cells from the innate immune system acting as the primary effector cells (35).

T cells and NK cells play complementary roles in the recognition of malignantly transformed cells. Naive CD8+ T cells recognise tumour cells through tumour antigens presented by major histocompatibility complex class I (MHC-I) molecules. MHC-I molecules are expressed on the surface of all nucleated cells and serve to present

peptide fragments derived from intracellular proteins to the immune system. These tumour antigen-MHC I complexes are displayed either directly on tumour cell surfaces, or on dendritic cells which have captured and processed these tumour antigens. Upon binding of the T-cell receptor (TCR) to the peptide-MHC I complex, naive CD8+ T cells undergo activation, resulting in clonal expansion and differentiation into effector T cells, known as CTLs, capable of eliminating tumour cells (36). In contrast, NK cells recognise tumour cells through a sophisticated mechanism involving a balance of inhibitory and activating signals. NK cells express inhibitory receptors that recognise MHC-I molecules, and activating receptors that recognise stress-induced ligands such as MICA, MICB, and ULBP1-6. Consequently, tumour cells, which commonly upregulate stress-induced ligands, and downregulate MHC-I expression to evade recognition by T cells, triggers NK cell activation and subsequent cytotoxic responses against the tumour (37).

Despite employing distinct tumour recognition mechanisms, T cells and NK cells utilise overlapping cytotoxic mechanisms to eliminate tumour cells. Both cell types employ two main mechanisms to induce tumour cell death: (i) the release of lytic granules and (ii) the upregulation of death ligands of the tumour necrosis factor (TNF) superfamily. In the first mechanism, T cells and NK cells release lytic granules containing perforin, a pore-forming protein, and granzyme B, a serine protease, at the immunological synapse formed with the tumour cell. Perforin form pores in the tumour cell membrane which facilitates the entry of granzymes into the cytoplasm, where it initiates apoptosis by activating caspases. The second mechanism involves the upregulation of death ligands such as Fas ligand and TNF-related apoptosis-inducing ligand (TRAIL) on the surface of T cells and NK cells. These ligands bind to their

respective death receptors, Fas and TRAIL receptors, on the tumour cell surface, initiating a caspase cascade that drives the tumour cell towards apoptosis (36, 37).

Overall, tumour immunosurveillance relies on the coordinated action of CTLs and NK cells, which employ complementary recognition mechanisms and overlapping cytotoxic pathways to effectively detect and eliminate malignant cells.

6.2.2 Cancer Immunoediting

Despite evidence for a protective role of the immune system against cancer development, tumours still develop in immunocompetent individuals, indicating that tumours can acquire mechanisms to evade immune detection or destruction. This observation gave rise to the concept of cancer immunoediting, an extension of the cancer immunosurveillance hypothesis, which postulates that the recognition and elimination of transformed cells by the immune system not only protects against cancer development, but concurrently exerts a selective pressure which sculpts the immunogenic phenotype of the emerging tumour. This dynamic process is classically delineated into three distinct phases: (i) elimination, (ii) equilibrium, and (iii) escape (30).

6.2.2.1 Elimination

The elimination phase of tumour immunoediting represents the initial interaction between the immune system and nascent tumour cells. This phase embodies the original concept of tumour immunosurveillance, involving the recognition and destruction of tumour cells through the coordinated action of the innate and adaptive immune systems before the tumour becomes clinically detectable. If the immune

system successfully eradicates the developing tumour, the immunoediting process concludes without progressing to subsequent phases. However, tumour immunosurveillance is not infallible; some tumour cells may acquire mutations or epigenetic changes which enable them to evade immune detection and destruction. These surviving cells consequently initiate the transition to the equilibrium phase of cancer immunoediting (30).

6.2.2.2 Equilibrium

The equilibrium phase of cancer immunoediting is characterised by a dynamic balance between the immune system and the surviving tumour cells, where the immune system manages to contain tumour growth but not completely eradicate it. During this phase, the immune system exerts selective pressure on the tumour cells, leading to the elimination of immune-sensitive cells while allowing immune-evasive cells to persist and proliferate. This dynamic equilibrium is maintained as the proliferation rate of immune-evasive tumour cells is counterbalanced by the immune system's ongoing elimination of immune-sensitive tumour cells. Consequently, the overall tumour mass remains relatively stable throughout the equilibrium phase, neither growing significantly nor being entirely eradicated. This phase can persist for years, and is characterised by a continuous adaptive struggle, wherein tumour cells continues to acquires and accumulate genetic and epigenetic changes that promote immune evasion, while the immune system concurrently strives to suppress tumour growth and prevent progression to clinically detectable tumours (30).

6.2.2.3 Escape

The escape phase marks the breakdown of the equilibrium state and the progression of the tumour to a clinically detectable stage. In this phase, tumour variants which have acquired genetic or epigenetic changes conferring resistance to immune-mediated killing begins to expand in an uncontrolled manner, leading to clinically apparent disease (30).

6.2.3 Mechanisms of immune evasion

In CRC, immune evasion mechanisms play a crucial role in tumour progression and resistance to treatment. Tumour cells adopt various strategies to evade detection and destruction by the immune system, which are summarised in Figure 4 (38-42).

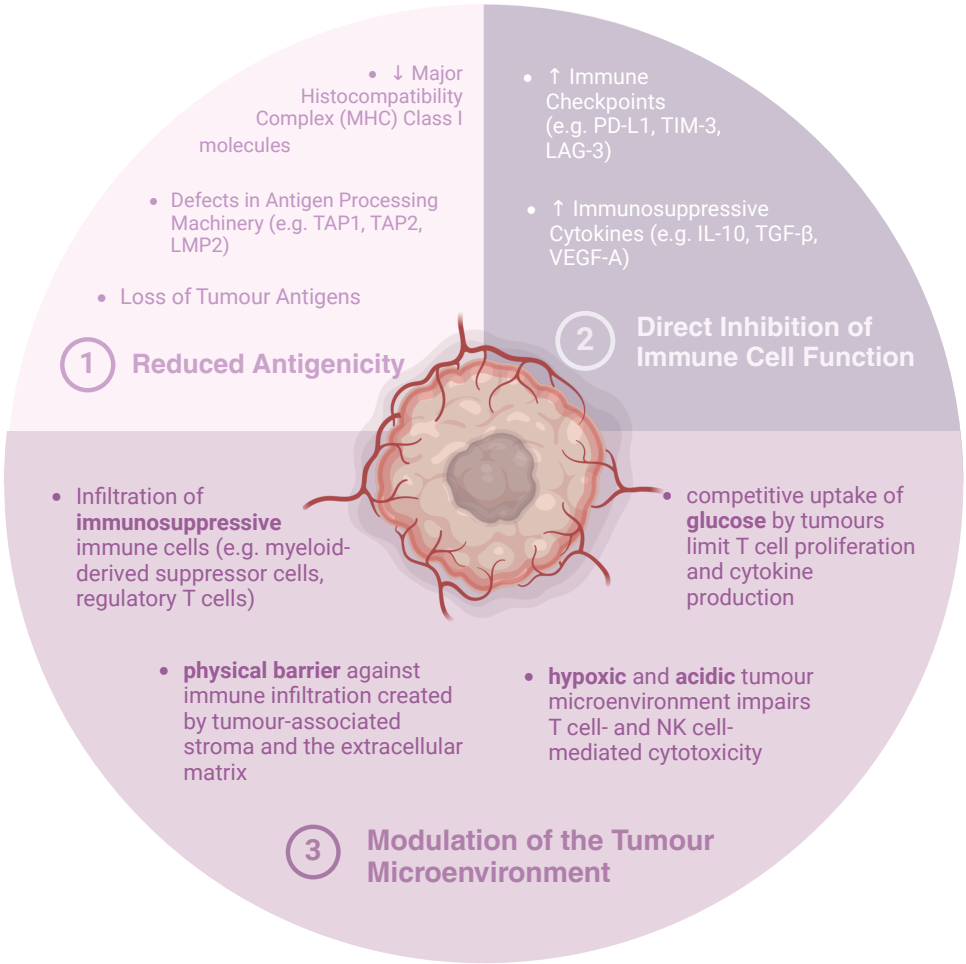

Figure 4. Overview of Immune Evasion Mechanisms in Cancer.

6.2.4 Immunotherapy

Cancer immunotherapy harnesses the immune system to fight cancer, encompassing a diverse array of therapeutic strategies including immune checkpoint blockade (ICB), adoptive cell transfer, and cancer vaccines. Unlike traditional therapies that directly target cancer cells, immunotherapy aims to enhance or restore the immune system's natural anti-tumour response. Notably, ICB has emerged as a promising therapeutic approach in the treatment of CRC. The concept of ICB is grounded in the understanding that while cancer cells can be recognised by the immune system, certain regulatory mechanisms, known as immune checkpoints, can inhibit the immune system's ability to destroy these cells. Immune checkpoints are regulatory pathways in the immune system that control the intensity and duration of immune responses to maintain self-tolerance, protecting from uncontrolled immune responses that may cause tissue damage. However, cancer cells often exploit these checkpoints to evade immune destruction. By targeting immune checkpoints, therapeutic interventions can remove these inhibitory signals to enhance endogenous anti-tumour immune responses. Currently approved immune checkpoint inhibitors (ICIs) target either the cytotoxic T-lymphocyte-associated protein 4 (CTLA-4) pathway or the programmed cell death protein 1 (PD-1)/programmed cell death ligand 1 (PD-L1) pathway (43).

Two PD-1-targeting monoclonal antibodies, pembrolizumab and nivolumab, as well as the combination of nivolumab with the anti-CTLA4 antibody ipilimumab, has been granted accelerated approval by the Food and Drug Administration (FDA) for the treatment of MSI-H metastatic CRC. This approval followed clinical trials demonstrating their remarkable efficacy in this patient population (Table 1). Notably,

the KEYNOTE-177 phase III trial further established pembrolizumab as a superior therapeutic approach for treating metastatic MSI-H CRC compared to traditional chemotherapies, as evidenced by the significantly improved progression-free survival of 16.5 months with pembrolizumab compared to 8.2 months with chemotherapy (44). These findings led to the FDA-approval of pembrolizumab as a first-line treatment for MSI-H metastatic CRC.

Table 1. Landmark Clinical Trials Leading to FDA-Approval of Immune Checkpoint Inhibitors in dMMR/MSI-H Metastatic Colorectal Cancer.

Name	Phase	Immune Checkpoint Inhibitor	ORR in MSI-H CRC	DCR ≥ 12 Weeks in MSI-H CRC	FDA Approval Date	Reference
Keynote 028	II	Pembrolizumab	40%	90%	May 2017	(45)
CheckMate 142	II	Nivolumab	31%	69%	August 2017	(46)
CheckMate 142	II	Nivolumab + Ipilimumab	55%	80%	July 2018	(47)

Abbreviations: DCR (Disease Control Rate); dMMR (Mismatch Repair Deficient); MSI-H (High Microsatellite Instability); ORR (Objective Response Rate); PFS (Progression-Free Survival).

However, the benefit of ICIs is primarily restricted to CRC patients with MSI-H tumours, which accounts for only 15-20% of all CRC cases (18). In contrast, patients with MSS tumours, which constitute most CRC cases, exhibit limited responses to ICIs (45). MSI-H tumours are characterised by a high mutational burden resulting from deficiencies in MMR machinery. Conversely, MSS tumours possess a proficient mismatch repair system, resulting in a lower mutational burden and stable microsatellite regions. This difference in mutational burden is thought to drive the variation in ICI response rates between MSI-H and MSS patients. The elevated mutational burden in MSI-H tumours is posited to lead to increased neoantigen production, which enhances recognition by T cells and consequently results in

augmented T cell-mediated responses against the tumour (48). Consistent with this hypothesis, MSI CRC tumours are characterised by high infiltration of CD8+ CTLs while MSS tumours lack significant CTL infiltrates (49). However, beyond microsatellite stability status, there are limited biomarkers available for predicting responses to ICIs. As mechanisms influencing tumour immunogenicity and responses to ICI in CRC remains underexplored, it is clear that a deeper understanding of such immunomodulatory mechanisms is necessary to unveil novel predicative biomarkers or immunosensitisation targets, which may ultimately expand the number of CRC patients who can benefit from ICIs.

6.3 Hedgehog Signalling

6.3.1 Hedgehog Proteins

The hedgehog (HH) signalling pathway is an evolutionarily conserved signalling cascade that plays an essential role in embryonic morphogenesis and the maintenance of adult tissue homeostasis. The *hh* gene was originally discovered during a genetic screen in *Drosophila melanogaster*, whereby mutations in the *hh* gene disrupted segment polarity in developing embryos, giving rise to a characteristic spiky or bristled appearance reminiscent of a hedgehog (50). While the *Drosophila* genome contains a single *hh* gene, the mammalian genome harbours three homologous genes: Sonic Hedgehog (*SHH*), Desert Hedgehog (*DHH*), and Indian Hedgehog (*IHH*). These HH genes encode secreted signalling proteins that can bind their cognate cell surface receptor patched homolog 1 (PTCH1) to initiate the HH signalling pathway. The three proteins share a high degree of amino acid sequence and structural homology in their N-terminal signalling domains, which are essential for binding of the PTCH1 receptor (51). Despite their structural and mechanistic similarities, SHH, IHH

and DHH exhibit distinct tissue expression patterns that underpin their unique roles in development and tissue homeostasis. SHH is predominantly expressed in regions such as the notochord and limb buds, where it is orchestrates neural patterning and limb formation (52). On the other hand, IHH is primarily expressed in developing bones and cartilage, where it regulates chondrocyte differentiation and bone formation (53). In contrast, DHH is expressed in the male gonads, where it is crucial for testicular development (54). These distinct expression patterns are critical for the specific biological functions of each HH protein, enabling specialised regulation of developmental processes and tissue maintenance.

The biogenesis of HH proteins involve a precise sequence of molecular events, beginning with the transcription of the HH gene in the nucleus and subsequent translation of the mRNA into a precursor protein in the cytoplasm. The precursor protein comprises an amino-terminal (N-terminal) signalling domain, a carboxy-terminal (C-terminal) autoprocessing domain, and a signalling peptide which directs the protein to the endoplasmic reticulum (ER) (52). Upon entry into the ER, the signal peptide is cleaved off by signal peptidases, and the precursor protein undergoes autoproteolytic cleavage to generate a mature N-terminal signalling domain and a C-terminal fragment (55). The mature N-terminal signalling domain undergoes two crucial post-translational lipid modifications, the addition of a cholesterol moiety to its C-terminus and a palmitate adduct to its N-terminus, which are essential for the protein's stability and activity (56-58). These palmitoyl and cholesteryl modifications tether the protein to the cell membrane, and its release from the cell surface is facilitated primarily by Dispatched-1 (DISP1), which extracts the lipid-modified HH protein from the membrane and packages it with its carrier, Signal peptide-CUB-EGF-

like domain-containing protein 2 (SCUBE2), to generate a soluble signalling protein (55).

6.3.2 Mechanism of HH signalling in Mammals

The mammalian HH genes, *SHH*, *IHH* and *DHH*, encode secreted signalling proteins that can bind to their cognate cell surface receptor PTCH1 and initiate the HH signalling pathway in an autocrine or paracrine fashion. Although the three HH genes exhibit distinct tissue expression patterns, they share a common signal transduction machinery (Figure 5) (55).

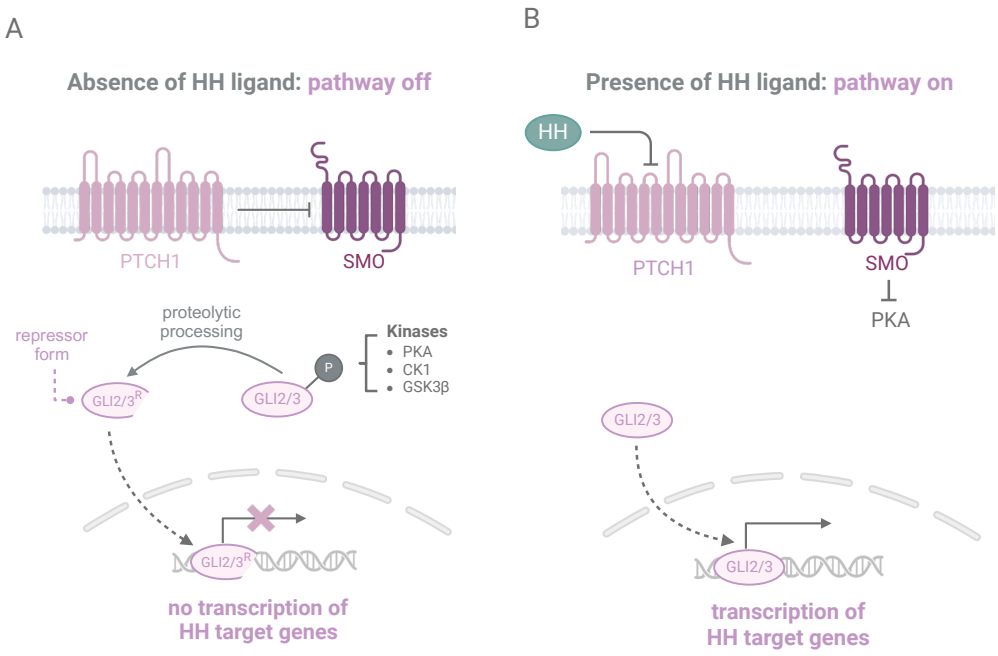

Figure 5. Overview of the Hedgehog (HH) Signalling Pathway in Vertebrates. (A) In the absence of HH proteins (SHH, IHH, DHH), the HH pathway is inactive. The transmembrane receptor PTCH1 inhibits the activity of the G protein-coupled receptor SMO. In this state, the transcription factors GLI2 and GLI3 are sequentially phosphorylated by the kinases PKA, CK1 and GSK3β. This phosphorylation primes GLI2/3 for ubiquitination by the $SCF^{\beta TRCP}$ E3 ubiquitin ligase complex, leading to their partial proteolysis into repressor forms ($Gli2/3^{R}$), which translocate into the nucleus to inhibit the transcription of HH target genes. **(B)** In the presence of HH ligands, HH binds PTCH1, relieving the inhibition on SMO. Activated SMO inhibits PKA activity, preventing the phosphorylation and proteolysis of GLI2/3. Full length GLI2/3 translocate into the nucleus to activate the transcription of HH target genes.

In the absence of HH ligands (Figure 5A), the HH signalling pathway is actively repressed by PTCH1, a 12-pass transmembrane protein. PTCH1 is enriched in the primary cilium, an antenna-like organelle that protrudes from the surface of diverse cell types, and is essential for the transduction of HH signalling in vertebrates (55, 59). At the primary cilium, PTCH1 inhibits the activity of the G protein-coupled receptor Smoothened (SMO) by controlling cholesterol distribution within the ciliary membrane. Specifically, evidence from structural and biochemical studies have indicated that PTCH1 transports cholesterol from the outer to the inner leaflet of the ciliary membrane (60, 61). This depletes the levels of accessible cholesterol within the outer membrane leaflet, which is essential for SMO activation (62-64). Consequently, in the absence of HH ligands, PTCH1 creates an environment that prevents the activation of SMO as it traffics into and out of the primary cilium. The activity of SMO critically influences the role of the bifunctional glioma-associated oncogene (GLI) transcription factors GLI2 and GLI3, which can function either as transcriptional activators or repressors to regulate the activity of the HH pathway (65). When SMO is inactivated, GLI2/3 undergoes sequential phosphorylation by protein kinase A (PKA), casein kinase 1 (CK1) and glycogen synthase kinase-3β (GSK3β), which creates a binding site for the E3 ubiquitin ligase complex $SCF^{\beta\text{-}TRCP}$. Ubiquitination by $SCF^{\beta\text{-}TRCP}$ targets GLI2/3 to the proteasome, where they are proteolytically processed into C-terminally truncated forms, $GLI2/3^{R}$, which act as transcriptional repressors. These repressor forms of GLI translocate into the nucleus and binds the promoter of HH target to facilitate transcriptional repression, thereby maintaining pathway quiescence (66).

The repression of the HH pathway is alleviated upon the binding of a HH ligand to its receptor PTCH1 (Figure 5B). The N-terminal palmitate of the HH ligand inserts

into the hydrophobic transport conduit within PTCH1, blocking its sterol transport activity (67-69). The inactivation of PTCH1 consequently leads to an increase in the concentration of accessible cholesterol within the outer leaflet of the ciliary membrane, which promotes the binding of cholesterol at the extracellular cysteine-rich domain of SMO, driving its activation (70). In its active conformation, SMO interacts less efficiently with the ciliary retrograde transport machinery, resulting in its accumulation in the primary cilium (55). At the primary cilium, activated SMO directly recruits PKA via a pseudosubstrate sequence found within its cytoplasmic domain. This interaction not only sequesters PKA away from the GLI transcription factors, but also occlude PKA's active site, thereby inhibiting its kinase activity (71). Consequently, GLI2/3 escapes proteolytic processing, and in their unprocessed full-length forms, act as transcriptional activators which translocate into the nucleus to induce the expression of HH target genes (55, 66).

Notably, HH target genes include components of the HH signalling pathway, including *GLI1*, *PTCH1*, and *HHIP*, which generates a feedback loop that ensures the HH signalling pathway remains tightly regulated. Specifically, GLI1, which acts exclusively as a transcriptional activator, amplifies HH signalling. Concurrently, the increase in negative regulators of the HH pathway, PTCH1 and HHIP, prevents excessive pathway activation which could lead to developmental abnormalities or tumourigenesis (72).

6.3.3 Hedgehog Signalling in Intestinal Homeostasis

The hedgehog proteins IHH and SHH are expressed within the adult mammalian intestine, with their expression localised to the intestinal crypts. In the

intestine, Hh signalling occurs primarily in a paracrine manner in the intestine, where IHH and SHH, secreted by epithelial cells, act on adjacent mesenchymal cells. This signalling facilitates crucial epithelial-mesenchymal crosstalk, playing a pivotal role in maintaining gut homeostasis (73).

6.3.3.1 Maintenance of intestinal epithelial homeostasis

Intestinal epithelial homeostasis is maintained through a dynamic balance between the proliferation of stem cells, their differentiation into specialised cell types, and the controlled shedding of old or damaged cells. This balance is essential for the continuous renewal of the intestinal lining, which is crucial for maintaining the intestine's barrier function, facilitating efficient nutrient absorption, and providing protection against pathogens (74, 75).

Accumulating evidence suggests that the HH pathway plays a key role in maintaining intestinal epithelial homeostasis, particularly by regulating stem cell self-renewal and differentiation. The conditional knockout of *Ihh* in the intestinal epithelium of adult mice led to an expansion of the stem cell pool within the intestinal crypts, indicating that *Ihh* may act as a negative regulatory signal that restricts the proliferation of intestinal stem cells (76). Supporting these findings, several studies have reported that the inhibition of the Hh pathway promoted epithelial proliferation and crypt fissioning, likely as a direct consequence of stem cell expansion (77, 78). In addition to regulating stem cell self-renewal, the inhibition of Hh signalling has been associated with defective enterocyte differentiation, suggesting that this pathway is also involved in the regulation of intestinal stem cell fate (76, 77, 79). Consistent with these findings, the expression of Ihh by differentiated colonic epithelial cells has been shown to

antagonise Wnt signalling, a key signalling pathway that promotes stem cell self-renewal and inhibits differentiation (79). Collectively, these studies highlight a role for HH signalling in maintaining intestinal epithelial homeostasis by acting as a negative regulatory signal that modulates the self-renewal and differentiation of intestinal stem cells.

Notably, as HH signalling occurs primarily in a paracrine manner, from the epithelium to the mesenchyme, this suggests that mesenchymal-derived factors, produced in response to HH signalling, are likely responsible for controlling the proliferation and differentiation of intestinal stem cells (73). Specifically, bone morphogenetic proteins (Bmps) have been identified as potential mesenchymal-derived factors mediating this process, as the inhibition of HH signalling in the murine intestine was associated decreased expression of Bmp4 and increased Wnt signalling (78). Bmp signalling, which is upregulated by Hh activity, is known to suppress intestinal stem cell self-renewal and promote its differentiation by negatively regulating the Wnt pathway (80). Consequently, this suggests that the HH pathway, by promoting Bmp signalling and consequently inhibiting Wnt signalling, regulates intestinal stem cell dynamics. This regulatory mechanism suppresses excessive proliferation of intestinal stem cells while encouraging its differentiation. Overall, existing data suggests that the crosstalk between Hh, Bmp, and Wnt signalling pathways establish a finely tuned regulatory network maintaining intestinal epithelial homeostasis. However, it remains possible that other, yet unidentified, mesenchymal factors also contribute to intestinal stem cell maintenance in response to Hh signalling.

6.3.3.2 Regulation of Intestinal Immunity

The immune system in the intestine maintains a delicate balance between tolerance and defence: protecting against invading pathogens while fostering tolerance to commensal microbes and dietary antigens. This balance is critical for maintaining homeostasis and preventing inappropriate inflammatory responses. However, dysregulation of this finely tuned balance can lead to uncontrolled inflammation, contributing to the development of inflammatory bowel disease (IBD) and other intestinal disorders (81).

Accumulating evidence suggests that the HH pathway plays a key role in regulating intestinal immune responses. Initial evidence for this role came from a study demonstrating that HH signalling is downregulated in IBD patients compared to healthy controls. Further analysis identified a *GLI1* variant (rs2228226C→G) with impaired transcriptional activity, which is associated with an increased susceptibility of developing IBD (82). Studies involving the manipulation of the Hh pathway in mice have further supported a role for Hh signalling in restraining intestinal inflammation. In a dextran sulfate-induced mouse model of colitis, genetic or pharmacological inhibition of Hh signalling exacerbated colon inflammation, while elevated HH signalling ameliorated colitis. The protective effect of HH signalling against colitis was partially attributed to the upregulation of the anti-inflammatory cytokine IL-10 by stromal cells, which promoted the differentiation of CD4+ T cells into immunosuppressive regulatory T cells (Tregs) (83). A similar study revealed that the conditional knockout of *Ihh* in the murine intestinal epithelium promoted intestinal inflammation, characterised the upregulation of inflammation-related genes and an increased infiltration of T cells and macrophages. Further investigation revealed that the immunosuppressive effects of

Ihh were, in part, attributed to the suppression of *CXCL12* expression in fibroblasts, a key chemokine involved in T cell recruitment (84). Collectively, these studies indicate that Hh signalling is crucial for the appropriate modulation of inflammatory responses in the gut.

6.3.4 Hedgehog Signalling in Cancer

6.3.4.1 Role in the Carcinogenesis and Progression of CRC

Multiple lines of evidence suggest that HH signalling, particularly through SHH, plays a role in the development and progression of CRC. Studies have demonstrated elevated expression of SHH and downstream HH pathway activation markers (*GLI1*, *PTCH1*, and *HHIP*) in colorectal carcinoma cells relative to normal colonic epithelial cells (85-87). Furthermore, a progressive upregulation of the HH pathway components, *SMO* and *GLI1*, was observed in a stepwise manner from normal colon to colonic adenoma and ultimately to colon adenocarcinoma, suggesting that the Hh pathway may contribute the carcinogenesis of CRC (87). Notably, while the expression of HH pathway activation markers was only slightly enriched in non-metastatic CRC tumours when compared to normal colonic tissue, a marked increase was observed in metastatic tumours, indicating a potential role for the HH pathway in promoting metastasis. Consistent with these findings, enhancing HH signalling in CRC cells has been shown to augment the formation and growth of lung metastases in a xenograft mouse model (86). Further supporting a role for the HH pathway in promoting metastasis, HH activity has been demonstrated to induce epithelial-mesenchymal transition (EMT), a process where carcinoma cells lose epithelial traits of cell-cell adhesion and cell polarity, and acquire mesenchymal traits of motility and invasion. Overexpression of GLI1, a key transcriptional effector of the HH pathway, in a human

CRC cell line has been shown to induce EMT, characterised by an upregulation of mesenchymal markers (*FOXC2*, *VIMENTIN*, *SNAIL1*, *ZFHX1B*) and a concurrent downregulation of the epithelial marker E-CADHERIN (86). Conversely, pharmacological inhibition of the Hh pathway using Cyclopamine reduced the expression of EMT-associated transcription factors (*SLUG*, *SNAIL* and *TWIST*) and markedly reduced the invasive capabilities of human CRC cells in vitro (88). In addition to the induction of EMT, HH activity has also been implicated in promoting the survival and self-renewal of CRC stem cells (89, 90). Collectively, these studies suggest that the HH pathway contributes to the carcinogenesis and progression of CRC, particularly through regulating cancer stem cell properties and promoting metastatic behaviour.

Interestingly, SHH and IHH exhibit distinct expression patterns in CRC. While an upregulation of *SHH* expression has consistently been observed in CRC, *IHH* expression tends to be downregulated. *IHH* transcript levels were shown to be markedly decreased in human colorectal adenocarcinomas compared to normal colonic tissue. Specifically, *IHH* expression has been shown to be negatively correlated with *APC* mutations in colorectal tumours (91). *APC* mutations, which occur early in the carcinogenesis of CRC, result in the constitutive activation of the Wnt pathway (9). Given that Wnt signalling has previously been implicated in the repression of IHH expression, it is plausible that constitutive Wnt activity, resulting from APC mutations, contributes to the downregulation of IHH expression in colorectal tumours (79). However, whether the repression of IHH expression contributes to the carcinogenesis and progression of CRC remains to be elucidated.

6.3.4.2 Role in Cancer Immunity

6.3.4.2.1 Polarisation of macrophages towards an immunosuppressive phenotype

Macrophages, a type of innate immune cell with versatile functions, play key roles in the regulation of anti-tumour immunity in a tissue-specific and context-dependent manner. These cells exhibit a spectrum of activation states in response to different environmental stimuli, which are often broadly categorised into two polarised states: classically activated (M1) and alternatively activated (M2). Polarisation of macrophages to the M1 state is induced by pro-inflammatory cytokines such as interferon-gamma (IFN-γ) and tumour necrosis factor alpha (TNF-α), as well as microbial components such as lipopolysaccharide (LPS). The M1 state is characterised by pro-inflammatory functions, promoting host defence against pathogens and malignant cells through phagocytosis, pro-inflammatory cytokine production and antigen presentation. On the other hand, M2 polarisation occurs in response to simulation with anti-inflammatory cytokines such as IL-4 and IL-13. These M2-polarised macrophages contribute to tissue repair, angiogenesis, and immunosuppression, playing crucial roles in resolving inflammation and maintaining tissue homeostasis (92). In tumours, infiltrating macrophages, also known as tumour-associated macrophages (TAMs), typically adopt an M2-like phenotype due to stimulation by factors present in the tumour microenvironment (TME), thereby contributing to an immunosuppressive and pro-angiogenic TME (93). Consequently, increased infiltration of TAMs has been shown to correlate with worse prognosis in human CRC patients (94).

Two independent studies have highlighted a role for HH signalling in promoting the polarisation of macrophages towards the immunosuppressive M2 phenotype (95, 96). In a murine model of breast cancer, the inhibition of Hh signalling via the administration of the Smo inhibitor vismodegib led to an increase in M1 macrophages and a decrease in M2 macrophages within the TME. This shift in the balance of M1 and M2 macrophages was accompanied by an increased infiltration of cytotoxic CD8+ T cells into the TME and a reduction in tumour growth (95). Similarly, myeloid-specific deletion of *Smo* in a mouse model of heptatocellular cancer promoted a pro-inflammatory phenotype in TAMs, characterised by a reduction in the expression of M2 markers (*Arg1*, *Cd206*, *Il10*, *Tgfb1*, and *Chil3*) and an increase in the expression of M1 markers (*Tnfa*, *iNos* and *Il6*) (96). In both studies, Hh signalling was shown to be activated in murine macrophages which were polarised to the M2 state (95, 96). Furthermore, treating M2-polarised murine macrophages with recombinant Shh further potentiated the expression of the Hh activation marker *Gli1*, as well as the M2 markers *Arg1* and *Cd206*. Accordingly, the inhibition of Hh signalling in M2 macrophages via treatment with the Gli inhibitor GANT61 attenuated the expression of the M2 markers *Arg-1* and *Cd206*, providing direct evidence that HH signalling in macrophages promote their polarisation towards the M2 phenotype. Conversely, inhibiting Hh signalling in M1-polarised murine macrophages via GANT61 treatment potentiated the expression of M1 markers *iNos, Il12*, and *Tnfα*, indicating that the activation of Hh signalling in macrophages suppress the pro-inflammatory M1 phenotype (95). Collectively, these results provide compelling evidence that Hh signalling in macrophages inhibit their polarisation towards the pro-inflammatory M1 phenotype while promoting their polarisation towards the immunosuppressive M2 phenotype.

6.3.4.2.2 PD-L1 Upregulation

Programmed death-ligand 1 (PD-L1), also known as cluster of differentiation 274 (CD274) or B7 homolog 1 (B7-H1), has emerged as a key negative regulator of the adaptive anti-tumour immune response. Expressed on the surface of antigen-presenting cells and tumour cells, PD-L1 can interact with the immune checkpoint receptor Programmed cell death protein 1 (PD-1) found on the surface of antigen-stimulated T cells and transduce inhibitory signals which restrain T cell activity (Figure 6) (97). Consequently, the upregulation of PD-L1 is a frequent mechanism exploited by tumours to evade host immune surveillance. Notably, tumours exhibiting PD-L1 expression, suggestive of the involvement of PD-1/PD-L1 pathway in immune evasion, correlates with response to PD-1 or PD-L1 blockade therapy (98-100).

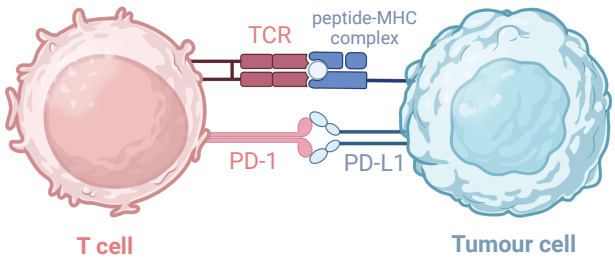

Figure 6. PD-1/PD-L1-Mediated Immune Checkpoint in Tumour Immune Evasion. The figure illustrates the interaction between programmed cell death protein 1 (PD-1) and its ligand, programmed death-ligand 1 (PD-L1), as a key immune checkpoint pathway regulating T cell activity. T cells can recognise tumour cells through their T cell receptor (TCR), which specifically binds to tumour antigens presented by major histocompatibility complex (MHC) molecules on the surface of the tumour cells, initiating T cell activation. However, tumour cells can express PD-L1 on their surface, which binds to PD-1, a receptor on activated T cells. This binding transmits an inhibitory signal which suppresses T cell activity, enabling tumours to evade T cell-mediated killing.

Several studies employing human cancer cell lines and animal models of cancer has demonstrated a role for HH signalling in regulating PD-L1 expression. This was initially reported in an in vitro study, which revealed that hypoxia-induced HH

signalling in human pancreatic ductal adenocarcinoma, gallbladder cancer, and small cell lung cancer cell lines induced the expression of PD-L1 (101). The role of Hh signalling in promoting PD-L1 expression was further demonstrated in a mouse model of Hh-driven gastric adenocarcinoma, whereby the administration of the Gli inhibitor GANT61 blocked adenocarcinoma development and attenuated the expression of PD-L1 within the gastric tissue of these mice (101). Beyond its role in regulating PD-L1 expression in tumour cells, Hh signalling is also involved in modulating PD-L1 expression in TAMs. Specifically, in a mouse model of heptatocellular carcinoma, paracrine signalling by tumour-derived Shh induced PD-L1 expression in TAMs via the STAT3 pathway, which was associated with suppressed intra-tumoural CD8+ T cell effector function (102). Collectively, these findings underscore the role of Hh signalling in promoting an immunosuppressive TME by upregulating PD-L1 expression on tumour cells and other cells within the TME.

Although the induction of PD-L1 expression through HH signalling suggest that cancers with high HH activity, and consequently high PD-L1 expression, may exhibit favourable responses to PD-1/PD-L1 blockade therapy, clinical data indicate otherwise. A recent pan-cancer analysis revealed that patients exhibiting high HH activity within the high PD-L1-expressing subgroup displayed a markedly lower response rate to ICIs and a significantly worse overall survival compared to those exhibiting low HH activity (103). This suggests that HH signalling likely activates additional immunosuppressive mechanisms, beyond merely inducing PD-L1 expression, that limit the efficacy of ICIs. Thus, integrating HH activity with PD-L1 expression may serve as a more robust predictor of response to ICIs than assessing PD-L1 expression alone.

6.3.4.2.3 Recruitment of myeloid-derived suppressor cells

Myeloid-Derived Suppressor Cells (MDSCs) are a heterogeneous population of immune cells originating from the myeloid lineage, characterised by their capacity to suppress both innate and adaptive immune responses. MDSCs are primarily divided into two major subsets based on their myeloid cell lineage origins: monocytic MDSCs (M-MDSCs) which arise from the monocytic lineage, and polymorphonuclear MDSCs (PMN-MDSCs) which originate from the granulocytic lineage. Essentially, M-MDSCs and PMN-MDSCs are monocytes and neutrophils, respectively, which have undergone pathological activation due to persistent stimulation by myeloid growth factors and inflammatory signals originating from sites of cancer or chronic inflammation. This is distinct from the classical activation of monocytes and neutrophils, which occurs in response to pathogens and tissue damage. While classically activated myeloid cells play crucial roles in host defence and tissue remodelling through mechanisms including phagocytosis and pro-inflammatory cytokine production, pathologically activated MDSCs acquire potent immunosuppressive properties which can impair anti-tumour responses (104). Hence, high MDSC infiltration is associated with poor disease prognosis and patient resistance to immunotherapy across many cancers, including CRC (105).

Several studies using murine cancer models have reported an association between HH signalling and MDSC infiltration in the TME. For instance, the pharmacological inhibition of Hh signalling in a mouse model of breast cancer resulted in a decrease in the infiltration of CD11b+ LY6G+ LY6C+ cells, indicative of MDSCs (95). Conversely, two independent studies found that epidermal-specific activation of Hh signalling in mouse models of Hh-driven basal cell carcinoma, either by expressing

a constitutively active form or Smo or through *Ptch1* deletion, led to an accumulation of CD11b+ cells at the tumour sites, suggesting an increased recruitment of MDSCs. In both studies, the enhanced recruitment of CD11b+ cells have been attributed, in part, to the elevated levels of the chemokine CCL2 within the TME (106, 107). However, it is crucial to note that, currently, no cell surface markers can distinctly differentiate classical neutrophils from PMN-MDSCs or classical monocytes from M-MDSCs in mice (104). Further qRT-PCR analysis of the CD11b+ Ly6G+ cells isolated from tumour sites in $Ptch^{\Delta ep}$ mice revealed that these cells do not express the MDSC marker arginase, suggesting that classical neutrophils rather than PMN-MDSCs infiltrate the tumour lesions in these mice. Accordingly, depleting neutrophils in $Ptch^{\Delta ep}$ mice using an anti-Ly6G depletion antibody enhanced tumour growth, indicating that these neutrophils contribute to anti-tumour immunity (107). These findings suggest that caution should be exercised when interpreting reports that associate HH signalling with MDSC infiltration. It is essential to critically assess whether the observed infiltrates are truly MDSCs or instead represent classical neutrophils and monocytes, which play distinct roles in tumour immunity.

6.3.4.2.4 Regulatory T cell differentiation

Regulatory T cells (Tregs) are a subset of immunosuppressive CD4+ T cells, characterised by the expression of the master transcription factor forkhead box protein P3 (FOXP3) (108). Naïve CD4+ T cells undergo differentiation into Tregs upon TCR activation in the presence of IL-2 and TGF-β (109). By consuming the T cell growth factor IL-2, interfering with antigen-presenting cell functions, and secreting immunosuppressive cytokines, Tregs create an immunosuppressive TME that allow cancer cells to evade immune detection and destruction (108).

Several studies have implicated a role for HH signalling in regulating the differentiation of CD4+ T cells into Tregs. Recent analysis of transcriptional data from The Cancer Genome Atlas (TCGA) across 14 different human cancer types revealed that tumours with high Hh activity generally displayed a higher abundance of Tregs and a lower abundance of CD8+ cytotoxic T cells compared to those with low Hh activity (103). Supporting this observation, epidermal-specific activation of Hh signalling in mouse models of Hh-driven basal cell carcinoma led to an accumulation of Tregs in both intra- and peri-tumoural regions. Consistent with this observation, elevated levels of TGF-β, a potent inducer of Treg differentiation, were found in tumour lesions compared to control skin (107). Conversely, two independent studies revealed that the pharmacological inhibition of Hh signalling in murine mammary cancer models resulted in a pronounced shift in CD8+ T cell:Treg ratio, characterised by an increase in CD8+ cytotoxic T cells and a decrease in immunosuppressive Tregs (95, 110). Specifically, inhibiting Hh signalling in these mice promoted the conversion of immunosuppressive Tregs into pro-inflammatory Th17 cells, indicating that Hh signalling activity is a key determinant in the fate and functionality of CD4+ T cells (110). Collectively, these results highlight a key role for HH signalling in regulating Treg differentiation, which may contribute to the formation of an immunosuppressive TME.

7 Materials and Methods

7.1 Cell Culture

All cell cultures were grown at 37 °C in a humidified atmosphere containing 5% CO_2 and were screened weekly for *Mycoplasma* contamination.

7.1.1 2D Cell Lines

7.1.1.1 SW948

The SW948 human colon adenocarcinoma cell line was purchased from American Type Culture Collection (ATCC) and cultured in DMEM/F-12 media (Gibco, 11320033) supplemented with 10% heat-inactivated foetal bovine serum (Gibco, 10082147) and 1% penicillin/streptomycin (Gibco, 15140122).

7.1.1.2 THP-1

The THP-1 human leukaemia monocytic cell line was kindly gifted by Dr Anjali Arora (Buffa lab, University of Oxford), and cultured in RPMI 1640 media (Gibco, 11875093) supplemented with 10% heat-inactivated fetal bovine serum (Gibco, 10082147).

7.1.1.3 Primary Human Colonic Fibroblasts

Primary human colonic fibroblasts were isolated by Yi Zhou (Buczacki lab, University of Oxford), and cultured in Fibroblast Growth Medium 2 (PromoCell, C-23020). These fibroblasts were isolated from normal human colon tissue. Briefly, the tissue was treated with ethylenediaminetetraacetic acid (EDTA) to remove the epithelial layer and subsequently cut into small fragments. The minced tissue was

subjected to enzymatic digestion with Liberase (Roche, 5401119001) for 60 minutes at 37 °C, with gentle agitation to facilitate cell dissociation. The digested mixture was passed through a 70 µm cell strainer to remove undigested material, and the resulting cell suspension was layered over a Percoll gradient and centrifuged at 900 x g for 20 minutes to separate fibroblasts from other cell types based on density. Fibroblasts were collected from the 30-70% interface and cultured in fibroblast growth medium at 37°C in a 5% CO_2 atmosphere. Non-adherent cells and debris were removed after 24 hours, and fibroblasts were passaged once large colonies were observed. The identity of fibroblasts was confirmed by immunofluorescence staining of alpha-smooth muscle actin and vimentin.

7.1.2 3D Organoid Lines

7.1.2.1 Pat-16-ID-8837

The patient-derived colon adenocarcinoma organoid line Pat-16-ID-8837 was kindly provided by Dr Scott Collins (Buczacki Lab, University of Oxford). The organoids were embedded in Cultrex Reduced Growth Factor Basement Membrane Extract (R&D Systems, 3533-010-02) and cultured in homemade organoid media, which was replaced every 2 days. The media consisted of Advanced DMEM/F-12 (Gibco, 12634010) supplemented with:

- 0.1% bovine serum albumin (Tocris, 5217)
- 1% GlutaMAX (Gibco, 35050061)
- 1% N-2 Supplement (Gibco, 17502048)
- 5% B-27 Plus Supplement (Gibco, A3582801)
- 10 mM HEPES (Gibco, 15630080)
- 100ug/mL Primocin (InvivoGen, ant-pm-2)

- 500 ng/mL recombinant human R-spondin-1 (PeproTech, 120-38)
- 1.25 mM N-acetylcysteine (MP Biomedicals, 0210009850)
- 100 ng/mL recombinant human epidermal growth factor (PeproTech, AF-100-15)
- 100 ng/mL recombinant human noggin (PeproTech, 120-10C)
- 10 µM SB 431542 (Tocris, catalog: 1614/1), 10mM Nicotinamide (Sigma-Aldrich, N3376)
- 10uM SB 202190 (Sigma-Aldrich, S7067)
- 1uM prostaglandin E_2 (Tocris, 2296/10)
- 10nM gastrin I (Sigma-Aldrich, 05-23-2301)
- recombinant human fibroblast growth factor-basic (PeproTech, 100-18B).

7.2 CRISPR/Cas9-Mediated Gene Editing

CRISPR/Cas9-mediated gene editing was used to knock out the Indian hedgehog (*IHH*) gene in the human colon adenocarcinoma cell line SW948 (see section 7.2.1) and the patient-derived organoid line Pat-16-ID-8837 (see section 7.2.2). An *IHH*-targeting multi-guide RNA, which is a set of 3 single guide RNAs (sgRNAs) targeting exon 1 of the *IHH* gene, was designed and purchased from Synthego. The three guide RNA sequences are (i) 5'-GCGAGCGGCACGAGUUUGCG-3', (ii) 5'-GGCCCGCAGCCCCAUGCCGC-3', and (iii) 5'-AGUGCAGUCGGGGCCGGAGC-3'.

7.2.1 2D Cell Line

SW948 cells were harvested and quantified using a haemocytometer. A suspension containing 100,000 cells was transferred into a microcentrifuge tube and centrifuged at 300g for 5 minutes to obtain a cell pellet. The pellet was resuspended

in 6 uL of Buffer R (Invitrogen, MPK1096), followed by the addition of 0.9 uL of Cas9 protein (Sigma-Aldrich, CAS9PROT) and 0.6 uL of the *IHH*-targeting multi-guide RNA. The mixture was incubated at room temperature for 10 minutes to facilitate the formation of ribonucleoprotein (RNP) complexes consisting of Cas9 protein and guide RNA. Using the NEON transfection system (Thermo Fisher Scientific), the RNP complexes were electroporated into the cells with the following parameters: 1320V, 30 ms, 1 pulse. Post-electroporation, the cells were plated onto a 12 well plate and allowed to grow to confluency, with media changes performed every 2 days. Once confluent, the cells were transferred to a T-25 flask for further culturing and analysis.

7.2.2 3D Organoid Line

4 fully confluent domes of organoids were prepared for a single CRISPR reaction. 500 uL of TrypLE (Gibco, 12604021) was initially added to each well containing a fully confluent dome to facilitate the breakdown of the BME matrix. The contents from the wells were pooled into a 15 mL centrifuge tube, and 10 uL of Y27632 (Tocris, 1254) was added. The centrifuge was submerged in a 37°C water bath for 10 minutes total. During this time, the organoid suspension was triturated 50 times every 2.5 minutes using a P1000 pipette to achieve a single-cell suspension. After 10 minutes of incubation, an equal volume of DMEM++ (Advanced DMEM/F-12 media (Gibco, 12634010), supplemented with 1% GlutaMAX (Gibco, 35050061), 1% HEPES (Gibco, 15630080), and 0.1% Y27632 (Tocris, 1254), was added to the organoid suspension. The mixture was then centrifuged at 400g for 6 minutes at 4°C to obtain a cell pellet. The pellet was resuspended in 10 uL of Buffer T (Invitrogen, MPK1096). In parallel, 7.2 uL of Buffer R (Invitrogen, MPK1096), 1.2 uL of Cas9 protein (Sigma-Aldrich, CAS9PROT) and 1.6 uL of the IHH-targeting multi-guide RNA were added to

a microcentrifuge tube and incubated at room temperature for 10 minutes to facilitate the formation of RNP complexes. Following incubation, the cell suspension was added to the RNP complex mixture. The RNP complexes were electroporated into the cells using the NEON Transfection System (Thermo Fisher Scientific) with the following parameters: 1350 V, 20 ms, and 2 pulses. Following electroporation, cells were transferred to a 1.5 mL microcentrifuge tube containing 750 uL of DMEM++, and the cell suspension was centrifuged at 400 g for 6 minutes at 4°C. The obtained cell pellet was resuspended in 320 uL of BME and aliquoted into eight 40uL domes in a 24-well plate. The plate was incubated at 37°C for 30 minutes to allow the domes to solidify. Following incubation, the domes were cultured overnight in antibiotic-free organoid media, after which the media was replaced with organoid media containing antibiotics (as described above) for further culturing.

7.3 Generation of Single Cell-Derived *IHH*-knockout clones

Single-cell cloning was performed using the limiting dilution technique to obtain clonal cell populations from a heterogeneous cell mixture. Cells were initially harvested and quantified using a haemocytometer. An initial suspension containing 1,000 cells in 1 mL of culture media was prepared, from which 250 uL was transferred to a 50 mL centrifuge tube, where it was further diluted with media to reach a total volume of 50 mL. 200 µL of the cell suspension was distributed into each well of a 96-well plate to achieve a target concentration of 1 cell per well. The plate was incubated at 37°C in a 5% CO_2 atmosphere for 14 days, allowing individual cells to grow into distinct colonies. After incubation, wells containing single colonies were identified and marked, and the colonies were subsequently expanded into larger culture vessels for further analysis.

7.4 Gene set enrichment analysis (GSEA)

GSEA was performed to identify differentially enriched gene signatures between tumours expressing high and low levels of IHH. The analysis utilised data from the Colon Adenocarcinoma cohort in The Cancer Genome Atlas (TCGA) PanCancer dataset, encompassing a total of 378 samples. Using cBioportal, samples were stratified based on IHH mRNA expression levels, defining the “high IHH-expressing” group as those in the upper quartile of IHH expression (n = 95) and the “low IHH-expressing” group as those in the lower quartile of IHH expression (n = 94). A pre-ranked gene list of the differentially expressed genes between the low and high *IHH*-expressing group was generated for GSEA, with genes ranked in descending order of log2 ratio between the two groups. In this context, genes with positive log2 fold change values were enriched in the high IHH-expressing group, while genes with negative log2 fold change values were enriched in the low IHH-expressing group. The pre-ranked gene list was input into the GSEA software (version 4.3.2), and a pre-ranked analysis was conducted with the hallmark gene set collection (n = 50 gene sets) from the Molecular Signatures Database (MSigDB). A false discovery rate (FDR) q-value cutoff of < 0.01 was applied to select for the most statistically significant differentially enriched gene sets.

7.5 Macrophage Polarisation Assay

THP-1 monocytes were harvested and quantified using a haemocytometer. The cells were plated at a density of 800,000 cells per well in 6-well plates and differentiated into macrophages by incubating with 10 ng/mL phorbol 12-myristate 13-acetate (PMA) for 24 hours. After differentiation, the wells were washed twice with PBS, and the macrophages were allowed to rest in PMA-free media for an additional

24 hours. The macrophages were subsequently polarised to M1 or M2 states by incubating with 20 ng/mL IFN-γ or IL-4, respectively, for 48 hours. When required, 3 ug/mL recombinant IHH (StemCell, 78197) or 7.5 uM GANT61 (StemCell, 73692) was added concurrently with the polarising agents and incubated for the same duration.

7.6 Processing and Analysis of RNA-sequencing data

The processing and analysis of RNA-sequencing data was performed by A. Mandal (Buczacki Lab, University of Oxford) in R (version 4.3.3). In brief, the quality of the raw reads were assessed using FastQC (version 0.11.9), and reads were filtered and trimmed using Cutadapt (version 3.5) to remove adapters and low-quality bases. The cleaned reads were mapped to the human reference genome GRCh38 (hg38) using STAR (version 2.7.3a) to obtain a gene-level read count matrix (61,541 Ensembl gene IDs across six samples). The edgeR package (version 4.0.16) was employed to estimate median library size across the samples (median library size: 59.2 million), with a count per million (CPM) threshold of 0.084 established to filter low-expressed genes. Genes were required to exceed this threshold in at least four samples, resulting in a final matrix of 21,461 genes that cleared this threshold. The 'voom' method from the limma package (version 3.58.1) was used for variance-stabilizing transformation and normalization of the count matrix. Ensembl gene IDs were converted to gene symbols using the biomaRt package (version 2.58.2), resulting in a matrix of normalized counts for 18,260 gene symbols. During this process, gene IDs lacking official gene symbol assignments (HGNC) or associated with multiple gene IDs were filtered out. The limma package was further used to conduct differential expression analysis, comparing wild-type and *IHH*-knockout samples (each with n = 3 replicates). Statistical significance was assessed by moderated t-test in limma, with significance

defined as adjusted p-value < 0.05. 141 genes were identified as statistically significant, including 43 upregulated and 98 downregulated in the *IHH*-knockout samples. Gene Set Enrichment Analysis (GSEA) was further performed using the fgsea package (version 1.28.0), utilizing the Hallmark gene set collection (n = 50 gene sets) from the Molecular Signatures Database (MSigDB) to identify differentially enriched biological processes or pathways between wild-type and *IHH*-knockout samples. Significant enrichment was defined as adjusted p-value < 0.05 and normalised enrichment score (NES) > |1.5|.

7.7 Profiling IHH-induced Immune-Related Genes Using an RT2 Profiler PCR Array

Primary human colonic fibroblasts were seeded in 6-well plates at a density of 35,000 cells per well and allowed to grow over 72 hours. After 72 hours, fibroblasts were treated with 3 µg/mL of recombinant IHH (StemCell, 78197). Total RNA was isolated from IHH-treated and control fibroblasts using the RNeasy mini kit (Qiagen, 74104), and RNA quality and concentration were assessed using a NanoDrop spectrophotometer (Thermo Fisher). Complementary DNA (cDNA) was synthesized from 500 ng of total RNA using the RT² First Strand Kit (Qiagen, 330401), according to manufacturer's protocol. The resulting cDNA was diluted to a final volume of 110 µL with RNase-free water. The "Human Cancer Inflammation & Immunity Crosstalk" RT² PCR Profiler Array (Qiagen, 330231) was used to analyse the expression of 84 genes involved in cancer-associated inflammation and immune response. For the PCR reaction, 102 µL of cDNA was mixed with 1,150 µL of 2x PowerTrack SYBR Green Master Mix (Applied Biosystems, A46109) and 1,048 µL of RNase-free water. This mixture was then distributed into the wells of the RT² Profiler PCR Array, with 25 µL of

the prepared reaction mix added to each well. The thermal cycling conditions were as follows: initial denaturation at 95°C for 10 minutes, followed by 40 cycles of 95°C for 15 seconds and 60°C for 60 seconds. The Ct values were obtained and input into the GeneGlobe Data Analysis Software (Qiagen) for analysis. The expression of the target genes were normalised to the endogenous control gene *ACTB*.

7.8 Sanger sequencing

Total DNA was extracted from harvested cells using the Quick-DNA Miniprep Kit (Zymo, D3024), and the quality and concentration of the extracted DNA was quantified using a NanoDrop Spectrophotometer (Thermo Fisher). The IHH gene was amplified via PCR using the forward primer 5'-GTTGCCAAAACAAACGGGCCGG-3' and the reverse primer 5'-GATCGCGCTCACCTGGGTCATG-3', which were designed using Primer3 on Benchling and purchased from Integrated DNA Technologies (IDT). PCR amplification was carried out in a 25 µL reaction volume consisting of 100-500 ng of genomic DNA, 1X Q5 Reaction Buffer (New England Biolabs, B9027SVIAL), 200 µM dNTPs (Invitrogen, 18427089), 0.02 U/µL Q5 High-Fidelity DNA Polymerase (New England Biolabs, M0491SVIAL), 0.5 µM each of the forward and reverse primers, and 1X 5X Q5 High GC Enhancer (B9028AVIAL). The thermal cycling conditions were as follows: initial denaturation at 98°C for 30 seconds, followed by 30 cycles of 98°C for 10 seconds, 60°C for 30 seconds, and 72°C for 30 seconds, with a final extension at 72°C for 2 minutes. Following PCR, the PCR products were purified using the QIAquick PCR Purification Kit (Qiagen, 28104), and the quality and concentration of the purified amplicons was quantified using a NanoDrop Spectrophotometer (Thermo Fisher). The purified amplicons were diluted with nuclease-free water to a

concentration of 10-50 ng/uL, and submitted to Genewiz (Oxford, United Kingdom) for Sanger Sequencing.

7.9 Sample Preparation for RNA-sequencing

CRC Organoids from the wild-type and IHH-knockout groups were cultured until reaching confluency. To ensure sufficient RNA yield, three confluent domes of organoids were pooled to form a single technical replicate. A total of 3 technical replicates were prepared for both the wild-type and IHH-knockout groups. RNA, DNA, and protein were simultaneously extracted from the organoids using the AllPrep DNA/RNA/Protein Mini Kit (Qiagen, 80004) according to manufacturers protocol, where Buffer RLT was added directly to the organoid domes in the 24-well plate to lyse the cells and initiate the extraction process. The quality and concentration of the extracted RNA and DNA were quantified using a NanoDrop Spectrophotometer (Thermo Fisher). All extracted RNA, DNA and protein were stored at -80°C until further use. The extracted RNA samples were sent to Genewiz (Oxford, United Kingdom) for RNA sequencing, where library preparation and sequencing were performed according to their standard protocols.

7.10 SiRNA knockdown of *IHH*

For siRNA-mediated knockdown of *IHH*, SW948 cells were seeded at a density of 250,000 cells/well in 6-well plates the day before transfection and allowed to adhere overnight. For each transfection reaction, Lipofectamine 3000 reagent (Invitrogen, L3000001) was mixed with 75 pmol of either *IHH*-targeting siRNA (Horizon Discovery, M-005901-01-0005) or a non-targeting control (Horizon Discovery, D-001206-13-05) in 250 uL of Opti-MEM media (Gibco, 31985062). This mixture was incubated at room

temperature for 15 minutes to facilitate the formation of transfection complexes. Following incubation, the medium in each well was replaced with 2 mL of Opti-MEM media, and 250 uL of the transfection complexes were added to the cells. The cells were incubated at 37°C and harvested at 48- and 72-hours post-transfection for qRT-PCR and Western blot analysis, respectively.

7.11 Western Blotting

7.11.1 Protein Extraction and Quantification

Extracted cells were pelleted and resuspended in RIPA lysis and extraction buffer (Thermo Scientific, 89900) supplemented with cOmplete protease inhibitor cocktail (Roche, 04693116001). The cell suspension was subjected to sonication (30 seconds on, 30 seconds off, for 10 cycles) to ensure complete lysis of cells. Following sonication, the cell lysate was centrifuged at 14,000 x g for 15 minutes (4°C) to pellet the cell debris. The supernatant was collected, and protein concentration was quantified using the Pierce BCA Protein Assay Kit (Thermo Scientific, 23225). The extracted protein was stored at -20°C until further use.

7.11.2 SDS-PAGE

Protein samples (15-50 ug) were mixed with NuPAGE LDS Sample Buffer (Invitrogen, NP0007) and NuPAGE Sample Reducing Agent (Invitrogen, NP0009), and incubated at 95°C for 5 minutes to facilitate protein denaturation. Proteins were separated by molecular weight using sodium dodecyl sulphate-polyacrylamide gel electrophoresis (SDS-PAGE) with 4-12% NuPAGE Bis-Tris gels (Invitrogen, NP0321BOX). The gels were run in 1X NuPAGE MES SDS Running Buffer (Invitrogen, NP0002) at 130V for 1 hour in a XCell SureLock Mini-Cell system

(Invitrogen). The molecular weight standard, Amersham ECL Rainbow Marker (Cytiva, GERPN800E), was loaded in the first lane to facilitate the estimation of protein sizes.

7.11.3 Immunoblotting

Following SDS-PAGE, the separated proteins were transferred onto a nitrocellulose membrane at 30 V for 1 hour using a XCell SureLock Mini-Cell system equipped with an XCell II Blot Module (Invitrogen). The membrane was subsequently blocked with 5% non-fat dry milk in Tris-buffered saline with 0.1% Tween 20 (TBST) for 1 hour at 4°C to prevent non-specific binding of antibodies. After blocking, the membrane was incubated overnight at 4°C in blocking buffer with primary antibodies against IHH (1:2000; Abcam, ab39634) and the loading control vinculin (1:5000; Sigma-Aldrich, V4505). Following primary antibody incubation, the membrane was washed three times with TBST for 10 minutes each, and incubated with anti-mouse (Proteintech, SA00001-1) and anti-rabbit (Proteintech, SA00001-2) IgG HRP-conjugated secondary antibodies for 1 hour at room temperature in blocking buffer. Following secondary antibody incubation, the membrane was again washed three times with TBST, and the protein bands were visualised using the Amersham ECL Prime Western Blotting Detection Reagent (Cytiva, RPN2236) and the ChemiDoc MP imaging system (Biorad).

7.12 Quantitative Reverse Transcription Polymerase Chain Reaction (qRT-PCR)

Total RNA was extracted from harvested cells using the RNeasy mini kit (Qiagen, 74104), and the quality and concentration of the extracted RNA was quantified using a NanoDrop Spectrophotometer (Thermo Fisher). Complementary DNA (cDNA) was

synthesized from 2 µg of total RNA using the SuperScript IV VILO Master Mix (Invitrogen, 11756050) in a 20 uL reaction volume, following the thermal cycling conditions: 25°C for 10 minutes, 50°C for 60 minutes, and 85°C for 5 minutes. The resulting cDNA was diluted 1:10 in nuclease-free water, and stored at -20°C until further use. Quantitative PCR was performed on a StepOnePlus Real-Time PCR System (Applied Biosystems) using either TaqMan-based (see section 7.12.1) or SYBR Green-based (see section 7.12.2) gene expression assays.

7.12.1 TaqMan

TaqMan gene expression assays (Applied Biosystems) were used to assess the expression of *IHH* (Hs00745531_s1) and *GLI1* (Hs00171790_m1). The expression of these target genes were normalised to the endogenous control gene *ACTB* (Hs01060665_g1). The PCR reactions were performed in a 20uL reaction volume containing 2 µL of cDNA, 1X TaqMan™ Gene Expression Assay, and 1X TaqMan™ Fast Advanced Master Mix. The qRT-PCR reactions were performed on a StepOnePlus Real-Time PCR System (Applied Biosystems), with the following thermal cycling conditions: initial denaturation at 95°C for 20 seconds, followed by 40 cycles of 95°C for 1 second and 60°C for 20 seconds. The threshold cycle (Ct) values were obtained and used to calculate relative expression levels of the target genes using the comparative Ct method ($2^{-\Delta\Delta Ct}$).

7.12.2 SYBR Green

SYBR Green gene expression assays were used to assess the expression of the M1 (*TNF, CD80, IL6, IL1B*) and M2 (*IL10, FN1, CD206, CCL18*) macrophage polarisation markers. The expression of these target genes was normalised to the

endogenous control gene *ACTB*. All primer pairs were supplied by Dr Anjali Arora (Buffa lab, University of Oxford), which were purchased from Invitrogen, with their sequences and catalogue numbers listed in Table 2. The PCR reactions were performed in a 10 uL reaction volume containing 2 uL of cDNA, 1X PowerTrack SYBR Green Master Mix (Applied Biosystems, A46109), and 300nM of forward and reverse primers. The qRT-PCR reactions were performed on a StepOnePlus Real-Time PCR System (Applied Biosystems), with the following thermal cycling conditions: initial denaturation at 95°C for 2 minutes, followed by 40 cycles of 95°C for 15 seconds and 60°C for 60 seconds. The Ct values were obtained and used to calculate relative expression levels of the target genes using the comparative Ct method ($2^{-\Delta\Delta Ct}$).

Table 2. Forward and Reverse PCR Primer Sequences for M1 and M2 Macrophage Polarization Markers.

Gene	Forward Primer	Reverse Primer
TNF	5'-CTCTTCTGCCTGCTGCACTTTG-3'	5'- ATGGGCTACAGGCTTGTCACTC-3'
CD80	5'- CTCTTGGTGCTGGCTGGTCTTT-3'	5'- GCCAGTAGATGCGAGTTTGTGC-3'
IL6	5'- AGACAGCCACTCACCTCTTCAG-3'	5'-TTCTGCCAGTGCCCTCTTTGCTG-3'
IL1B	5'- CCACAGACCTTCCAGGAGAATG-3'	5'- GTGCAGTTCAGTGATCGTACAGG-3'
IL10	5'- TCTCCGAGATGCCTTCAGCAGA-3'	5'- TCAGACAAGGCTTGGCAACCCA-3'
FN1	5'- ACAACACCGAGGTGACTGAGAC-3'	5'- GGACACAACGATGCTTCCTGAG-3'
CD206	5'- AGCCAACACCAGCTCCTCAAGA-3'	5'- CAAAACGCTCGCGCATTGTCCA-3'
CCL18	5'- GTTGACTATTCTGAAACCAGCCC-3'	5'- GTCGCTGATGTATTTCTGGACCC-3'

7.13 Statistical analyses

All statistical analyses, unless stated otherwise, were performed using GraphPad Prism (version 10.2.0). Due to the small number of biological replicates obtained per experiment ($n \leq 3$), normality tests were not conducted; however, all qRT-PCR data were assumed to follow a normal Gaussian distribution based on the continuous nature of the data and prior research indicating that similar biological measurements

typically follow a normal distribution. For normally distributed data, comparisons between two groups were conducted using Student's t-test. For multiple group comparisons, one-way analysis of variance (ANOVA) was employed.

8 Results

8.1 In Silico Analysis: Identifying IHH Expression as a Potential Regulator of CRC Immunogenicity

ICIs have revolutionised the treatment paradigm for CRC, offering significant benefits primarily to MSI-H patients. In contrast, MSS tumours, which constitute the majority (80-85%) of CRC cases, exhibit limited responses to ICIs. The differential response to ICIs is largely attributed to variations in tumour immunogenicity, defined as the ability of a tumour to provoke an immune response. The differences in immunogenicity are primarily driven by tumour mutational burden; MSI-H tumours exhibit a higher mutational burden that results in increased neoantigen production, facilitating enhanced recognition by T cells. However, beyond tumour mutational burden, the factors driving the variation in immunogenicity in CRC, especially within MSS tumours, remain inadequately understood. This limitation underscores the need for a deeper exploration of the underlying mechanisms that influence tumour immunogenicity and immune evasion in CRC. Consequently, our research group aims to address this knowledge gap by identifying and exploring potential factors that may regulate immunogenicity in CRC. By uncovering these regulatory factors, we aim to identify novel predictive biomarkers or immunosensitisation targets that could enable a broader range of CRC patients, particular those harbouring MSS tumours, to benefit from ICI therapy.

To uncover potential regulators of immunogenicity in CRC, our laboratory conducted a gene expression analysis to identify genes which were differentially expressed between colorectal tumours exhibiting high immunogenicity and those characterised by low immunogenicity. Specifically, by leveraging multi-omic data from The Cancer Genome Atlas (TCGA) colon adenocarcinoma dataset alongside a curated set of 340 immunogenicity parameters, Jack Flower performed a k-means based clustering analysis which identified 5 subgroups of patients with related immunogenicity, designated as immune subtypes (IS) 1 through 5 (Figure 7). Notably, IS1 and IS2 comprised tumours exhibiting MSI, while IS3-5 encompassed tumours which were MSS. A differential gene expression analysis was subsequently performed to identify differentially expressed genes between tumours classified as having high versus low immunogenicity within the MSI (IS1 versus IS2) and MSS (IS3 versus IS5) groups. This analysis revealed an upregulation of *IHH* expression in tumours exhibiting low immunogenicity across both MSS and MSI cases, suggesting that IHH may play an immunosuppressive role in CRC. Among the PRIs identified, IHH emerges as a compelling target for further investigation due to its epithelial-specific expression (see Figure 9 on page 62). Given that most of the other identified PRIs are highly expressed by immune cells, their differential expression may simply reflect differences in immune cell infiltration or activity between tumours with high and low immunogenicity, rather than signifying a genuine role in regulating CRC immunogenicity. In contrast, *IHH* expression is epithelial-specific, which negates this concern and suggests a genuine immunoregulatory role in CRC. Additionally, the selection of IHH for further analysis is supported by existing literature demonstrating the involvement of the HH signalling pathway in suppressing tumour immune responses in other malignancies, including breast and basal cell carcinoma (see section 6.3.4.2). Based on these findings, we

hypothesise that IHH signalling contributes to the formation of an immunosuppressive tumour microenvironment in CRC.

Figure 7. Schematic Overview of the Bioinformatic Analysis Conducted by Jack Flower to Identify Potential Regulators of Immunogenicity in Colorectal Cancer. Abbreviations: IS (Immune Subtype); MSI (Microsatellite Instable); MSS (Microsatellite Stable); PRI (Potential Regulator of Immunogenicity).

To investigate the potential link between *IHH* expression and immune response in CRC, a gene set enrichment analysis (GSEA) was performed to identify differentially enriched gene signatures between tumours expressing high and low levels of *IHH* (Figure 8). Colon Adenocarcinoma samples from The Cancer Genome Atlas (TCGA) PanCancer dataset, encompassing both MSI and MSS cases, were stratified into high and low *IHH*-expressing groups based on mRNA expression (Figure 8A). GSEA using the hallmark gene set collection from MSigDB revealed that the 8 most significantly differentially enriched gene sets between the two groups were immune-related (Figure 8B-C), indicating a strong association between *IHH* expression and CRC immunogenicity. These gene sets, which were enriched in the low *IHH*-expressing group, included pathways associated with inflammatory responses, interferon-mediated immune responses, and T cell effector functions, suggesting that reduced *IHH* expression is linked to enhanced anti-tumour immune responses. To further explore the potential mechanisms by which IHH may regulate CRC immunogenicity, we examined the leading-edge subset of these immune-related gene sets, referring to the core group of genes within a gene set that most strongly contribute to the enrichment signal. Notably, the enrichment of immune-related gene sets in the low *IHH*-expressing group was primarily driven by leading-edge genes such as *CXCL9*, *CXCL10*, *CXCL11*, *CXCL13*, *CCL4*, *TNFSF9*, and *GZMA* (Table 3). These genes are known to play crucial roles in T cell cytotoxicity (*TNFSF9*, *GZMA*) and the recruitment of immune cells such as T cells, B cells, and NK cells (*CXCL9*, *CXCL10*, *CXCL11*, *CXCL13*, *CCL4*) (111-115). This suggests that the recruitment of immune effector cells and T cell-mediated responses may be enhanced in tumours with low *IHH* expression compared to those with high *IHH* expression. Collectively, these findings strongly support the hypothesis that IHH plays an immunosuppressive role in CRC.

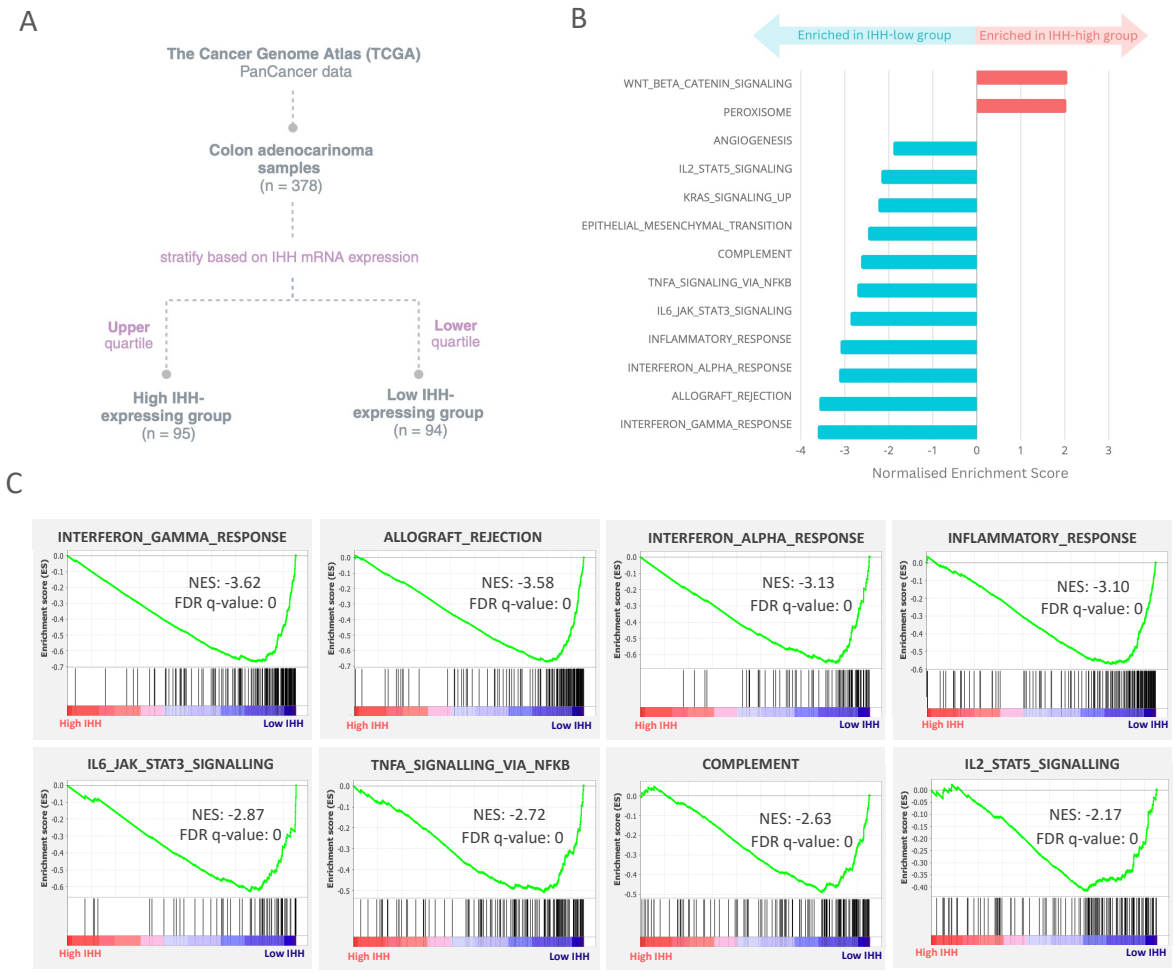

Figure 8. Gene Set Enrichment Analysis (GSEA) Identified Enrichment of 8 Immune-Related Gene Sets in Low *IHH*-Expressing Colon Adenocarcinoma Samples Compared to High *IHH*-expressing Samples. (A) Flow chart depicting the stratification of The Cancer Genome Atlas (TCGA) colon adenocarcinoma samples based on *IHH* mRNA expression levels. Samples were divided into low and high *IHH*-expressing groups, corresponding to the lower and upper quartiles of *IHH* mRNA expression, respectively. **(B)** Bar plot showing Hallmark gene sets (MSigDB) that were differentially enriched between low and high *IHH*-expressing groups, as identified by GSEA. Significant enrichment was defined by a false discovery rate (FDR) q-value < 0.01. **(C)** Enrichment plots depicting the 8 significantly enriched (FDR q-value < 0.01) immune-related gene sets from the Hallmark collection in CRC samples with low IHH expression compared to those with high IHH expression.

Table 3. Top 10 Leading-Edge Genes Contributing to the Enrichment of the 8 Immune-Related Hallmark Gene Sets in Low *IHH*-expressing Colon Adenocarcinoma samples.

Hallmark Gene Set	Top 10 Leading-Edge Genes
INTERFERON_GAMMA_RESPONSE	*IDO1, CXCL9, CXCL10, PLA2G4A, CXCL11, CIITA, GZMA, GBP4, CD274, OAS2*
ALLOGRAFT_REJECTION	*CXCL13, CXCL9, CCL13, KLRD1, GZMA, IFNG, PRKCG, CRTAM, HLA-DRA, CCL4*
COMPLEMENT	*PLA2G4A, SERPINB2, GZMA, KYNU, MMP12, OLR1, CP, GZMK, CCL5, RASGRP1*
IL2_STAT5_SIGNALING	*CXCL10, GBP4, SPP1, EOMES, CD86, IL2RA, TNFRSF9, IL2RB, NRP1, CTLA4*
IL6_JAK_STAT3_SIGNALING	*REG1A, CXCL13, CXCL9, PLA2G2A, CXCL10, CXCL11, IL2RA, CCL7, STAT1, IL6*
INFLAMMATORY_RESPONSE	*CXCL9, CXCL10, CXCL11, AQP9, MARCO, CXCL8, CLEC5A, OLR1, TNFAIP6, TNFSF9*
INTERFERON_ALPHA_RESPONSE	*CXCL10, CXCL11, GBP4, SAMD9L, IFI44L, SAMD9, BST2, IFIT3, IFI44, IFIT2*
TNFA_SIGNALING_VIA_NFKB	*DUSP4, CXCL10, CXCL11, SERPINB2, KYNU, OLR1, BIRC3, TNFAIP6, TNFSF9, CCL4*

8.2 Exploring the Potential Immunosuppressive Mechanisms of IHH in CRC

IHH is a signalling molecule that activates the HH signalling pathway by binding to its receptor, PTCH1, which is expressed on the surface of diverse cell types. Thus, to elucidate the potential mechanisms by which IHH influences the immune landscape in CRC, the expression of IHH and its receptor PTCH1 was evaluated to identify the cell types that may be involved in mediating IHH's immunosuppressive effects. Data from a publicly available single-cell expression atlas, which transcriptionally profiled 371,223 cells from colorectal tumours and adjacent normal tissues of 28 MSS and 34 MSI patients, revealed that *IHH* is expressed predominantly within the epithelial compartment in CRC (Figure 9B) (116). In contrast, its receptor *PTCH1* is expressed primarily in the stromal compartment, with some expression also seen in epithelial and

immune cells (Figure 9C). This expression pattern suggests that IHH is likely secreted by colorectal carcinoma cells and may exert both autocrine signalling effects on tumour cells themselves and paracrine signalling effects on surrounding stromal and immune cells. This implies a complex interplay where IHH not only influences the immunogenicity of CRC through direct effects on the tumour cells, but by also modulating the surrounding TME. Based on these findings, investigation into the effects of IHH signalling on colorectal cancer cells, cancer-associated fibroblasts, and immune cells was warranted.

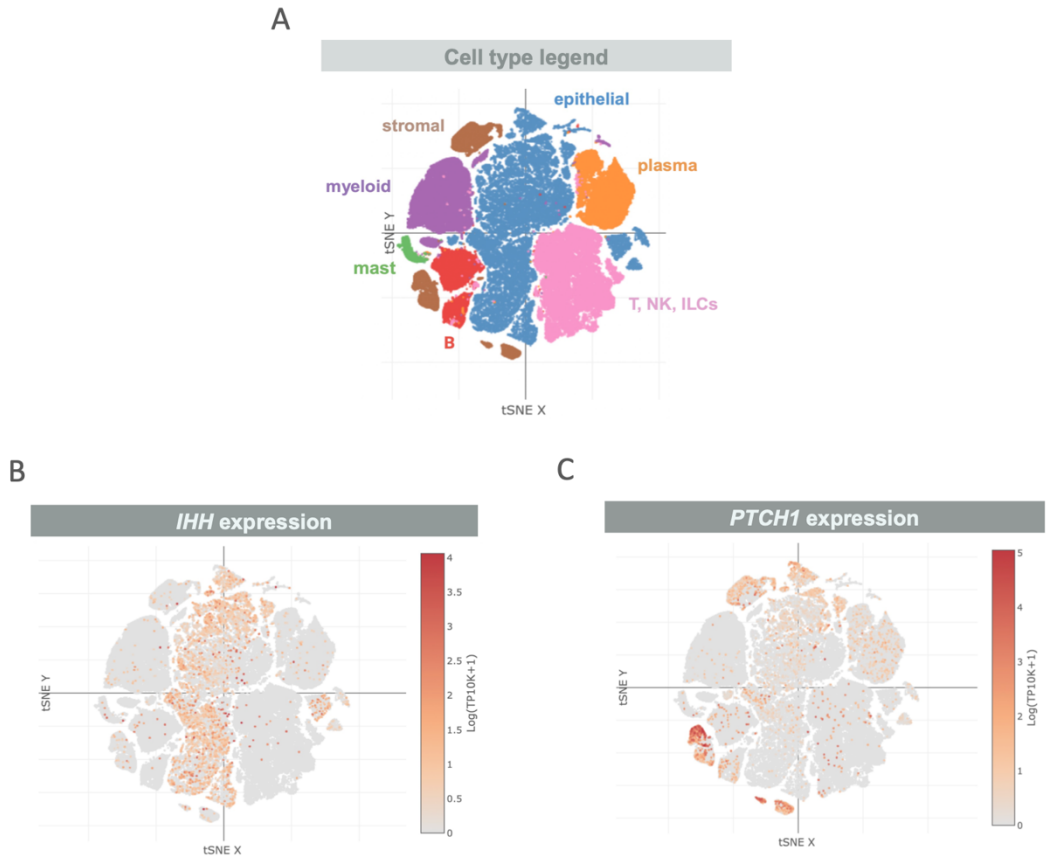

Figure 9. tSNE Plots Illustrating the Expression of *IHH* and Its Receptor *PTCH1* in Colorectal Cancer (CRC). (A) Different cell types within the CRC tumour microenvironment are colour-coded as follows: epithelial cells (blue), stromal cells (brown), plasma cells (orange), B cells (red), mast cells (green), myeloid cells (purple), and T, NK, and innate lymphoid cells (pink). **(B-C)** The tSNE plots display the expression levels of **(B)** *IHH* and **(C)** *PTCH1* across the identified cell types. Data source: Broad Institute Single Cell Portal - Human Colon Cancer Atlas (c295) (116).

8.2.1 Autocrine Effects on Cancer Cells

Given that PTCH1 is expressed on colorectal carcinoma cells (Figure 9C), it is plausible that IHH signalling can operate in an autocrine manner, where IHH secreted by CRC cells bind to PTCH1 receptors on the same cells to initiate signalling. In light of this, I hypothesise that IHH regulates CRC immunogenicity, at least in part, through these autocrine signalling mechanisms.

8.2.1.1 Generation of an IHH-knockout CRC organoid line

To elucidate the potential autocrine role of IHH in modulating CRC immunogenicity, the CRISPR-Cas9 system was employed to knockout the *IHH* gene in CRC organoids. This approach allows for subsequent transcriptomic analysis to investigate the downstream effects of IHH loss on gene expression and pathways related to immune regulation.

Initial experiments involved knocking out *IHH* in the colorectal adenocarcinoma cell line SW948 to validate the effectiveness of the *IHH*-targeting multi-guide RNA in generating a functional knockout. The SW948 cell line was employed due to its high endogenous *IHH* expression (Figure 10A), which enables clear and sensitive detection of decreases in IHH levels following gene knockout. Initial electroporation of Streptococcus pyogenes-derived Cas9 (SpCas9) protein and the *IHH*-targeting multi-guide RNA into SW948 cells achieved a knockout efficiency of 100%, which was validated by Sanger sequencing (Data not shown). Single cells were isolated and clonally expanded from the heterogenous population of *IHH*-knockout cells to obtain single cell-derived *IHH*-knockout clones, with clone A1 selected for further analysis.

The *IHH*-knockout in clone A1 was assessed at the gene, transcript, and protein level (Figure 10D-G). Gene-level validation through Sanger sequencing revealed a uniform 55 base-pair fragment deletion in the *IHH* gene across all A1 cells (Figure 10D-E). At the transcript level, qRT-PCR analysis demonstrated a reduction of *IHH* mRNA levels in A1 cells relative to wild-type cells (Figure 10F). However, Western blot analysis using an antibody targeting the C-terminus of IHH showed no difference in IHH protein levels between A1 cells and wild-type SW948 cells (Figure 10G).

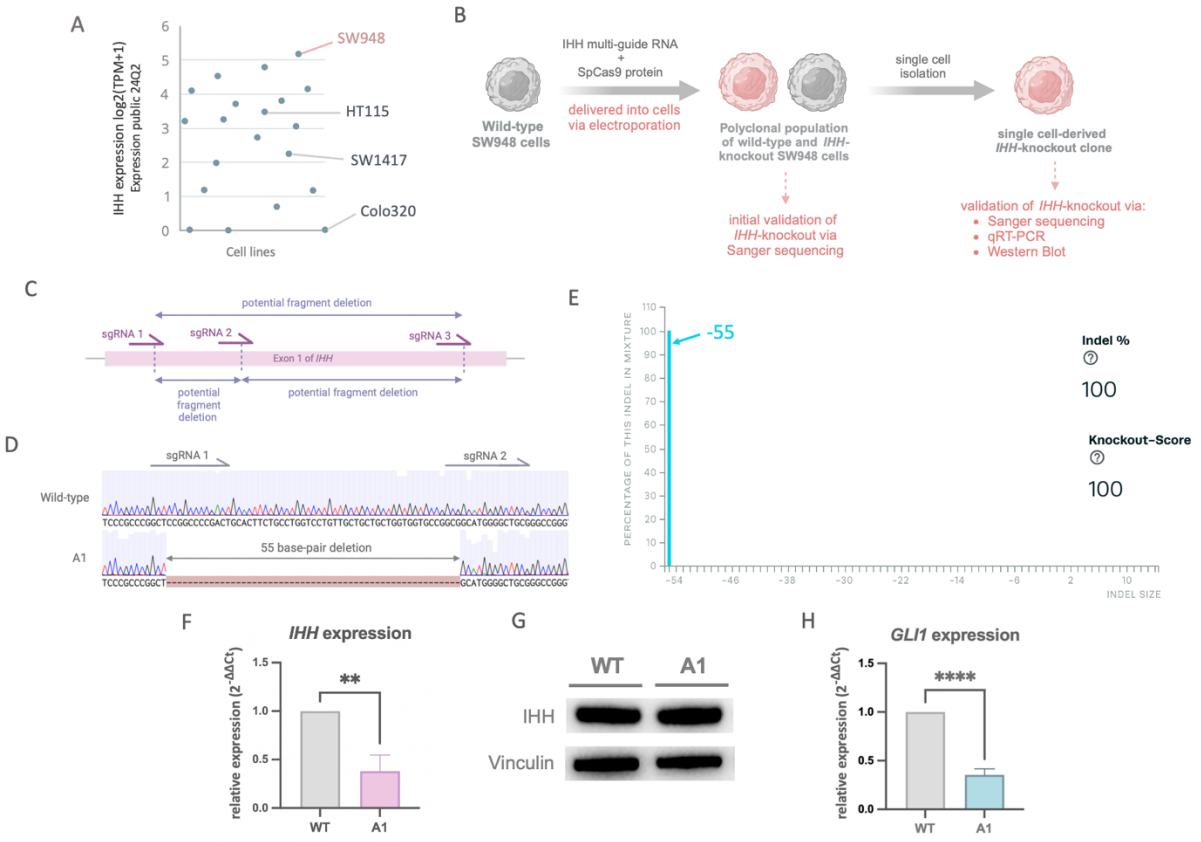

Figure 10. Characterisation and Validation of *IHH*-Knockout in the Human Colorectal Adenocarcinoma Cell Line SW948. (A) Dot plot showing the mRNA expression levels of *IHH* in microsatellite stable primary human colorectal adenocarcinoma cell lines. Each dot represents a different cell line. Data source: The Cancer Dependency Map (DepMap) (117). **(B)** Schematic workflow for knocking out the *IHH* gene in SW948 cells using the CRISPR/Cas9 gene-editing system. **(C)** The multi-guide RNA strategy for targeting the *IHH* gene, which comprises three spatially coordinated single guide RNAs, all targeting exon 1 of the *IHH* gene. The sgRNAs are positioned to facilitate the generation of large fragment deletions. **(D-H)** Validation of IHH-knockout in the single cell-derived clone A1. **(D)** DNA sequencing alignment

comparing exon 1 from the *IHH* gene in the IHH-knockout clone A1 with wild-type SW948 cells. A 55-base pair deletion is identified in the A1 clone compared to the wild-type sequence. **(E)** Analysis of Sanger sequencing data from the A1 clone using Synthego ICE analysis software reveals that all cells within the A1 clone harbours a 55-base pair deletion in the IHH gene. The knockout score, defined as the proportion of indel events that result in frameshifts or are greater than 21 base pairs in length, is reported at 100%. **(F)** qRT-PCR analysis of *IHH* expression in A1 cells compared to wild-type SW948 cells (n = 3). Data are presented as mean ± SD of fold changes in expression relative to the wild-type control, with statistical significance assessed by Student's t-test. **(G)** Western blot analysis of IHH expression in A1 cells compared to wild-type SW948 cells using the anti-IHH antibody ab39634. Vinculin serves as the loading control. **(H)** qRT-PCR analysis of *GLI1* expression in A1 cells compared to wild-type SW948 cells (n = 3). Data are presented as mean ± SD of fold changes in expression relative to the wild-type control, with statistical significance assessed by Student's t-test (**, $p < 0.01$; ****, $p < 0.0001$).

To validate the specificity of the IHH-targeting antibody, siRNA was employed to knockdown *IHH* expression in wild-type SW948 cells. qRT-PCR analysis confirmed that the transfection of siRNA into SW948 cells downregulated *IHH* expression at the transcript level (Figure 12A). However, Western blot analysis showed no reduction in IHH protein levels following siRNA transfection (Figure 12B).

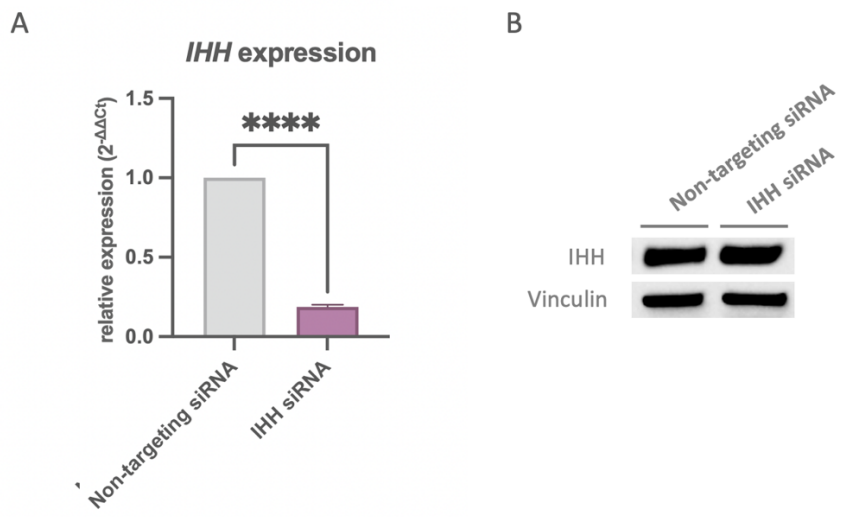

Figure 11. Assessment of the specificity of the IHH-targeting antibody ab39634 using siRNA-mediated knockdown. Analysis of IHH expression levels following siRNA-mediated knockdown of IHH in SW948 cells using **(A)** qRT-PCR (n = 3) and **(B)** Western blot, with vinculin serving as the loading control. qRT-PCR data are presented as mean ± SD of fold changes in expression relative to the non-targeting siRNA control, with statistical significance assessed by Student's t-test (****, $p < 0.0001$).

To confirm whether the 55 base-pair fragment deletion in *IHH* resulted in a loss-of-function in A1 cells, autocrine HH signalling activation was compared between A1 cells and wild-type SW948 cells. qRT-PCR analysis revealed a marked reduction in the expression of *GLI1*, a transcriptional target of the HH pathway, in A1 cells relative to wild-type cells (Figure 10H).

Following the validation of the IHH-targeting multi-guide RNA's efficacy in SW948 cells, the knockout strategy was implemented in a more physiologically relevant model: CRC patient-derived organoids (Figure 12). Among three transcriptomically-profiled and whole-exome sequenced, patient-derived CRC organoid lines preserved in our laboratory's biobank, the organoid line Pat-16-ID-8837 was selected for conducting the knockout experiments. As all three organoid lines exhibited similar levels of *IHH* expression, the selection of Pat-16-ID-8837 was based

on the organoid line's minimal inter-replicate variability and the absence of deleterious mutations in components of the canonical HH pathway (Figure 12A; Table 6 in Appendix). This organoid line was derived from an 81-year-old female who underwent a robotic right hemicolectomy in March 2023 for an ascending colon adenocarcinoma. Pathology from the surgery demonstrated a pT4a pN0 (0/23) V0 L0 R0 poorly differentiated adenocarcinoma. The tumour was MSS and wild-type for *BRAF*, *KRAS* and *NRAS*. Whole-exome sequencing found mutations in *APC, TP53, PIK3CA, ARID1B, SETD1B* and *KDM5A*. Sanger sequencing analysis revealed that electroporation of SpCas9 protein and *IHH*-targeting multi-guide RNA into Pat-16-ID-8837 organoids resulted in an 88% knockout efficiency (Figure 12D). Although achieving a 100% knockout through further isolation and clonal expansion of single organoids is theoretically ideal, it presents substantial technical challenges. Specifically, while CRC organoid lines are theoretically immortal, they present a finite lifespan in practice, remaining viable for only a limited number of passages. Moreover, the whole process, from isolation and expansion to screening, would take several months, which is impractical given the limited timeframe of a Master's research project. Consequently, the 88% knockout score was deemed adequate to induce meaningful transcriptomic changes detectable through RNA-sequencing (RNA-seq).

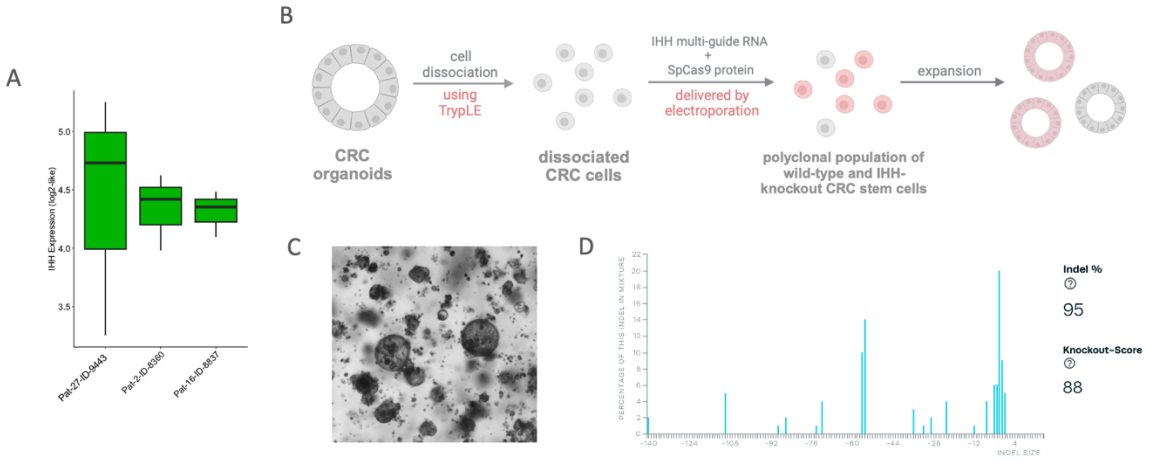

Figure 12. Knockout of the *IHH* Gene in Patient-Derived Colon Adenocarcinoma Organoid Line Pat-16-ID-8837. (A) Box-and-whisker plots comparing the transcript levels of *IHH* between three patient-derived colon adenocarcinoma organoid lines. The plots display the median (horizontal line), 25th to 75th percentiles (box), and 10th to 90th percentiles (whiskers). No significant differences ($p < 0.05$) in *IHH* expression levels were observed between the three organoid lines, as assessed by moderated t-test. **(B)** Schematic workflow for knocking out the *IHH* gene in the colorectal adenocarcinoma organoid line Pat-16-ID-8837 using the CRISPR/Cas9 system. **(C)** 4X brightfield image of the Pat-16-ID-8837 organoids taken 7 days post-CRISPR treatment. **(D)** Sanger sequencing data of the *IHH*-knockout Pat-16-ID-8837 line analysed using the Synthego ICE analysis software, revealing the proportion of different indel events detected in the knockout line, along with the corresponding knockout score, defined as the proportion of indel events that result in frameshifts or are greater than 21 base pairs in length.

8.2.1.2 RNA-seq analysis: IHH-knockout Alters Transcriptomic Profile in CRC Organoids

To investigate the impact of *IHH*-knockout on the transcriptomic landscape of the CRC organoids, RNA-seq was performed to identify genes that were differentially expressed between wild-type and *IHH*-knockout samples (Figure 13). This analysis aimed to determine whether the loss of IHH induces distinct changes in gene expression that could shed light on the underlying mechanisms through which IHH influences CRC immunogenicity, specifically through autocrine signalling within cancer cells.

To examine whether *IHH*-knockout samples exhibit distinct gene expression profiles from wild-type samples, principal component analysis (PCA) and hierarchical clustering were performed. PCA revealed a clear separation between *IHH*-knockout and wild-type samples along PC1, which accounted for 33.5% of the total variance (Figure 13A). This separation suggests that the loss of IHH function results in distinct transcriptional changes. Hierarchical clustering corroborated these findings, showing that IHH-knockout samples cluster separately from wild-type samples (Figure 13B).

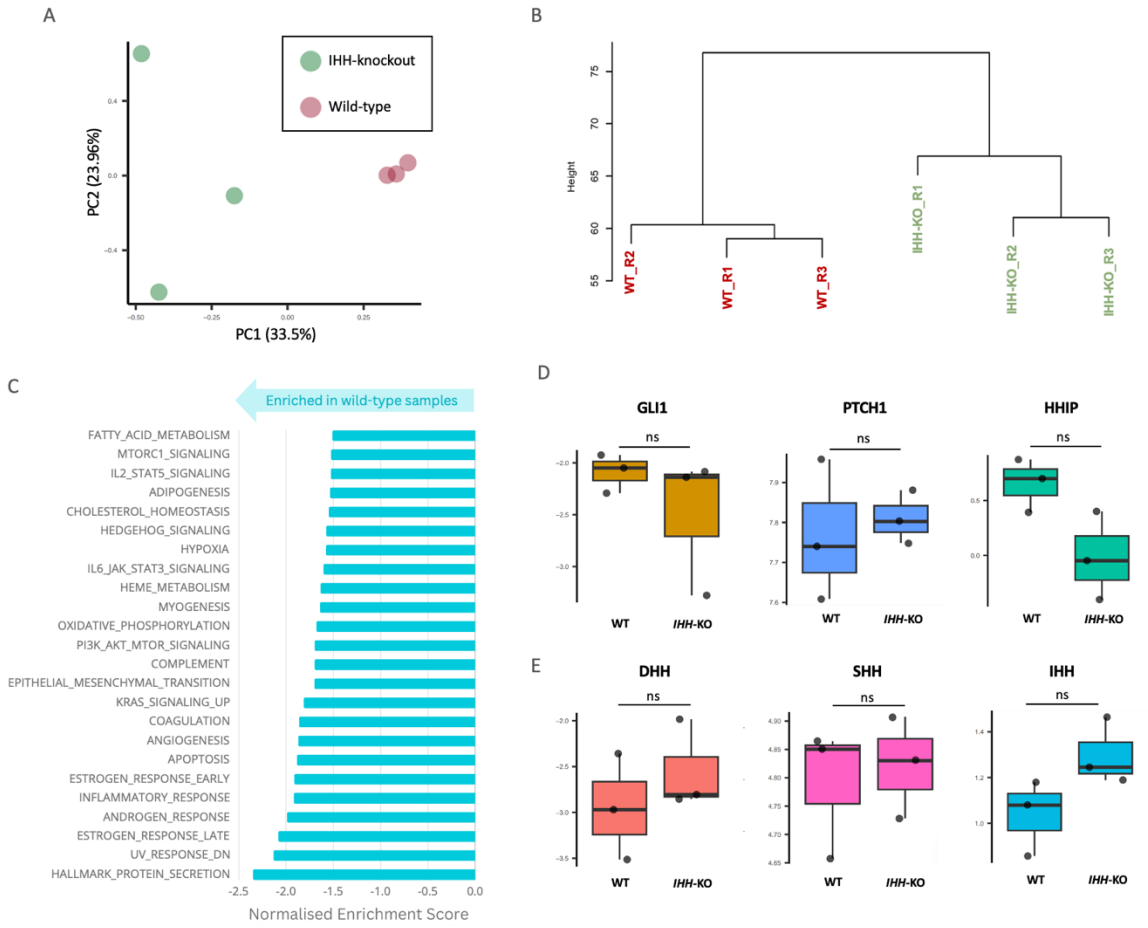

Figure 13. Transcriptomic Comparison of Wild-type and *IHH*-knockout CRC organoid line Pat-16-ID-8837 using RNA-sequencing. (A) Principal Component Analysis (PCA) plot showing the distribution of wild-type and IHH-knockout samples along principal components (PC) 1 and 2, which accounts for 33.5% and 23.96% of the total variance, respectively. **(B)** Hierarchical clustering of differentially expressed genes reveals the relationship between wild-type (red) and IHH-knockout (green) samples. **(C)** Gene Set Enrichment Analysis (GSEA) comparing wild-type and *IHH*-knockout samples using the Hallmark gene sets collection. The analysis highlights 24 differentially enriched gene sets, with significant enrichment defined by an adjusted p-value < 0.05 and a normalised enrichment score (NES) > |1.5|. **(D-E)** Box-and-whisker plots comparing the transcript levels of **(D)** Hedgehog (HH) pathway activation markers (*GLI1*, *PTCH1*, *HHIP*) and **(E)** HH family ligands (*IHH*, *SHH*, and *DHH*) between wild-type and *IHH*-knockout samples (n = 3). The plots display the median (horizontal line), 25th to 75th percentiles (box), and 10th to 90th percentiles (whiskers). Statistical significance was assessed by moderated t-test (ns, $p \geq 0.05$).

RNA-seq analysis revealed a total of 141 genes that were differentially expressed (p < 0.05) between wild-type and *IHH*-knockout organoids, with 43 upregulated and 98 downregulated genes upon the knockout of *IHH*. To gain deeper insights into the biological implications of these transcriptomic changes, GSEA was performed, identifying biological pathways and processes that were significantly affected by *IHH*-knockout. GSEA revealed that 24 gene sets from the hallmark gene set collection were differentially enriched (adjusted p-value < 0.05, NES > |1.5|) between wild-type and *IHH*-knockout samples (Figure 13C). Notably, these included an enrichment of gene sets associated with immune response (ALLOGRAFT_REJECTION, COMPLEMENT, IL2_STAT5_SIGNALING, IL6_JAK_STAT3_SIGNALING, INFLAMMATORY RESPONSE) and cancer-related processes such as hypoxia, EMT, and angiogenesis in wild-type samples. The enrichment of the 5 immune-related gene sets in the wild-type samples were driven by leading-edge genes (Table 4) which included pro-inflammatory cytokines (*IL18*, *CSF2*), cytokine receptors (*IL3RA*, *IL-10RA*, *CCRL2*, *CCR1*, *IL1R1*), complement regulatory proteins (*CD55*, *CD59*), immune checkpoints (*LGALS3*), cathepsin proteases (*CTSS*, *CTSB*), metalloprotease inhibitors (*TIMP1*, *TIMP2*), and antigen presentation machinery (*B2M*).

Table 4. Top 10 Leading-Edge Genes Contributing to the Enrichment of the 5 Immune-Related Hallmark Gene Sets in Wild-Type CRC Organoid Samples Compared to *IHH*-Knockout Samples.

Hallmark Gene Set	Top 10 Leading-edge genes
ALLOGRAFT_REJECTION	*IL18, FYB1, B2M, HDAC9, ETS1, CTSS, TLR6, TIMP1, GALNT1, EGFR*
COMPLEMENT	*CD36, DOCK4, TIMP2, PIK3CG, FYN, CTSB, CD59, CD55, F3, LGALS3*
IL2_STAT5_SIGNALING	*MYO1E, AHNAK, EMP1, IL3RA, KLF6, PTGER2, CST7, IL10RA, ST3GAL4, ABCB1*
IL6_JAK_STAT3_SIGNALING	*CD36, ACVRL1, IL3RA, IL13RA1, CD44, CCR1, IL6ST, MYD88, IL1R1, CSF2*
INFLAMMATORY_RESPONSE	*IL18, PDE4B, SGMS2, KLF6, PTGER2, CD55, CCRL2, IL10RA, F3, MET*

To assess whether the knockdown of *IHH* impacted autocrine HH signalling, the mRNA expression of the HH target genes *GLI1*, *PTCH1* and *HHIP* were examined. No significant changes in the transcript levels of *GLI1*, *PTCH1* or *HHIP* were observed between wild-type and IHH-knockout samples (Figure 13D). However, GSEA revealed an enrichment of the hallmark HH signalling gene set in wild-type samples compared to *IHH*-knockout samples (Figure 13C), with the enrichment driven by the 7 genes *NRCAM*, *AMOT*, *NRP2*, *L1CAM*, *CELSR1*, *NF1*, and *CDK6* (Data not shown).

Given the functional redundancy among HH family members in activating the HH pathway, it is possible that the loss of IHH function could be offset by compensatory signalling from other HH ligands. To assess whether IHH knockout induces compensatory upregulation of other HH family members, the mRNA expression of *SHH* and *DHH* were evaluated. No significant changes in *SHH* or *DHH* mRNA expression were observed between wild-type and IHH-knockout samples (Figure 13E).

8.2.1.3 Discussion

Although the expression of PTCH1 receptors by colorectal carcinoma cells indicates the possibility of autocrine HH signalling, the precise role and impact of this autocrine mechanism in CRC remains inadequately characterised. In this chapter, I established an *IHH*-knockout CRC organoid model and employed RNA-sequencing to examine the transcriptomic alterations induced by the knockout of *IHH*. These transcriptomic data were subsequently analysed to elucidate the potential role of IHH in modulating CRC progression, with a particular emphasis on its possible immunomodulatory functions.

The initial phase of this chapter involved the validation of the IHH-targeting multi-guide RNA in the 2D CRC cell line SW948 (Figure 10). Traditional CRISPR knockout strategies typically employ an individual sgRNA to induce random indels at the target locus. While this approach can generate functional knockouts by inducing frameshift mutations, its efficacy is inconsistent, with frameshifts occurring in only about two-thirds of cases where indels occur. To address these limitations, we employed a multi-guide strategy that utilises three spatially coordinated sgRNAs targeting exon 1 of the *IHH* gene. By targeting the gene with multiple sgRNAs, this approach aims to induce one or more large fragment deletions within the *IHH* gene, which increases the likelihood of disrupting gene function compared to smaller, random indels. Our group has found this approach to have vastly improved knockout efficiencies in cell lines and organoids compared to alternative approaches such as plasmid transfection and lenti-CRISPR (118). Consequently, the multi-guide strategy enhances the predictability and reliability in generating a functional knockout of IHH. Notably, gene-level analysis by Sanger sequencing revealed that the multi-guide

strategy achieved an *IHH*-knockout efficiency of 100% in SW948 cells (Data not shown), highlighting the high efficacy of the *IHH*-targeting multi-guide RNA in mediating gene disruption. This high efficacy is particularly valuable for gene editing in organoids, as it circumvents the need for the time-consuming and labour-intensive step of isolating and clonally expanding individual IHH-knockout organoids to ensure uniform gene knockout.

Full confirmation of a functional knockout of IHH requires both gene-level and protein-level validation to ensure that the genetic alterations result in corresponding loss of IHH protein. However, our evaluation of the single cell-derived *IHH*-knockout clone A1 revealed challenges in validating IHH-knockout at the protein level. Gene-level validation through Sanger sequencing revealed a 55 base-pair fragment deletion in exon 1 of the *IHH* gene (Figure 10D-E). This deletion is expected to induce a frameshift in the coding sequence that would disrupt normal protein function. At the transcript level, qRT-PCR analysis revealed a marked reduction in *IHH* transcripts in A1 cells compared to wild-type SW948 cells, suggesting that the 55 base-pair deletion in the *IHH* gene impaired the stability of the transcribed mRNA (Figure 10F). However, Western blot analysis revealed no detectable differences in IHH protein levels between A1 cells and wild-type SW948 cells (Figure 10G).

The lack of an observable alterations at the protein level was unexpected given the significant changes observed at the gene and transcript level. The observation that IHH protein levels remain unchanged in A1 cells, despite the presence of a frameshift mutation induced at the gene level, is unlikely to reflect the true biological situation. A frameshift mutation occurring early in the coding sequence, in exon 1 of *IHH*, would

disrupt the downstream protein coding sequence, including the C-terminal region targeted by the anti-IHH antibody used for analysis. Therefore, the observed unchanged IHH protein levels in the Western blot are more plausibly attributed to technical artifacts, including antibody cross-reactivity with homologous proteins such as SHH, which may mask the true reduction in IHH protein levels. To further address the observed discrepancies and validate the specificity of our IHH-targeting antibody, siRNA was employed to knockdown *IHH* expression in wild-type SW948 cells. Despite successful downregulation of *IHH* mRNA levels as confirmed by qRT-PCR, Western blot analysis again failed to show a corresponding reduction in IHH protein levels (Figure 11A-B). This suggests that the antibody used may lack specificity for IHH, indicating the need for more specific antibodies or alternative protein detection strategies, such as mass spectrometry, to accurately assess IHH protein levels. Additionally, evaluating whether siRNA-mediated knockdown of *SHH* in A1 cells leads to a decrease in the immunoreactive signal could confirm whether the observed signal is attributable to cross-reactivity with SHH.

The most definitive evidence of a functional IHH knockout in A1 cells was the reduction in autocrine HH signalling. The decreased expression of *GLI1* (Figure 10H), a key transcriptional target of the HH pathway, in the A1 clone provided good evidence that the 55 base-pair deletion in the IHH gene impaired the protein's signalling function.

Following the validation of the *IHH*-targeting multi-guide RNA in SW948 cells, we successfully applied the same knockout approach to patient-derived CRC organoids, achieving an 88% knockout efficiency in the Pat-16-ID-8837 organoid line

(Figure 12D). CRC organoids offer a more physiologically relevant model compared to traditional 2D cell lines for investigating CRC, as CRC organoids form 3D structures that mimic in vivo crypt-like organisation of epithelial cells and their associated cellular interactions. Unlike 2D cell lines, which typically consist of a monolayer of homogeneous cells, CRC organoids preserve the cellular heterogeneity of the tumour, encompassing both stem cells and differentiated epithelial cell types (119, 120). Such cellular complexity is particularly important for studying the role of HH signalling in CRC, as the HH pathway has been reported to play a crucial role in regulating stem cell dynamics (see section 6.3.3.1). Although a complete knockout was not achieved in the Pat-16-ID-8837 organoid line, the 88% *IHH*-knockout efficiency was deemed sufficient to induce meaningful transcriptomic changes that may reveal potential autocrine functions of IHH in CRC, while circumventing the need for the labour-intensive and time-consuming process of isolating and clonally expanding single organoids.

In the final phase of this chapter, I employed RNA-sequencing to examine transcriptomic alterations resulting from the knockout of *IHH* in CRC organoids. PCA and hierarchal clustering indicated significant alterations in the transcriptomic profile of the CRC organoids following *IHH*-knockout (Figure 13A-B). Notably, the loss of IHH drove the upregulation of 43 genes and the downregulation of 98 genes in the CRC organoids ($p < 0.05$).

The primary mechanism of action for IHH, as described in literature, involves the activation of the canonical HH signalling pathway through interactions with its receptor PTCH1, which is expressed on the surface of various cell types, including

colorectal carcinoma cells. Consequently, we investigated whether the knockout of *IHH* affected autocrine HH signalling in the CRC organoids. The mRNA levels of three well-established transcriptional targets of the canonical HH pathway, *GLI1*, *PTCH1*, and *HHIP*, remained unchanged following *IHH*-knockout (Figure 13D), suggesting that HH signalling was not significantly perturbed. Contrary to these findings, GSEA showed that the HEDGEHOG_SIGNALING hallmark gene set was enriched in wild-type samples compared to *IHH*-knockout samples (Figure 13C). However, this enrichment was driven by genes with no direct involvement in the HH pathway (*NRCAM*, *AMOT*, *NRP2*, *L1CAM*, *CELSR1*, *NF1*, and *CDK6*). This suggests that the observed gene set enrichment may reflect broader cellular changes rather than specific alterations in HH signalling. Given the functional redundancy among HH proteins, I further examined whether the unaltered HH signalling activity could be attributed to compensatory signalling by other HH family members. However, no significant changes were observed in the transcript levels of *SHH* or *DHH* (Figure 13E), indicating that the unchanged HH pathway activity is unlikely attributed to compensatory upregulation of other HH proteins. Although, the possibility of compensatory mechanisms occurring at the protein level or through other, yet unexplored, mechanisms cannot be excluded. These findings suggest that the transcriptomic alterations resulting from *IHH*-knockout are unlikely a consequence of impaired canonical HH signalling but may instead be attributed to other non-canonical functions of IHH.

To explore the potential role of IHH in modulating CRC immunogenicity, transcriptomic alterations following *IHH*-knockout in CRC organoids were analysed by GSEA to identify potential changes in immune-related pathways. GSEA revealed an

enrichment of gene expression associated with 5 immune-related gene signatures in wild-type CRC organoids relative to *IHH*-knockout samples (Figure 13C), suggesting that the knockout of *IHH* may have shifted the immunogenic profile of the CRC organoids. Further analysis revealed that this enrichment was driven by a combination of genes with opposing roles in tumour immunogenicity (Table 4). For instance, the knockout of *IHH* resulted in a downregulation of the pro-immunogenic genes *B2M* and *IL18*, potentially contributing to decreased immunogenicity of the CRC organoids. B2M is a key component of the MHC-I molecule, crucial for presenting tumour antigens to CD8+ T cells; its downregulation may therefore facilitate immune evasion by impairing tumour recognition by the adaptive immune system (121). Concurrently, the reduction of IL-18 expression, a cytokine known to enhance the cytotoxic activity of T and NK cells, implies a diminished capacity of these immune cells to effectively target and destroy tumour cells (122). Conversely, *IHH*-knockout also led to the downregulation of immunosuppressive genes such as *LGALS3*, *CD55*, and *CD59*, potentially enhancing tumour immunogenicity. *LGALS3* encodes galectin-3, which can bind to glycoproteins on T cells to inhibit their activation and proliferation; consequently, its downregulation could impair T cell-mediated responses (123). Meanwhile, CD55 and CD59 are regulatory receptors which protect cells from complement-mediated lysis; their depletion may therefore increase the susceptibility of the CRC organoids to immune-mediated destruction via the complement system (124). Since both pro-immunogenic and immunosuppressive genes are concurrently downregulated upon the knockout of *IHH*, it is difficult to definitively determine the overall impact of *IHH*-knockout on CRC immunogenicity from transcriptomic alterations alone. Instead, further functional studies, particularly utilising in vivo CRC models, are essential to evaluate the biological significance of these transcriptomic changes and to clarify how

they may affect tumour immune responses. The lack of a clear direction regarding whether immunogenicity has increased or decreased based on the transcriptomic data could also suggest that autocrine or tumour-intrinsic pathways may not be the primary mechanism through which IHH exerts its immunosuppressive effects in CRC. Instead, its immunosuppressive effects may be mediated predominantly through paracrine signalling interactions with the TME.

While the role of SHH in the carcinogenesis and progression of CRC is well-established (see section 6.3.4.1), the role of IHH remains largely unexplored. Our GSEA results revealed that knocking out *IHH* led to a downregulation of gene expression associated with hypoxia, angiogenesis, EMT, and PI3K/AKT/mTOR signalling—key processes and implicated in tumour progression (Figure 13C). This suggests that, similar to SHH, IHH may contribute to tumour growth and metastasis in CRC through regulating these processes. However, since canonical HH signalling was unperturbed following *IHH*-knockout (Figure 13D), it is likely that these effects are mediated through non-canonical mechanisms independent of the well-characterised GLI-mediated transcriptional programme. Given that the majority of existing literature has predominantly focused on the canonical arm of HH signalling in cancer, our findings underscore the importance of expanding research efforts to explore the non-canonical arms of HH signalling. Further research into these non-canonical pathways could uncover novel therapeutic targets and offer new strategies for the treatment of CRC.

Overall, although transcriptomic analysis following *IHH*-knockout in the patient-derived CRC organoid line Pat-16-ID-8837 did not establish a clear role for autocrine

IHH signalling in regulating tumour immunogenicity, it has uncovered a potential involvement in driving tumour progression. However, it is crucial to recognise that these insights are based on a single biological replicate; thus, further validation with the knockout of *IHH* in additional CRC organoid lines are needed to substantiate these preliminary findings.

8.2.2 Paracrine Signalling to Macrophages

Macrophages are functionally versatile immune cells which constitute a key component of the TME. The functional plasticity of tumour-infiltrating macrophages, commonly known as tumour-associated macrophages (TAMs), enable them to adopt either anti-tumoural or pro-tumoural roles depending on the specific conditions within the TME. Macrophages display a range of activation states in response to different environmental cues, which are typically classified into two functionally contrasting states: classically activated (M1) and alternatively activated (M2) (Figure 14). M1 macrophages, characterised by the production of pro-inflammatory cytokines such as TNF-α, IL-12, and IFN-γ, contributes to anti-tumour immunity by enhancing cytotoxic T cell responses, presenting tumour antigens to the adaptive immune system, and generating reactive oxygen and nitrogen species that can directly induce tumour cell apoptosis. In contrast, M2 macrophages, characterised by an anti-inflammatory phenotype, secretes growth factors and anti-inflammatory cytokines that promote the formation of an immunosuppressive and pro-angiogenic TME (92). Tumours are known to exploit macrophages to foster a tumour-supportive milieu, particularly by skewing their polarisation towards the M2 phenotype (93). Consistent with the pro-tumoural role of M2 macrophages, increased infiltration of TAMs into the TME is associated with poor prognosis in CRC patients (94).

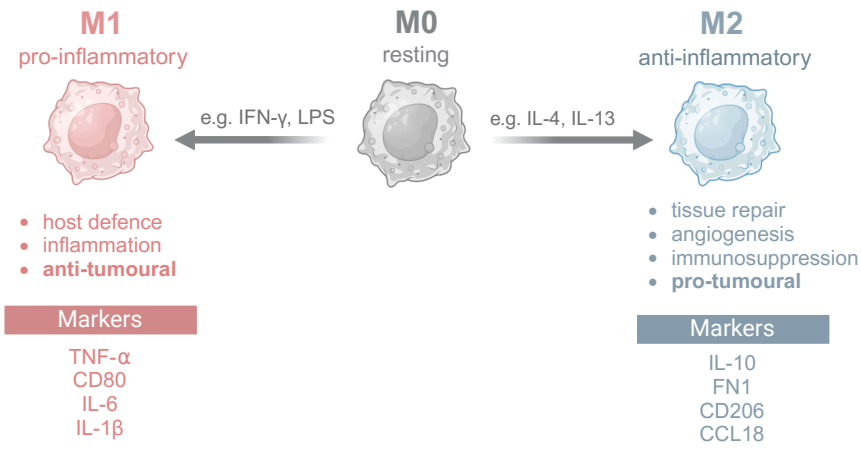

Figure 14. M1 and M2 Polarisation of Macrophages. Polarisation of macrophages to the M1 state is induced by pro-inflammatory cytokines such as IFN-γ or microbial components such as lipopolysaccharide (LPS). M1 macrophages are characterised by the upregulation of markers including *TNF, CD80, IL6, IL1B*, and exhibit pro-inflammatory and anti-tumoural properties, playing key roles in mediating inflammation and facilitating the elimination of pathogens and tumour cells. Conversely, M2 macrophage polarisation is typically induced by anti-inflammatory cytokines, including IL-4 and IL-13. M2 macrophages are characterised by the upregulation of markers such as *IL10, FN1, CD206, CCL18*, and are known for their anti-inflammatory and pro-tumoural functions, contributing to processes such as tissue repair, angiogenesis, and immunosuppression. Importantly, it should be noted that M1 and M2 states do not represent discrete phenotypes, but rather the extremities of a continuum of macrophage phenotypes.

Several murine studies have implicated the Hh signalling pathway, particularly through Shh, in promoting the polarisation of TAMs toward the immunosuppressive M2 phenotype in breast and hepatocellular cancer (95, 96, 125). However, its role in influencing TAM polarisation in CRC remains unexplored. Analysis of *Gli1* promoter activity has identified CD11b-positive cells as Hh-responsive cells in the murine colon, suggesting that colonic macrophages may also respond to stimulation by HH proteins (126). Based on these findings, I hypothesise that IHH may contribute to an immunosuppressive TME in CRC by driving macrophage polarisation towards a more immunosuppressive phenotype.

8.2.2.1 Recombinant IHH treatment Alters Expression of M1 and M2 Markers in THP-1 Macrophages

To investigate the role of IHH in regulating human macrophage function, macrophages derived from the immortalised human monocytic cell line THP-1 were employed as a model to study macrophage polarisation dynamics in response to IHH ligand stimulation. THP-1 monocytes were differentiated into resting M0 macrophages through exposure to phorbol 12-myristate 13-acetate (PMA), and were subsequently polarised to the M1 state through stimulation with IFN-γ or alternatively polarised to the M2 state via stimulation with IL-4 and IL-13 (Figure 15A). The successful polarisation of THP-1 macrophages to the M1 state was confirmed by an upregulation of the M1 markers *TNF*, *IL1B*, *CD80*, and *IL6* (Figure 15B), while successful polarisation to the M2 state was confirmed by an augmented expression of the M2 markers *IL10*, *FN1*, *CD206*, *CCL18* (Figure 15C).

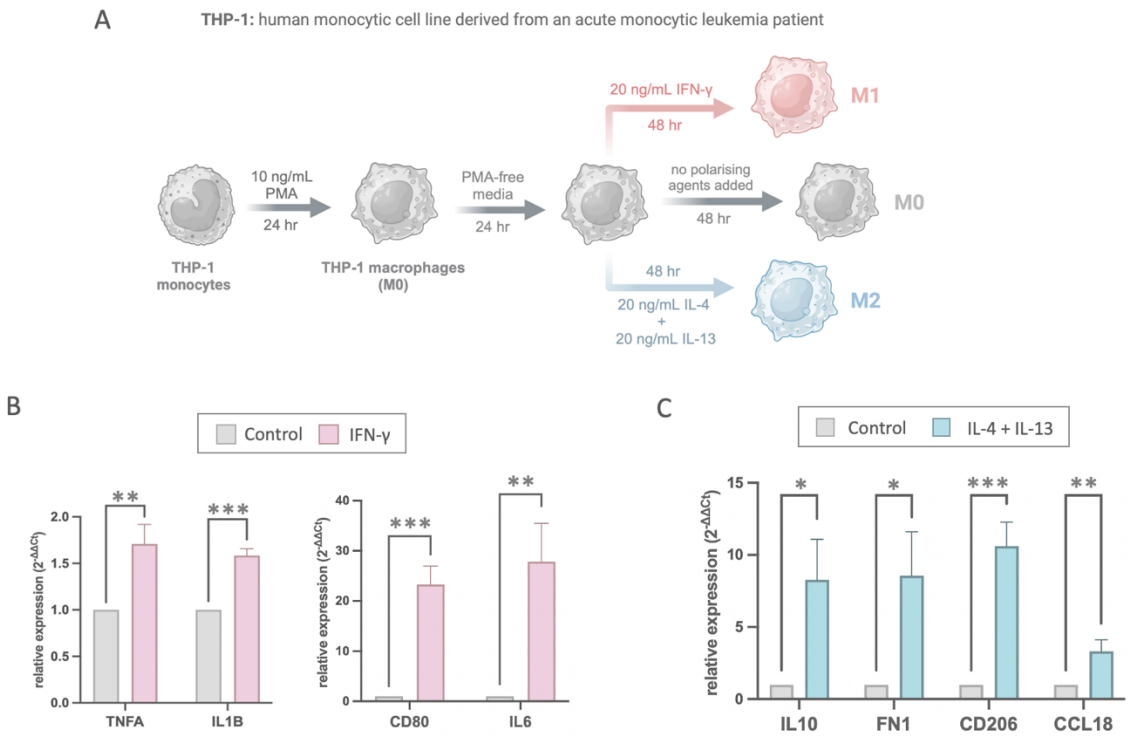

Figure 15. IFN-γ and IL-4+IL-13 Induce Polarization of THP-1 Macrophages to M1 and M2 States, Respectively. (A) Schematic workflow of the macrophage polarization assay. THP-1 monocytes were differentiated into macrophages by treatment with 10 ng/mL PMA for 24 hours, followed by a resting phase of 24 hours. THP-1 macrophages were then polarized to the M1 state by incubation with 20 ng/mL IFN-γ for 48 hours or to the M2 state by incubation with 20 ng/mL IL-4 and IL-13 for 48 hours. **(B)** qRT-PCR analysis of M1 marker expression (TNF, CD80, IL6, IL1B) in IFN-γ-treated THP-1 macrophages compared to untreated controls (n = 3). **(C)** qRT-PCR analysis of M2 marker expression (FN1, CD206, CCL18, IL10) in IL3 and IL-14-treated THP-1 macrophages compared to untreated controls (n = 3). Data for both qRT-PCR analyses are represented as mean ± SD of fold changes in expression relative to untreated controls, with statistical significance assessed using Student's t-test (*, $p < 0.05$; **, $p < 0.01$; ***, $p < 0.001$).

To investigate whether IHH influences the polarization state of THP-1 macrophages, the expression of M1 and M2 markers was evaluated following treatment of IFN-γ or IL-4 and IL-13-stimulated THP-1 macrophages with recombinant IHH. Preliminary data suggests that the addition of recombinant IHH to IFN-γ-stimulated macrophages reduced the expression of the M1 markers *TNF*, *CD80*, *IL6*,

and *IL1B* (Figure 16A). Meanwhile, treatment of IL-4 and IL-13-stimulated macrophages with recombinant IHH led to non-uniform changes in the expression of M2 markers, specifically resulting in a moderate decrease in the expression of *FN1* and *CD206*, a moderate increase in *CCL18* expression, and a marked augmentation in *IL10* expression (Figure 16B). However, given that only a single biological replicate was performed due to challenges with the commercial supply of recombinant IHH, additional replicates are needed to confirm these initial promising observations.

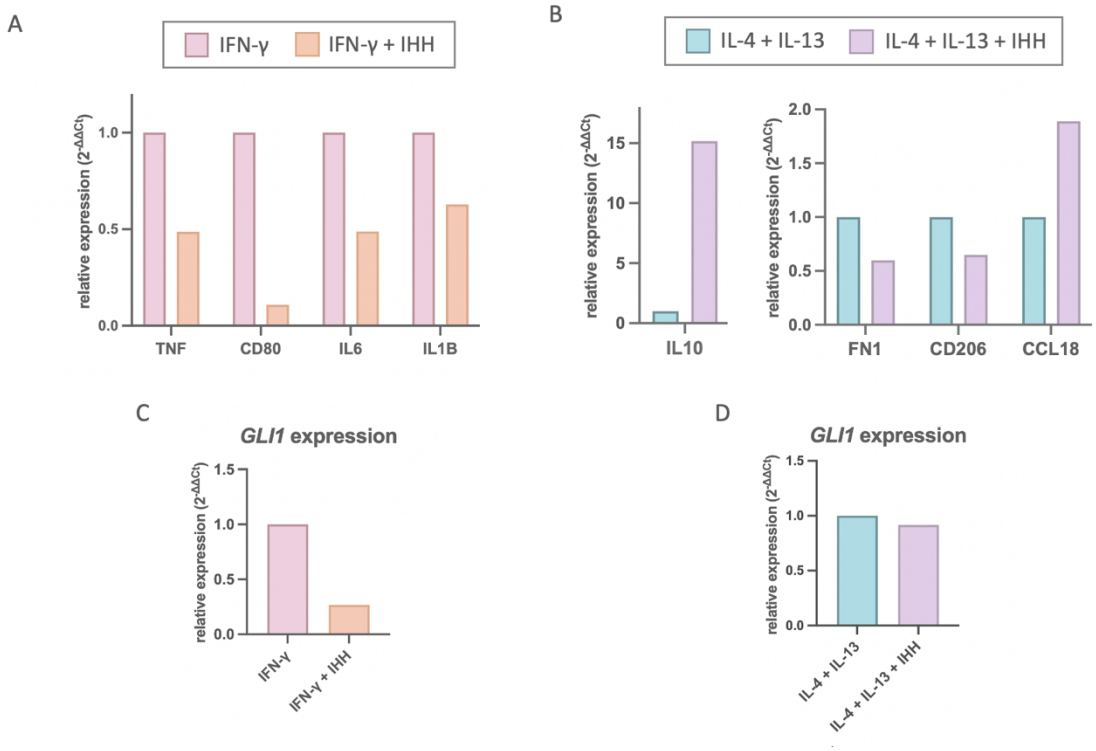

Figure 16. Recombinant IHH Alters the Expression of M1 and M2 Markers in THP-1 Macrophages Without Activating the HH Pathway. (A-B) qRT-PCR analysis of the changes in expression of **(A)** M1 markers (*TNF*, *CD80*, *IL6*, *IL1B*) in IFN-γ-stimulated THP-1 macrophages and **(B)** M2 markers (*FN1*, *CD206*, *CCL18*, *IL10*) in IL3 and IL-14-stimulated THP-1 macrophages following treatment with recombinant IHH (n = 1). **(C-D)** qRT-PCR analysis of changes in *GLI1* expression in **(C)** IFN-γ-stimulated THP-1 macrophages and **(D)** IL-3 and IL-14-stimulated THP-1 macrophages following treatment with recombinant IHH (n = 1). *Only one biological replicate was performed due to commercial supply issues with recombinant IHH.*

To further investigate whether the HH pathway was activated in THP-1 macrophages following recombinant IHH treatment, the expression of the HH pathway activation marker *GLI1* was assessed. Preliminary data suggest that in IFN-γ- or IL-13 and IL-14-stimulated macrophages, no increase in *GLI1* expression was observed upon recombinant IHH treatment (Figure 16C-D); however, additional replicates again are needed to confirm these observations.

8.2.2.2 Activation of HH Signalling in IL-4 and IL-13-stimulated THP-1 Macrophages Contributes to M2 Polarization

A. Hanna et al. previously demonstrated that IL-4 stimulation of RAW 264.7 macrophages resulted in the activation of HH signalling (95). To determine whether IL-4 and IL-13 treatment similarly activates the HH pathway in THP-1 macrophages, the expression of *GLI1*, a key transcriptional target of the HH pathway, was examined. Stimulation of THP-1 macrophages with IL-4 and IL-13 was observed to markedly increase *GLI1* expression, with a concurrent upregulation of the M2 markers *IL10*, *FN1*, *CD206* and *CCL18* (Figure 17A).

To further determine whether the activation of HH signalling in THP-1 macrophages treated with IL-4 and IL-13 contributed to M2 polarisation, the GLI inhibitor GANT61 was used to inhibit the HH pathway in these M2-polarised macrophages. GANT61 acts downstream of SMO and selectively inhibits GLI1- and GLI2-mediated transcription by impairing their DNA binding capabilities (127). GANT61 treatment reduced the expression of the HH activation marker *GLI1* and concurrently attenuated the expression of the M2 markers *IL10*, *FN1*, *CD206* and

CCL18 (Figure 17A). Interestingly, *FN1* expression was reduced by GANT61 to levels below those observed in unpolarised M0 controls (Figure 17A).

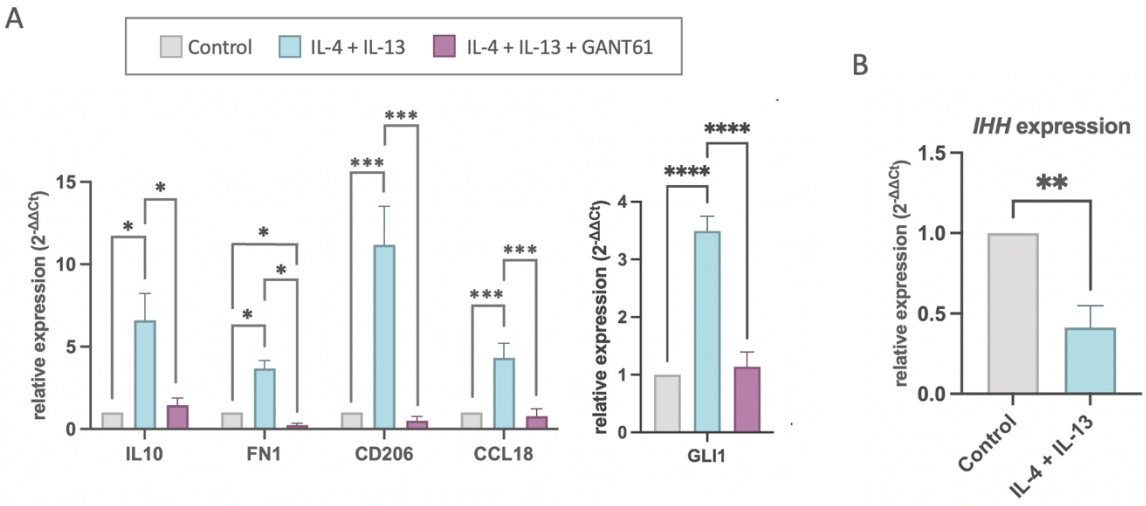

Figure 17. Activation of HH Signaling in IL-4 and IL-13-stimulated THP-1 Macrophages Contributes to M2 Polarization. (A) qRT-PCR analysis of the expression levels of M2 polarization markers (*FN1, CD206, CCL18, IL10*) and *GLI1* in THP-1 macrophages under three conditions: (i) untreated (ii) treatment with IL-4 and IL-13, and (iii) treatment with IL-4, IL-13, and GANT61 (n = 3). Data are presented as mean ± SD of fold changes in expression relative to untreated control, with statistical significance assessed by one-way ANOVA (No asterisk, $p \geq 0.05$; *, $p < 0.05$; ***, $p < 0.001$; ****, $p < 0.0001$). **(B)** qRT-PCR analysis of changes in *IHH* expression in THP-1 macrophages following stimulation with IL-4 and IL-13 (n = 3). Data are presented as mean ± SD of fold changes in expression relative to untreated control, with statistical significance assessed by Student's t-test (**, $p < 0.01$).

8.2.2.3 Activation of HH Signalling in IL-4 and IL-13-Stimulated THP-1 Macrophages Was Not Attributed to IHH Upregulation

A. Hanna et al. previously demonstrated that stimulation of murine RAW 264.7 macrophages with IL-4 led to an upregulation of *Ihh*, which was proposed to contribute to the elevated HH signalling through autocrine mechanisms (95). To assess whether the activation of HH signalling in THP-1 macrophages stimulated with IL-4 and IL-13 can be attributed to the upregulation of IHH, the expression of *IHH* was evaluated.

Contrary to expectations, *IHH* mRNA levels were downregulated in THP-1 macrophages upon stimulation with IL-4 and IL-13 (Figure 17B).

8.2.2.4 Discussion

The rising recognition of macrophages as key contributors to an immunosuppressive TME in CRC has prompted significant interest in targeting these cells to enhance anti-tumour immune responses. In this chapter, we employed THP-1 macrophages as a model to investigate the role of IHH in modulating macrophage polarisation, aiming to understand how IHH may contribute to the immunosuppressive characteristics of the TME.

Through the use of recombinant IHH, we present preliminary evidence that IHH may attenuate pro-inflammatory macrophage functions while enhancing their immunosuppressive capabilities. Specifically, recombinant IHH treatment reduced the expression of M1 markers *TNF*, *CD80*, *IL6*, and *IL1B* in THP-1 macrophages stimulated with IFN-γ, suggesting that IHH may inhibit the polarisation of macrophages toward the pro-inflammatory and anti-tumoural M1 phenotype (Figure 16A). Notably, the most substantial reduction was observed in CD80 expression, a co-stimulatory molecule critical for T cell activation (128). This suggests that IHH may indirectly suppress T cell activity through inhibiting CD80 expression on TAMs.

Conversely, in macrophages stimulated with IL-4 and IL-13, recombinant IHH treatment substantially potentiated the expression of the M2 marker *IL10*, moderately increased the expression of the M2 marker *CCL18*, and moderately decreased the expression of the M1 markers *FN1* and *CD206* (Figure 16B). While FN1 and CD206

are associated with the tissue-repairing functions of M2 macrophages by facilitating extracellular matrix remodelling and phagocytosis, respectively, IL-10 and CCL18 are linked to their immunosuppressive roles (129-132). Specifically, IL-10 is an immunosuppressive cytokine which suppresses tumour immune responses primarily by inhibiting the production of pro-inflammatory cytokines and antigen presentation by dendritic cells and macrophages (132). Meanwhile, the chemokine CCL18 has been implicated in the recruitment of immunosuppressive Tregs to the TME (131). Consequently, these findings suggest that IHH may shift M2 macrophages towards a phenotype with diminished tissue-repair functions and an enhanced immunosuppressive capacity, potentially enhancing tumour immune evasion. These findings are consistent with our hypothesis that IHH may contribute to immunosuppression in CRC by driving macrophage polarisation towards a more immunosuppressive phenotype. The functional consequences of these transcriptional changes in macrophage M1 and M2 markers on T cell responses will need to be further assessed using T cell activation and cytotoxicity assays. However, it is crucial to note that these observations are derived from a single biological replicate, therefore additional experiments are needed to confirm these preliminary findings.

Interestingly, preliminary data suggested that recombinant IHH treatment did not increase HH pathway activity in THP-1 macrophages (Figure 16C-D), indicating that its effects on macrophage polarisation may be independent of canonical HH signalling. The observation that canonical HH signalling was not increased in THP-1 cells following recombinant IHH treatment aligns with the fact that macrophages lack primary cilia, which are structures essential for activating the HH pathway in response to HH ligands in vertebrates (59). However, this observation contrasts with earlier

studies demonstrating that recombinant SHH can still activate the HH pathway in murine RAW 264.7 macrophages, as evidenced by elevated *Gli1* expression (95). This discrepancy may be attributed to differences in the biological activity of IHH versus SHH, variations in receptor expression or downstream signalling mechanisms between human THP-1 macrophages and murine RAW 264.7 macrophages. Thus, further research is needed to clarify the mechanisms through which HH ligands exert their effects on human macrophages. Moreover, although both SHH and IHH engage the common receptor PTCH1, it remains uncertain whether they exhibit distinct biological activities. Therefore, exploring the potential for differential downstream signalling cascades and cellular effects initiated by each ligand may provide deeper insights into their respective roles in CRC.

In this chapter, I provided further evidence for an involvement of the HH pathway in promoting M2 polarisation of THP-1 macrophages. Stimulation with IL-3 and IL-14 led to elevated HH pathway activity in THP-1 cells, as indicated by increased *GLI1* expression (Figure 17A). Importantly, inhibiting HH signalling with the GLI inhibitor GANT61 resulted in reduced expression of the M2 markers *IL10*, *FN1*, *CD206*, and *CCL18* in IL-3 and IL-14 stimulated macrophages (Figure 17A), suggesting that the HH pathways play a role in driving M2 macrophage polarisation downstream of IL-4 and IL-13. This observation is consistent with a previous report by A. Hanna et al., which noted that inhibiting HH signalling similarly impaired M2 polarisation in IL-4-stimulated murine RAW 264.7 macrophages. The study also detailed an upregulation of *Ihh* in these macrophages upon IL-4 stimulation, which may contribute to the elevated HH signalling through autocrine mechanisms (95). Contrary to these findings, I found that *IHH* was downregulated in THP-1 macrophages

stimulated with IL-4 and IL-13 (Figure 17B), suggesting that the activation of HH signalling in these macrophages was not attributed to the upregulation of *Ihh*. Although, potential upregulation of other members of the HH family cannot be excluded. Consequently, further experiments using HH-neutralising antibodies are required to clarify whether the activation of HH signalling in THP-1 macrophages downstream of IL-4 and IL-13 stimulation occurs through the upregulation of HH ligands or alternatively through cell-intrinsic mechanisms.

While THP-1 macrophages offer valuable insights into the role of IHH and the HH pathway in modulating macrophage polarization and function, further experiments involving primary macrophages from CRC patients, including primary monocyte-derived macrophages and intestinal resident macrophages, can help confirm the relevance of our observations to CRC. HH signalling has been proposed to drive M2-polarisation of macrophages through distinct mechanisms, all of which involves the modulation of STAT6, a key transcription factor involved in the transcription of M2-associated genes. One proposed mechanism by J. Petty et al. indicates that HH signalling transcriptionally upregulates *Klf4*, a co-transcriptional activator that enhances STAT6-driven gene expression, thereby promoting M2 polarization (96). In contrast, A. Hanna et al. suggest that the HH pathway transcriptionally upregulates *Il4* and its receptor *Il4ra*, creating a feed-forward loop that amplifies STAT6 phosphorylation and activation (95). Additionally, D. Hinshaw et al. proposes that HH signalling potentiates O-GlcNAc modification of STAT6, enhancing its transcriptional activity and thus contributing to M2 macrophage polarisation (125). While these studies provide valuable insights, it is important to note that they were all conducted in murine macrophages, highlighting the necessity of further research to ascertain

whether these mechanisms are conserved in human macrophages. Further experiments involving non-biased approaches, such as ChIP-seq and RNA-seq, may provide a fuller picture of the mechanisms by which the HH pathway promotes M2 polarization in THP-1 macrophages stimulated with IL-4 and IL-13. ChIP-seq can delineate the binding sites of GLI transcription factors, revealing direct targets of the HH pathway. In parallel, RNA-seq can validate the upregulation of these HH targets and unveil potential downstream effects on the broader transcriptome. This complementary approach may offer a more comprehensive understanding of how the HH pathway orchestrates M2 macrophage polarization, which may reveal novel targets for the re-polarisation of TAMs from the immunosuppressive M2 phenotype towards the anti-tumoral M1 phenotype.

It is important to note that, although IL-4 and IL-13 were employed in this study to induce M2 polarisation in THP-1 macrophages, these cytokines are not the primary mediators of M2 polarisation in TAMs. In the TME, TAM polarisation is driven predominantly by IL-6, adenosines, and Toll-like receptor (TLR) agonists. With our increasing understanding of macrophage biology, M2 macrophages have been further subdivided into four subtypes (M2a, M2b, M2c, and M2d) based on their distinct gene expression profiles and specialised functions (Table 5). While IL-4 and IL-13 promotes macrophage polarisation to the M2a subtype, typically associated with wound healing and tissue repair, tumour-derived factors including IL-6 typically drive polarisation towards the M2d subtype, which is linked to pro-tumourigenic functions, including immunosuppression and angiogenesis (133, 134). Therefore, IL-4 and IL-13-stimulated macrophages may not accurately recapitulate the phenotypic and functional characteristics of TAMs. Future experiments should employ tumour-derived

factors, such as IL-6 or conditioned media from CRC cell lines, to induce M2 polarisation, thereby providing a more accurate model of TAMs and their functional dynamics within the TME.

Table 5. Four M2 Macrophage Subtypes: M2a, M2b, M2c and M2d.

M2 Subtypes	Induced by	Cell surface markers	Secreted Factors	Primary Roles	References
M2a	IL-4, IL-13	CD206, CD209, Dectin-1	IL-10, TGF-β, CCL17, CCL18, CCL22, IL-1Ra	Defense against parasites, wound healing, allergic responses	(133-135)
M2b	Immune complexes, IL-1β, TLR agonists	CD80, CD86, MHC-II	IL-10, TNF-α, IL-1β, IL-6, IL-4, CCL1, IL-1	Immunoregulation (production of both pro- and anti-inflammatory cytokines)	
M2c	glucocorticoids, IL-10, TGF-β	CD163, MerTK, CD14, CD86, CD16, CD206, TLR-1, TLR-8	IL-10, TGF-β, CCL16, CCL18, CXCL13	Resolution of inflammation, clearance of apoptotic cells (efferocytosis)	
M2d	IL-6, TLR agonists, adenosines	CD163, CD14, CD86	IL-10, VEGF, TGF-β, CCL18, MMP-9	Angiogenesis, ECM remodelling, immunosuppression, promoting tumour progression	

Abbreviations: CCL (C-C Motif Chemokine Ligand); ECM (Extracellular Matrix); IL (Interleukin); MMP (Matrix metalloproteinase); TGF-β (Transforming Growth Factor Beta); TLR (Toll-Like Receptor); TNF-α (Tumour Necrosis Factor Alpha); VEGF (Vascular Endothelial Growth Factor).

Overall, my investigation highlights a role for IHH and the HH pathway in regulating macrophage polarisation, with important implications for CRC immunotherapy. The preliminary evidence presented indicates that IHH can attenuate the pro-inflammatory M1 phenotype while promoting an immunosuppressive M2 phenotype, potentially enhancing tumour immune evasion. Furthermore, the observation that these effects may operate independently of canonical HH signalling underscores the necessity for further exploration of the non-canonical mechanisms

underlying IHH's influence on macrophage behaviour. A deeper understanding of these mechanisms could unveil novel therapeutic targets for reprogramming TAMs, ultimately enhancing the efficacy of immunotherapies in CRC patients.

8.2.3 Paracrine Signalling to Fibroblasts

Given that *PTCH1* is predominantly expressed by the stromal compartment in CRC (Figure 9 on page 62), this suggests that HH signalling primarily functions in a paracrine manner, where HH ligands secreted by colorectal carcinoma cells activate signalling in adjacent stromal cells. Cancer-associated fibroblasts (CAFs), the most abundant stromal cell type in CRC, represents a major source of immunosuppressive factors that support tumour immune evasion (136-138). Based on these observations, I hypothesise that IHH secreted by colorectal carcinoma cells may contribute to an immunosuppressive TME by regulating the expression of CAF-derived factors.

8.2.3.1 Recombinant IHH Treatment Downregulated CCL4, CCL5, CXCL10 and CXCL11 expression in Primary Human Colonic Fibroblasts

To examine whether IHH may induce an immunosuppressive TME in CRC by regulating CAFs, primary human colonic fibroblasts were treated with recombinant IHH, and changes in the expression of 84 immune-related genes were assessed. Using qRT-PCR, a significant reduction (fold-regulation > |1.5|, $p < 0.05$) in the expression of the cytokines *CCL4*, *CCL5*, *CXCL10* and *CXCL11* was observed in IHH-treated fibroblasts compared to untreated controls (Figure 18B-D). Furthermore, activation of the HH pathway in IHH-treated fibroblasts was confirmed by the upregulation of *GLI1* expression in IHH-treated fibroblasts compared to untreated controls (Figure 18A).

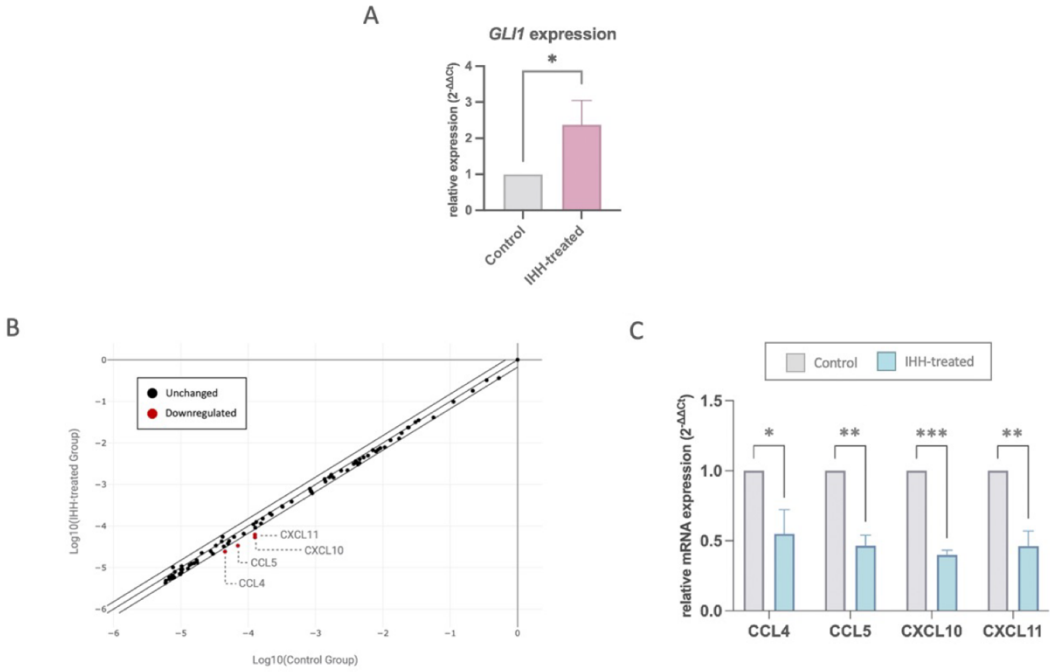

Figure 18. Recombinant IHH (3 µg/mL) Treatment Downregulates *CCL4*, *CCL5*, *CXCL10*, and *CXCL11* Expression in Primary Human Colonic Fibroblasts. (A) qRT-PCR analysis of changes in *GLI1* expression in fibroblasts following treatment with recombinant IHH (n = 3). Data are presented as mean ± SD of fold changes in expression relative to untreated controls, with statistical significance assessed via Student's t-test (*, $p < 0.05$). **(B-C)** qRT-PCR analysis of the changes in the expression of 84 immune-related genes in fibroblasts following IHH treatment (n = 3). **(B)** Scatter plot depicting changes in the expression of 84 immune-related genes in fibroblasts following treatment with recombinant IHH (n = 3). Each point represents an individual gene, with red dots representing genes that are downregulated by more than 1.5-fold regulation. Dotted lines denote the ±1.5-fold regulation threshold, used to define significant changes in gene expression relative to untreated control. **(C)** Bar plots comparing the expression of chemokines *CCL4*, *CCL5*, *CXCL10*, and *CXCL11* between IHH-treated fibroblasts and untreated controls (n = 3). Data are shown as mean ± SD of fold changes in expression relative to untreated controls, with statistical significance assessed using Student's t-test (*, $p < 0.05$; **, $p < 0.01$; ***, $p < 0.001$).

8.2.3.2 Discussion

Growing evidence suggests a pivotal role for CAFs in fostering an immunosuppressive TME, particularly through the secretion of immunomodulatory factors such as cytokines and chemokines (136-138). Although it is well-established

that cancers modulate CAFs to promote a TME conducive to tumour progression, the precise mechanisms by which tumours regulate CAF behaviour remains incompletely understood. In this chapter, I hypothesised that IHH, secreted by colorectal tumours, may regulate adjacent fibroblasts to promote an immunosuppressive TME.

Using qRT-PCR, I analysed transcriptomic changes in 84 immune-related genes following treatment of primary human colonic fibroblasts with recombinant IHH. My results indicate that treatment with recombinant IHH led to a notable decrease in the expression of the chemokines *CCL4*, *CCL5*, *CXCL10*, and *CXCL11* in IHH-treated fibroblasts (Figure 18B-D). The most prominently downregulated chemokines, CXCL10 and CXCL11, are potent chemoattractants for CXCR3-positive immune cells, and their expression in CRC is associated with enhanced intratumoural CD8+ T cell infiltration and improved prognosis in patients (139-142). Similarly, the expression of CCL4 and CCL5, which recruits CCR1+ and CCR5+ immune cells, are also positively correlated with the infiltration of CD8+ T cells in cancer (140, 143). These findings suggest that IHH may inhibit the recruitment of CTLs to the TME by suppressing the expression of these chemokines in CAFs. However, further T cell migration assays will be necessary to validate whether these transcriptomic changes truly impair T cell recruitment.

While CXCL10 and CXCL11 have consistently been linked to CD8+ T cell infiltration and a favourable prognosis in CRC, the role of CCL4 and CCL5 in modulating tumour immune responses appears to be more complex. Specifically, while CCL4 and CCL5 can recruit CTLs to the TME, they have also been shown to attract immunosuppressive Tregs and TAMs (115, 144-146). The nuanced roles of

CCL4 and CCL5 in tumour immunity highlights the complexity of the TME and suggest that more sophisticated models of CRC, particularly in vivo systems, are essential for understanding how IHH signalling in CAFs shapes the immune landscape in CRC.

Interestingly, the chemokines *CCL4*, *CCL5*, *CXCL10*, and *CXCL11*, were previously identified among the leading-edge genes driving the enrichment of immune-related gene sets in TCGA colon adenocarcinoma samples with low *IHH* expression (see Table 3 on page 61). This finding supports the hypothesis that paracrine signalling to CAFs is a critical mechanism through which IHH mediates its immunosuppressive effects in CRC, potentially by impairing CTL recruitment.

The activation of the canonical HH signalling pathway in IHH-treated fibroblasts was confirmed through the observed upregulation of the HH target gene *GLI1* (Figure 18A). This finding suggests that the transcriptional changes in *CCL4*, *CCL5*, *CXCL10*, and *CXCL11* may be, at least in part, mediated through the canonical HH pathway. However, further experiments involving the inhibition of this pathway using the GLI inhibitor GANT61 will be necessary to validate whether these transcriptional changes occur downstream of the canonical GLI-mediated transcriptional programme, or alternatively through a non-canonical pathway. Moreover, it is important to note that treatment with 3 µg/mL of recombinant IHH for 24 hours resulted in only a modest upregulation of *GLI1* expression in fibroblasts. This suggests that further optimization of both the concentration and duration of IHH treatment is warranted to achieve more substantial effects, potentially revealing additional insights into the mechanisms by which IHH influences CAF behaviour and the TME. Furthermore, it is important to acknowledge that only a small number of immune-related genes were assessed using

our qPCR array; therefore, expanding our analysis to include a broader range of immune-related genes may also reveal additional mechanisms by which IHH influences CRC immunogenicity.

In summary, my findings elucidate the role of IHH in modulating fibroblast behaviour and highlight its potential contribution to an immunosuppressive TME in CRC. The observed downregulation of key chemokines *CCL4*, *CCL5*, *CXCL10*, and *CXCL11* in IHH-treated fibroblasts indicate that paracrine IHH signalling to CAFs may impede the recruitment of CTLs to the tumour site. Given that the lack of T cell infiltration is a significant barrier to the efficacy of ICIs in CRC, our findings suggest that targeting IHH signalling in CAFs may represent a promising therapeutic strategy to enhance T cell infiltration and improve ICI efficacy.

9 Concluding Remarks

The present thesis provides a preliminary understanding of the role of IHH in regulating CRC immunogenicity, elucidating several mechanisms by which IHH may contribute to an immunosuppressive TME. Specifically, my results indicate that IHH primarily exerts its immunomodulatory effects through paracrine signalling mechanisms to the surrounding TME. This paracrine interaction with surrounding fibroblasts and macrophages appears to suppress CTL recruitment by downregulating key chemokines in CAFs, while skewing TAM polarization towards a more immunosuppressive, less pro-inflammatory phenotype, thereby facilitating immune evasion in CRC. Although a definitive role for autocrine IHH signalling in regulating CRC immunogenicity was not established, our findings point to a potential involvement of this autocrine mechanism in driving tumour progression through other pathways, such as EMT and angiogenesis.

Notably, we observed that IHH may exert many of its effects through non-canonical GLI-independent pathways. Accumulating evidence underscores the significance of non-canonical mechanisms activated by HH ligands, illustrating their capacity to influence a variety of cellular processes, including cell survival, proliferation, and migration. For instance, HH ligands have been demonstrated to promote angiogenesis by regulating RhoA activity in endothelial cells, promoting cell survival and facilitating actin cytoskeletal rearrangements that drive cell migration (147). Additionally, binding of SHH to PTCH1 has been reported to facilitate cell cycle progression by disrupting PTCH1-CYCLINB1 interactions (148). Moreover, there is growing evidence of crosstalk between the HH pathway and several other signalling cascades, such as the Wnt, Notch, and TGF-β pathways (149-151). This growing

recognition of non-canonical HH signalling mechanisms suggest that the functional repertoire of IHH is broader than previously recognised, potentially implicating non-canonical mechanisms as critical mediators of its role in CRC. Therefore, further research into the non-canonical mechanisms through which IHH exerts its effects is essential to fully elucidate the role of IHH in CRC and to identify potential therapeutic targets that could more effectively disrupt its influence on tumour progression and the immunosuppressive TME.

In light of these findings, IHH signalling emerges as a compelling therapeutic target in CRC, particularly given its potential involvement in fostering an immunosuppressive TME and in driving tumour progression. Targeting IHH signalling offers a novel strategy to reprogram the immunosuppressive TME in CRC, potentially enhancing anti-tumour immune responses. Furthermore, the broader implications of IHH's non-canonical effects suggest that therapeutic interventions should not solely focus on blocking canonical GLI-dependent HH signalling but also investigate inhibitors that target alternative pathways through which IHH exerts its influence. Such an approach could complement existing immunotherapies by addressing IHH-driven resistance mechanisms, potentially improving treatment outcomes for CRC patients.

While this thesis provides valuable insights into the role of IHH in CRC, it is important to acknowledge its preliminary nature. Although not exhaustive, these findings represent a promising starting point for understanding the complex mechanisms through which IHH influences tumour progression and immunogenicity. Further research involving additional experimental validation of these preliminary findings, along with broader investigations across different CRC models, will be crucial

to fully elucidate the role of IHH in CRC and to assess its potential as a therapeutic target. Given that the current findings detailed in this thesis are derived exclusively from in vitro experiments, which inherently lack the complexity and dynamic interactions present in a living organism, future studies should incorporate in vivo models to better simulate the complex interactions between the tumour and its surrounding TME. This continued exploration may pave the way for novel strategies to enhance treatment outcomes for CRC patients.

10 Appendix

Table 6. Gene Mutations Revealed by Whole Exome Sequencing of Patient-Derived Orgnaoid Line Pat-16-ID-8837. The softwares SIFT and PolyPhen were used to predict the functional impact of gene mutations.

Chromosome	Gene	Consequence	SIFT	PolyPhen	Variant Allele Frequency
chr2	ABCA12	missense_variant	deleterious(0.01)	possibly_damaging(0.726)	45.95
chr7	ABCB5	missense_variant&splice_region_variant	deleterious(0.04)	probably_damaging(0.944)	45.8
chr6	ABCF1	missense_variant	deleterious(0)	probably_damaging(0.994)	41.92
chr3	ACAD11	missense_variant	deleterious(0)	probably_damaging(1)	40.56
chr3	ACTL6A	missense_variant	deleterious(0)	probably_damaging(1)	52.38
chr2	ACTR3	stop_gained	NA	NA	51.57
chr10	ADAMTS14	missense_variant	tolerated(0.32)	benign(0)	51.74
chr15	ADAMTS17	missense_variant	tolerated(0.06)	possibly_damaging(0.877)	48.31
chr19	ADGRE2	splice_polypyrimidine_tract_variant&intron_variant	NA	NA	51.52
chr3	ADIPOQ	missense_variant	deleterious(0)	probably_damaging(1)	51.7
chr7	AGAP3	missense_variant	deleterious(0.04)	probably_damaging(0.964)	25
chr7	AGAP3	missense_variant	deleterious(0)	probably_damaging(0.998)	22.86
chr10	AGAP4	missense_variant	tolerated(0.06)	benign(0.003)	40.13
chr10	AGAP4	missense_variant	deleterious(0.05)	possibly_damaging(0.697)	11.69
chrX	AGTR2	missense_variant	tolerated(0.2)	possibly_damaging(0.838)	49.77
chr11	AHNAK	frameshift_variant	NA	NA	25.52
chr11	AHNAK	frameshift_variant	NA	NA	24.73
chr14	AHNAK2	missense_variant	tolerated(0.09)	possibly_damaging(0.774)	49.09
chr1	AK2	missense_variant	deleterious(0)	probably_damaging(0.931)	7.55
chr14	AK7	splice_donor_variant	NA	NA	50.89
chr6	ALDH5A1	missense_variant	deleterious(0.02)	probably_damaging(0.983)	49.46
chr3	ALG1L2	missense_variant	tolerated(0.16)	possibly_damaging(0.751)	40.22
chr2	ALK	missense_variant	deleterious(0)	probably_damaging(1)	40.91
chr2	ALMS1	inframe_deletion	NA	NA	100
chrX	AMER1	missense_variant	deleterious(0.02)	benign(0.029)	45.1
chr18	ANKRD30B	missense_variant	tolerated(0.13)	benign(0.159)	26.87
chr12	ANKRD33	missense_variant	tolerated(0.61)	benign(0.303)	55.25
chr1	ANKRD35	missense_variant	tolerated(0.5)	benign(0.279)	48.6
chr12	ANKS1B	frameshift_variant	NA	NA	51.21
chr9	ANKS6	missense_variant	tolerated(0.22)	benign(0.003)	42.23
chr10	ANXA8	missense_variant	tolerated(0.46)	benign(0.025)	100
chr17	AOC3	missense_variant	tolerated(1)	benign(0.003)	67.91
chr14	AP5M1	missense_variant	tolerated(0.62)	benign(0.003)	54.47
chr5	APC	splice_acceptor_variant	NA	NA	53.42
chr22	APOL4	frameshift_variant	NA	NA	100
chrX	AR	inframe_insertion	NA	NA	92.31
chr4	ARFIP1	frameshift_variant	NA	NA	41.54

chr2	ARHGAP15	missense_variant	deleterious(0)	probably_damaging(0.999)	51.7
chr10	ARHGAP22	missense_variant	deleterious(0)	probably_damaging(1)	41.98
chr7	ARHGEF5	stop_gained&frameshift_variant	NA	NA	9.39
chr6	ARID1B	missense_variant	deleterious_low_confidence(0)	probably_damaging(0.939)	50
chr10	ASCC1	missense_variant	deleterious(0.02)	possibly_damaging(0.857)	42.86
chr12	ASCL4	missense_variant	deleterious(0)	possibly_damaging(0.87)	52.03
chr17	ATAD5	missense_variant	tolerated(0.73)	benign(0)	68.08
chr14	ATG2B	missense_variant	deleterious(0.02)	probably_damaging(0.995)	51.59
chr12	ATN1	inframe_deletion	NA	NA	44.08
chr15	ATP10A	missense_variant	deleterious(0)	possibly_damaging(0.886)	53.04
chr15	ATP10A	missense_variant	tolerated(0.76)	benign(0.059)	48.36
chr1	ATP1A4	missense_variant	tolerated(0.11)	benign(0.027)	38.78
chr15	BAHD1	missense_variant	tolerated(0.11)	probably_damaging(0.991)	48.59
chr16	BAIAP3	missense_variant	tolerated(0.13)	possibly_damaging(0.759)	98.94
chr2	BAZ2B	missense_variant	deleterious(0)	probably_damaging(1)	36.88
chr17	BECN1	missense_variant&splice_region_variant	deleterious(0.02)	possibly_damaging(0.447)	29.69
chrX	BHLHB9	missense_variant	deleterious(0)	benign(0.083)	56.94
chr2	BIRC6	splice_region_variant&splice_polypyrimidine_tract_variant&intron_variant	NA	NA	50.47
chrX	BMX	missense_variant	deleterious(0)	benign(0.32)	56.68
chr17	BPTF	missense_variant	tolerated(0.26)	benign(0.027)	36.07
chr17	BPTF	inframe_insertion	NA	NA	25.31
chr19	BRME1	frameshift_variant	NA	NA	50.62
chr6	BTN3A3	missense_variant	tolerated(0.1)	probably_damaging(0.952)	44.39
chr13	C13orf46	splice_donor_variant	NA	NA	100
chr2	CALCRL	frameshift_variant	NA	NA	42.96
chr14	CARMIL3	missense_variant	tolerated(0.43)	probably_damaging(0.922)	56.31
chr3	CASR	missense_variant	deleterious(0)	probably_damaging(1)	46.43
chr9	CBWD5	missense_variant	deleterious(0.01)	benign(0.102)	52.94
chr10	CC2D2B	missense_variant	tolerated(0.05)	benign(0.249)	50
chr3	CCDC13	missense_variant	deleterious(0.03)	benign(0.147)	42.8
chr9	CCDC171	missense_variant	deleterious(0)	probably_damaging(0.995)	52.73
chr14	CCDC177	missense_variant	tolerated(0.11)	possibly_damaging(0.497)	47.62
chr3	CCDC39	missense_variant	tolerated(0.34)	benign(0.104)	51.55
chr2	CCDC88A	missense_variant	deleterious(0.01)	benign(0.14)	35.81
chr6	CD24	missense_variant	tolerated(0.08)	benign(0.009)	100
chr20	CD40	missense_variant	deleterious(0)	possibly_damaging(0.722)	20.75
chr20	CD93	frameshift_variant	NA	NA	36.89
chr20	CDC25B	missense_variant	tolerated(0.58)	benign(0)	98.11
chr16	CDH1	missense_variant&splice_region_variant	deleterious(0.01)	probably_damaging(0.986)	54.94
chr5	CDH6	missense_variant	deleterious(0)	probably_damaging(0.998)	48.67
chr19	CEP89	stop_gained	NA	NA	11.61
chr7	CFAP69	missense_variant	tolerated(0.51)	probably_damaging(0.996)	44.3
chr8	CHCHD7	missense_variant	deleterious(0)	probably_damaging(0.998)	10.59
chr15	CHRNA5	missense_variant	deleterious(0.01)	probably_damaging(1)	56.91

chrX	CLCN5	missense_variant	deleterious(0.01)	possibly_damaging(0.879)	52.04
chr4	CLOCK	missense_variant	tolerated(0.26)	benign(0.028)	50.6
chr1	CNKSR1	stop_gained	NA	NA	37.59
chr16	CNOT1	stop_gained	NA	NA	47.3
chr4	CRACD	missense_variant	tolerated(1)	benign(0.173)	43.8
chrX	CRLF2	missense_variant	tolerated(0.06)	probably_damaging(0.985)	46.61
chr1	CROCC	missense_variant	tolerated(0.37)	possibly_damaging(0.859)	33.33
chr8	CSMD1	missense_variant	tolerated(0.24)	benign(0.117)	100
chr14	CTSG	missense_variant	deleterious(0.02)	probably_damaging(0.912)	47.79
chr11	CYB5R2	splice_donor_region_variant&intron_variant	NA	NA	48.31
chr1	CYP4B1	missense_variant	deleterious(0)	probably_damaging(0.927)	41.41
chr8	CYRIB	missense_variant	deleterious(0)	probably_damaging(0.956)	68.65
chr13	DACH1	inframe_deletion	NA	NA	74.31
chrX	DCAF8L1	missense_variant	tolerated(0.14)	benign(0.003)	47.42
chr4	DCLK2	missense_variant&splice_region_variant	deleterious(0)	probably_damaging(1)	37.16
chr10	DDX21	missense_variant	tolerated_low_confidence(0.19)	benign(0.051)	50
chr14	DHRS4	missense_variant	tolerated(0.12)	benign(0.075)	52.17
chr17	DNAH17	missense_variant	deleterious(0.02)	probably_damaging(0.999)	35.77
chr17	DNAH17	missense_variant	tolerated(0.11)	benign(0.24)	65.5
chr17	DNAH17	missense_variant	tolerated(0.29)	benign(0.131)	31.76
chr2	DNAH7	missense_variant&splice_region_variant	deleterious(0.04)	possibly_damaging(0.776)	46.75
chr3	DOCK3	missense_variant	deleterious(0.02)	possibly_damaging(0.836)	51.43
chr14	DPF3	missense_variant	deleterious(0.05)	benign(0.023)	45.92
chr8	DPYS	missense_variant	tolerated(0.4)	benign(0)	29.81
chr11	DRD4	inframe_insertion	NA	NA	90.24
chr11	DTX4	missense_variant	deleterious(0)	probably_damaging(0.999)	41.04
chr11	DYNC2H1	frameshift_variant	NA	NA	62.35
chr16	E2F4	missense_variant	deleterious(0.01)	probably_damaging(0.999)	44.44
chr5	EBF1	missense_variant	deleterious_low_confidence(0)	benign(0.284)	53.54
chr7	EEPD1	missense_variant	deleterious(0.01)	benign(0.217)	50.47
chr2	EFEMP1	missense_variant	tolerated(0.09)	benign(0.011)	46.55
chr7	ELAPOR2	missense_variant	tolerated(1)	benign(0.001)	42.65
chr5	EMB	missense_variant	tolerated(0.79)	benign(0.031)	50.39
chr14	EML5	missense_variant	deleterious(0.03)	benign(0.127)	67.03
chr16	ENKD1	stop_gained	NA	NA	38.64
chr7	EPHB6	inframe_deletion	NA	NA	96.41
chr13	EPSTI1	frameshift_variant	NA	NA	27.8
chrX	ERCC6L	missense_variant	deleterious(0)	probably_damaging(1)	47.37
chr2	ETAA1	missense_variant	deleterious(0)	probably_damaging(0.999)	50.26
chr8	FAM110B	missense_variant	tolerated(0.9)	benign(0.012)	66.45
chr17	FAM171A2	missense_variant	deleterious(0.04)	benign(0.04)	66.87
chr12	FAM186B	missense_variant	tolerated(0.28)	benign(0.007)	46.07
chr1	FAM189B	missense_variant	tolerated(0.49)	possibly_damaging(0.837)	47.78
chr9	FAM205A	missense_variant	deleterious(0.01)	possibly_damaging(0.878)	56.25
chr10	FAM25G	missense_variant	deleterious_low_confidence(0.01)	benign(0.039)	32.73
chrX	FAM47B	missense_variant	deleterious(0.03)	benign(0.108)	39.73
chr2	FASTKD2	missense_variant	deleterious(0.02)	benign(0)	46

chr11	FAT3	missense_variant	deleterious(0.05)	possibly_damaging(0.648)	47.77
chr5	FBN2	missense_variant	deleterious(0)	possibly_damaging(0.847)	45.99
chr5	FBN2	missense_variant	deleterious(0.02)	probably_damaging(0.981)	44.26
chr5	FBXL7	missense_variant	deleterious(0)	probably_damaging(0.995)	47.14
chr17	FBXO47	missense_variant	tolerated(0.15)	benign(0.001)	11.36
chr1	FCRLB	missense_variant	tolerated(0.45)	benign(0.165)	41.7
chr3	FGD5	missense_variant	tolerated(0.07)	benign(0.215)	32.88
chr10	FHIP2A	missense_variant	deleterious(0.02)	possibly_damaging(0.85)	50.37
chr14	FKBP3	missense_variant	tolerated(0.11)	benign(0)	42.72
chr17	FLCN	missense_variant	deleterious(0)	probably_damaging(0.961)	96.95
chr19	FLT3LG	missense_variant	tolerated(0.65)	benign(0)	44.93
chr1	FMO5	stop_gained	NA	NA	45.69
chr11	FOLR3	frameshift_variant	NA	NA	100
chrX	FOXP3	missense_variant	deleterious_low_confidence(0.01)	benign(0.424)	47.25
chrX	GAGE12J	missense_variant&splice_region_variant	deleterious(0.04)	benign(0.003)	58.33
chr4	GAK	missense_variant	tolerated(0.31)	benign(0)	40.17
chr2	GBX2	inframe_insertion	NA	NA	19.82
chr4	GK2	missense_variant	tolerated(0.24)	possibly_damaging(0.626)	37.21
chr2	GLI2	missense_variant	tolerated(0.06)	benign(0.192)	40.6
chr7	GLI3	missense_variant	tolerated(1)	benign(0.052)	56.73
chr15	GOLGA6L2	inframe_insertion	NA	NA	57.26
chr15	GOLGA8A	frameshift_variant	NA	NA	100
chr3	GOLGB1	missense_variant	tolerated(0.14)	benign(0)	38.64
chr4	GPM6A	missense_variant	tolerated(0.18)	benign(0.342)	55.14
chr3	GPR149	missense_variant	deleterious(0)	probably_damaging(0.991)	54.49
chr5	GPRIN1	missense_variant	tolerated(0.13)	benign(0.015)	47.56
chr10	GPRIN2	inframe_insertion	NA	NA	45.2
chr19	GRIK5	missense_variant	deleterious(0.03)	benign(0.052)	48.21
chrX	GRIPAP1	missense_variant	tolerated(0.33)	benign(0)	100
chrX	GRIPAP1	missense_variant	deleterious(0.01)	probably_damaging(0.989)	14.01
chr3	GRM7	missense_variant	tolerated(0.06)	benign(0.232)	52.5
chr4	GRXCR1	missense_variant	deleterious(0.03)	benign(0.088)	48.76
chr4	GRXCR1	missense_variant	tolerated(0.11)	possibly_damaging(0.473)	47.72
chr7	GTF2IRD2B	missense_variant	tolerated(0.08)	benign(0.019)	29.44
chr6	H4C12	missense_variant	tolerated(0.06)	benign(0.33)	36.76
chr14	HEATR5A	missense_variant	deleterious(0)	possibly_damaging(0.682)	45.9
chr20	HELZ2	missense_variant	tolerated(0.1)	benign(0.062)	21.5
chr6	HLA-B	missense_variant	deleterious_low_confidence(0)	probably_damaging(1)	37.8
chr1	HMCN1	missense_variant	deleterious(0.02)	probably_damaging(1)	47.77
chr14	HOMEZ	splice_donor_variant	NA	NA	49.15
chr10	HSPA12A	missense_variant	tolerated(0.49)	benign(0.003)	45.04
chr5	HTR1A	missense_variant	deleterious(0)	possibly_damaging(0.88)	47.58
chr4	HTT	inframe_deletion	NA	NA	76.6
chr16	HYDIN	missense_variant	tolerated(0.32)	benign(0)	17.57
chr10	IDI1	frameshift_variant	NA	NA	43.93
chr10	IFIT3	frameshift_variant	NA	NA	52.88
chr2	IFT172	splice_region_variant&splice_polypyrimidine_tract_variant&intron_variant	NA	NA	37.04
chr2	IFT172	missense_variant	tolerated(0.78)	benign(0)	47.4

chr1	IGFN1	inframe_insertion	NA	NA	99.44
chr21	IGSF5	missense_variant	tolerated_low_confidence(0.18)	benign(0.062)	49.56
chr4	IL2	missense_variant	deleterious(0.01)	probably_damaging(0.998)	50
chr2	IMP4	missense_variant	tolerated(1)	benign(0)	48.59
chr15	INSYN1	missense_variant	deleterious_low_confidence(0)	benign(0.215)	50.71
chr3	IP6K2	missense_variant	deleterious(0.02)	probably_damaging(0.979)	54.89
chr7	IQCA1L	frameshift_variant	NA	NA	51.11
chr12	ITPR2	missense_variant	tolerated(0.18)	benign(0.005)	42.31
chr1	IVL	inframe_insertion	NA	NA	55.75
chr5	JAKMIP2	missense_variant	tolerated(0.33)	probably_damaging(0.978)	45.11
chr9	KANK1	missense_variant	tolerated(0.15)	possibly_damaging(0.621)	48.31
chr16	KATNIP	missense_variant	deleterious(0)	possibly_damaging(0.588)	55.56
chr1	KCND3	missense_variant	tolerated(0.07)	possibly_damaging(0.832)	45.49
chr18	KCNG2	missense_variant	tolerated(0.19)	benign(0.01)	100
chr19	KCNN1	missense_variant	deleterious(0.05)	possibly_damaging(0.5)	47.64
chr19	KCNN1	splice_polypyrimidine_tract_variant&intron_variant	NA	NA	53.11
chr12	KDM5A	frameshift_variant	NA	NA	48.13
chr1	KIAA1522	missense_variant	tolerated(0.2)	benign(0.056)	45.45
chr1	KIF14	missense_variant	deleterious(0.01)	possibly_damaging(0.771)	53.37
chr19	KIR2DL4	missense_variant	deleterious(0.01)	possibly_damaging(0.593)	100
chr19	KIR3DL2	missense_variant	tolerated(0.08)	benign(0.041)	100
chr7	KLF14	missense_variant	tolerated(0.2)	benign(0.054)	100
chr7	KLRG2	missense_variant	deleterious(0)	probably_damaging(0.998)	50.23
chr12	KMT2D	missense_variant	deleterious_low_confidence(0.01)	benign(0.171)	53.49
chr10	KNDC1	missense_variant	deleterious(0)	possibly_damaging(0.685)	43.78
chr15	KNL1	missense_variant	tolerated(0.11)	benign(0.037)	51.03
chr22	KREMEN1	missense_variant	deleterious(0)	benign(0.072)	47.22
chr12	KRT1	missense_variant	deleterious(0.01)	probably_damaging(0.99)	46.07
chr17	KRT20	missense_variant	tolerated(0.13)	benign(0.355)	33.42
chr17	KRT34	missense_variant	deleterious(0)	possibly_damaging(0.612)	28.61
chr17	KRTAP2-3	missense_variant	tolerated(0.07)	possibly_damaging(0.464)	40
chr17	KRTAP4-7	inframe_insertion	NA	NA	96.72
chr11	KRTAP5-10	inframe_insertion	NA	NA	49.21
chr11	KRTAP5-5	inframe_insertion	NA	NA	43.86
chr11	KRTAP5-7	inframe_insertion	NA	NA	99.25
chr1	LACTBL1	missense_variant	deleterious(0)	benign(0.109)	50
chr20	LBP	missense_variant	deleterious(0.02)	benign(0.083)	16.17
chr2	LCLAT1	missense_variant	deleterious(0)	possibly_damaging(0.577)	50.26
chr12	LMBR1L	missense_variant	tolerated(0.07)	possibly_damaging(0.843)	51.72
chr3	LMCD1	missense_variant	deleterious(0)	probably_damaging(0.992)	38.75
chr3	LMLN	missense_variant	tolerated(1)	possibly_damaging(0.759)	15.2
chr3	LNP1	inframe_insertion	NA	NA	42.11
chr2	LONRF2	missense_variant	deleterious(0)	probably_damaging(0.999)	46.69
chr9	LRRC26	missense_variant	tolerated(0.35)	benign(0.077)	44.44
chr12	LRRC43	missense_variant	deleterious(0)	possibly_damaging(0.674)	55.79
chr11	LRRC56	missense_variant	tolerated_low_confidence(0.11)	benign(0.003)	51.54
chr19	LRRC8E	missense_variant	tolerated(0.41)	benign(0)	93.24

chr7	LRRN3	missense_variant	deleterious(0)	probably_damaging(0.998)	42.86
chr19	LSM4	missense_variant	tolerated(0.08)	probably_damaging(0.937)	48.37
chr14	LTBP2	missense_variant	tolerated(0.25)	probably_damaging(0.997)	47.4
chr1	LYPD8	missense_variant	tolerated(0.55)	benign(0)	100
chr1	MACF1	missense_variant	deleterious_low_confidence(0.04)	benign(0.059)	49.11
chr1	MACF1	missense_variant	deleterious(0.03)	probably_damaging(0.997)	50.33
chr6	MAN1A1	splice_region_variant&synonymous_variant	NA	NA	48.15
chr4	MAN2B2	missense_variant	deleterious(0.01)	probably_damaging(0.981)	44.24
chr15	MAP1A	missense_variant	tolerated(0.22)	benign(0.197)	8.63
chr14	MAP3K9	missense_variant	deleterious(0)	probably_damaging(0.992)	45.61
chr19	MAST3	missense_variant&splice_region_variant	NA	NA	49.19
chr19	MAST3-AS1	downstream_gene_variant	NA	NA	40.38
chr3	MBD4	missense_variant	deleterious(0.02)	possibly_damaging(0.66)	44.81
chr21	MCM3AP	missense_variant	tolerated(0.36)	benign(0.122)	46.81
chr8	MCMDC2	frameshift_variant	NA	NA	15.38
chr6	MDC1	missense_variant	deleterious(0.02)	possibly_damaging(0.906)	45.36
chr12	MED13L	missense_variant	tolerated(1)	benign(0)	50.3
chr1	MED18	missense_variant	tolerated(0.12)	probably_damaging(0.998)	49.37
chr18	MEX3C	missense_variant	deleterious(0)	probably_damaging(0.997)	100
chr7	MGAM2	missense_variant	tolerated_low_confidence(1)	unknown(0)	41.18
chr11	MICAL2	inframe_insertion	NA	NA	40.35
chr22	MICAL3	missense_variant	deleterious_low_confidence(0)	possibly_damaging(0.862)	47.91
chr13	MPHOSPH8	missense_variant	deleterious_low_confidence(0)	possibly_damaging(0.721)	67.19
chr1	MPL	missense_variant	tolerated(0.08)	benign(0.003)	37.86
chr10	MRC1	splice_donor_region_variant&intron_variant	NA	NA	43.9
chr11	MRGPRE	missense_variant	tolerated(0.2)	benign(0.398)	50.57
chr8	MROH1	missense_variant	tolerated(0.16)	benign(0.197)	69.77
chr5	MROH2B	missense_variant	deleterious(0.01)	possibly_damaging(0.689)	24.29
chr9	MRPL50	missense_variant	tolerated(0.11)	benign(0.046)	26.06
chr2	MRPS5	missense_variant	deleterious(0)	probably_damaging(0.993)	50.45
chr11	MS4A12	missense_variant	tolerated(1)	benign(0.001)	47.24
chrM	MT-ATP6	missense_variant	tolerated(0.1)	benign(0.003)	98.94
chrM	MT-ATP6	missense_variant	tolerated(0.1)	benign(0.399)	100
chrM	MT-ND2	missense_variant	tolerated(0.29)	benign(0.005)	100
chrM	MT-ND4	missense_variant	deleterious_low_confidence(0)	probably_damaging(0.999)	10.05
chrM	MT-ND4	missense_variant	deleterious_low_confidence(0)	probably_damaging(0.997)	34.3
chr19	MUC16	missense_variant	deleterious_low_confidence(0)	benign(0)	98.36
chr3	MUC4	missense_variant	deleterious_low_confidence(0.03)	possibly_damaging(0.821)	11.11
chr17	MYCBPAP	missense_variant	tolerated(0.09)	possibly_damaging(0.511)	15.68
chr12	MYF6	missense_variant	deleterious(0)	probably_damaging(1)	38.79

chr5	MYO10	missense_variant	deleterious(0.01)	probably_damaging(0.986)	48.17
chr15	MYO1E	missense_variant	tolerated(0.11)	benign(0)	47.33
chr7	MYO1G	missense_variant	tolerated(0.48)	possibly_damaging(0.56)	48.25
chr11	MYRF	missense_variant	deleterious(0)	possibly_damaging(0.551)	41.63
chr7	NAPEPLD	missense_variant	tolerated_low_confidence(0.77)	benign(0)	52.05
chr3	NBEAL2	stop_gained	NA	NA	44.2
chr1	NBPF14	missense_variant	tolerated(0.17)	probably_damaging(0.988)	38.64
chr19	NCLN	missense_variant	deleterious(0)	probably_damaging(0.989)	93.44
chr2	NEB	missense_variant	deleterious(0)	probably_damaging(0.998)	47.83
chr1	NENF	missense_variant	tolerated(0.09)	benign(0.237)	26.23
chr19	NFKBIB	missense_variant	deleterious_low_confidence(0.02)	benign(0.081)	47.8
chr14	NIN	missense_variant	tolerated(0.19)	benign(0)	50.54
chr3	NIT2	stop_gained	NA	NA	45.83
chr19	NLRP9	missense_variant	tolerated(0.33)	benign(0)	43.33
chr5	NNT	splice_polypyrimidine_tract_variant&intron_variant	NA	NA	61.22
chr7	NOM1	missense_variant	deleterious(0)	probably_damaging(0.93)	44.68
chr14	NOP9	inframe_insertion	NA	NA	93.94
chr14	NOP9	inframe_insertion	NA	NA	92.38
chr9	NOTCH1	missense_variant	deleterious(0)	probably_damaging(1)	54.9
chr1	NOTCH2	missense_variant	tolerated(0.56)	possibly_damaging(0.617)	51.35
chr1	NPHP4	missense_variant	tolerated(0.26)	benign(0)	48.56
chr9	NPR2	downstream_gene_variant	NA	NA	57.53
chr7	NRF1	missense_variant	deleterious(0.02)	benign(0.009)	44.55
chr8	NSMAF	missense_variant	deleterious(0)	probably_damaging(0.999)	26.55
chr6	NT5E	missense_variant	tolerated(0.35)	benign(0.079)	46.15
chr9	NTNG2	missense_variant	deleterious(0.01)	probably_damaging(0.994)	50.6
chr9	OLFML2A	missense_variant	deleterious(0.01)	probably_damaging(0.999)	53.1
chr11	OR10D3	missense_variant	tolerated(0.06)	benign(0.009)	46.86
chr14	OR10G2	missense_variant	tolerated(1)	benign(0)	57.35
chr1	OR2L8	missense_variant	tolerated(1)	benign(0)	7.74
chr11	OR5F1	missense_variant	tolerated(1)	benign(0.175)	41.38
chr12	ORAI1	frameshift_variant	NA	NA	100
chr2	OSGEPL1	frameshift_variant	NA	NA	52.75
chr11	OTOG	missense_variant	deleterious(0.01)	probably_damaging(0.979)	47.33
chr12	OTOGL	missense_variant	deleterious(0)	probably_damaging(0.999)	50.65
chr1	PADI2	missense_variant	deleterious(0)	possibly_damaging(0.845)	46.31
chr22	PANX2	missense_variant	deleterious(0)	possibly_damaging(0.678)	57.28
chr22	PARVB	splice_acceptor_variant	NA	NA	46.58
chr5	PCDHA12	missense_variant	tolerated_low_confidence(0.73)	benign(0.024)	45.75
chr5	PCDHB3	missense_variant	tolerated_low_confidence(1)	benign(0)	100
chr5	PCDHGA7	missense_variant	deleterious_low_confidence(0.02)	probably_damaging(0.96)	48.07
chr5	PCDHGB1	missense_variant	tolerated(0.2)	possibly_damaging(0.474)	48.48

chr4	PCGF3	missense_variant	deleterious(0)	probably_damaging(0.922)	51.43
chr8	PDE7A	missense_variant	deleterious(0.02)	benign(0.039)	72.49
chrX	PDZD4	missense_variant	deleterious(0)	probably_damaging(0.964)	50.64
chr16	PERCC1	inframe_insertion	NA	NA	85.07
chr3	PFKFB4	missense_variant	NA	benign(0.006)	51.58
chr2	PGAP1	missense_variant	tolerated(1)	benign(0.007)	46.74
chr3	PIK3CA	missense_variant	tolerated(0.06)	possibly_damaging(0.655)	46.89
chr3	PIK3CA	missense_variant	tolerated(0.06)	benign(0.026)	42.22
chr11	PLCB3	missense_variant	tolerated(0.28)	benign(0.001)	8.94
chr11	PLCB3	missense_variant	tolerated(0.45)	benign(0.053)	8.77
chr11	PLCB3	missense_variant	tolerated(0.52)	benign(0.01)	7.93
chr8	PLEC	missense_variant	tolerated(0.06)	benign(0.034)	73.32
chr2	POLE4	splice_donor_region_variant&intron_variant	NA	NA	43.72
chr15	POTEB3	missense_variant	tolerated_low_confidence(1)	benign(0)	30.73
chrX	POU3F4	missense_variant	deleterious(0)	probably_damaging(0.998)	48.3
chr19	PPM1N	missense_variant	tolerated(0.08)	benign(0.055)	12.18
chr1	PRAMEF10	stop_gained	NA	NA	21.88
chr1	PRAMEF33	missense_variant	tolerated(1)	benign(0)	35.04
chr1	PRAMEF7	missense_variant	deleterious(0.01)	benign(0.162)	25.17
chr14	PRKD1	missense_variant	tolerated(0.12)	possibly_damaging(0.571)	21.43
chr8	PRKDC	missense_variant	deleterious(0.02)	benign(0.079)	75.12
chr5	PRRC1	missense_variant	tolerated(0.12)	possibly_damaging(0.851)	42.33
chr19	PSG7	stop_gained	NA	NA	99.27
chr7	PTCD1	missense_variant	deleterious(0.02)	possibly_damaging(0.781)	49.7
chr14	PTGDR	frameshift_variant	NA	NA	33.47
chr20	PTGIS	missense_variant	tolerated(0.14)	probably_damaging(0.931)	19.24
chr10	PTPRE	splice_polypyrimidine_tract_variant&intron_variant	NA	NA	52.41
chr20	PTPRT	missense_variant	tolerated(0.19)	benign(0.146)	22.34
chr7	PURB	missense_variant	tolerated(0.12)	possibly_damaging(0.858)	50.47
chr2	RAB3GAP1	stop_lost	NA	NA	47.06
chr22	RASD2	missense_variant	tolerated(0.24)	probably_damaging(0.976)	48.12
chr16	RBBP6	missense_variant	tolerated_low_confidence(0.06)	benign(0.437)	94.02
chr1	RBM15	missense_variant	deleterious(0)	probably_damaging(0.998)	53.95
chr15	RBPMS2	missense_variant	deleterious(0.03)	probably_damaging(0.962)	46.46
chr19	RCN3	missense_variant	tolerated(0.11)	benign(0.056)	55.72
chr1	RCSD1	missense_variant	deleterious(0)	probably_damaging(0.996)	42.66
chr6	REV3L	missense_variant	tolerated(0.16)	benign(0.062)	52.69
chr3	RFC4	missense_variant	tolerated(0.5)	benign(0.001)	52.99
chr11	RIC8A	missense_variant	tolerated(0.38)	benign(0)	52
chr3	RNF168	missense_variant	tolerated(0.11)	possibly_damaging(0.629)	37.95
chr5	RNF180	missense_variant	tolerated(0.1)	benign(0.342)	46.04
chr6	RNF217	missense_variant	deleterious_low_confidence(0.01)	possibly_damaging(0.676)	61.42
chr1	RPAP2	frameshift_variant	NA	NA	49.21
chr12	RPH3A	missense_variant	tolerated(0.11)	benign(0.25)	49.08

chr11	RSF1	missense_variant	tolerated(0.93)	benign(0.003)	51.85
chrX	RTL4	missense_variant	deleterious(0.02)	probably_damaging(0.999)	55.4
chr21	RUNX1	missense_variant	deleterious(0.04)	probably_damaging(0.945)	38.18
chr21	RUNX1	missense_variant	deleterious(0)	benign(0.079)	34.92
chr1	RUSC1	missense_variant	deleterious_low_confidence(0)	benign(0)	37.87
chr5	RXFP3	missense_variant	tolerated(0.5)	benign(0)	47.47
chr1	RYR2	missense_variant	deleterious(0.03)	benign(0.031)	55.86
chr9	SARDH	missense_variant	deleterious(0.01)	benign(0.006)	51.48
chr15	SCG3	missense_variant	deleterious_low_confidence(0)	probably_damaging(1)	37.85
chr17	SCGB1C2	missense_variant	tolerated(0.18)	benign(0.319)	61.38
chr17	SCGB1C2	missense_variant	deleterious(0)	possibly_damaging(0.56)	41.81
chrX	SCML2	missense_variant	deleterious(0.03)	benign(0.062)	39.63
chr2	SCN2A	missense_variant	deleterious(0)	probably_damaging(0.995)	21.7
chr18	SERPINB4	missense_variant	deleterious(0.02)	probably_damaging(0.999)	9.46
chr12	SETD1B	missense_variant	tolerated_low_confidence(0.05)	benign(0.009)	54.29
chr10	SFTPA1	missense_variant	tolerated(0.1)	possibly_damaging(0.566)	47.78
chrX	SH2D1A	missense_variant	tolerated(0.95)	probably_damaging(0.976)	37.09
chr9	SHC3	missense_variant	deleterious(0)	benign(0.398)	52.5
chr20	SLA2	missense_variant	tolerated(0.67)	benign(0.003)	78.05
chr17	SLC16A5	missense_variant	deleterious(0)	probably_damaging(0.933)	36.59
chr6	SLC17A2	stop_gained	NA	NA	45.86
chr2	SLC1A4	missense_variant	deleterious(0.01)	possibly_damaging(0.762)	40.84
chr13	SLC25A15	missense_variant	deleterious(0)	probably_damaging(0.998)	30.89
chr1	SLC30A7	missense_variant	deleterious(0)	probably_damaging(1)	54.39
chr2	SLC35F6	missense_variant	tolerated(0.44)	benign(0.001)	34.62
chr8	SLC45A4	stop_gained	NA	NA	14.53
chr12	SLC6A12	missense_variant	deleterious(0)	probably_damaging(0.99)	44.12
chr1	SMCP	inframe_deletion	NA	NA	36.42
chr6	SNAP91	missense_variant	deleterious(0.02)	probably_damaging(0.962)	54.05
chr7	SND1	missense_variant	tolerated(0.1)	benign(0.119)	51.59
chr2	SNTG2	missense_variant&splice_region_variant	tolerated(0.23)	benign(0)	43.9
chr10	SORCS1	missense_variant	tolerated(0.3)	benign(0)	38.41
chr2	SP140	missense_variant	deleterious(0)	benign(0.349)	40.86
chrX	SPANXD	missense_variant	tolerated(0.3)	benign(0.003)	19.9
chr9	SPATA31A6	missense_variant	tolerated(0.07)	benign(0.076)	45.13
chr9	SPATA31C1	inframe_insertion	NA	NA	44.15
chr1	SPEN	missense_variant	tolerated_low_confidence(0.3)	benign(0.037)	46.64
chr16	SPN	missense_variant	deleterious(0.04)	probably_damaging(0.96)	54.01
chr4	SPOCK3	missense_variant	tolerated_low_confidence(0.31)	benign(0.234)	43.87
chr1	SPRR1B	stop_gained	NA	NA	40.4
chr5	SPRY4	missense_variant	tolerated(1)	possibly_damaging(0.748)	43.9
chr1	SPTA1	missense_variant	tolerated(1)	benign(0)	48.75
chr12	SRGAP1	splice_acceptor_variant	NA	NA	48.78
chr1	STMN1	missense_variant	tolerated(0.17)	possibly_damaging(0.471)	50.25

chr12	STRAP	missense_variant	deleterious(0)	possibly_damaging(0.73)	40.31
chr4	SULT1B1	missense_variant	deleterious(0)	probably_damaging(1)	46.67
chr9	SVEP1	missense_variant	deleterious(0)	benign(0.253)	37.11
chr3	SYN2	inframe_insertion	NA	NA	55.56
chr6	SYNE1	missense_variant	deleterious(0.05)	benign(0.04)	42.19
chr6	SYNJ2	missense_variant	tolerated_low_confidence(0.06)	benign(0.003)	55.81
chr14	SYT16	missense_variant	deleterious(0)	probably_damaging(0.997)	47.76
chr6	TAF8	missense_variant	tolerated_low_confidence(0.11)	benign(0.026)	45.3
chr19	TBC1D17	missense_variant	tolerated(0.59)	benign(0.244)	50.2
chr6	TBC1D32	missense_variant&splice_region_variant	deleterious(0)	probably_damaging(0.99)	48.51
chr17	TBC1D3B	missense_variant	deleterious_low_confidence(0)	possibly_damaging(0.902)	100
chr17	TBC1D3F	missense_variant	tolerated(0.98)	benign(0)	64.97
chr5	TBC1D9B	missense_variant	deleterious(0)	probably_damaging(1)	54.42
chrX	TCP11X2	missense_variant	tolerated(0.19)	probably_damaging(0.967)	28.12
chrX	TCP11X2	missense_variant	tolerated(0.05)	benign(0.329)	22.37
chr1	TESK2	missense_variant	deleterious(0)	probably_damaging(0.999)	45.41
chrX	TEX13C	missense_variant	tolerated(0.15)	benign(0.013)	53.7
chrX	TEX13C	missense_variant	tolerated(0.53)	probably_damaging(0.97)	46.06
chr8	TEX15	missense_variant	tolerated(0.09)	possibly_damaging(0.687)	97.4
chr2	THADA	missense_variant	tolerated(0.13)	benign(0.204)	44.05
chr15	TMC3	stop_gained&splice_region_variant	NA	NA	51.01
chr2	TMEM247	inframe_insertion	NA	NA	60.43
chr12	TMTC3	frameshift_variant	NA	NA	48.91
chr9	TNC	missense_variant	deleterious(0)	probably_damaging(1)	49.01
chr3	TNIK	missense_variant	tolerated(0.12)	probably_damaging(0.954)	40.32
chr16	TNRC6A	missense_variant	tolerated(0.09)	benign(0.047)	100
chr17	TP53	stop_gained	NA	NA	97.85
chr20	TP53RK	missense_variant	tolerated_low_confidence(0.38)	benign(0)	18.1
chr11	TPCN2	missense_variant	deleterious(0)	probably_damaging(1)	39.63
chr12	TPH2	missense_variant	tolerated(0.13)	benign(0.325)	42.86
chr1	TPR	missense_variant	tolerated(0.13)	benign(0)	48.54
chr8	TRHR	missense_variant	tolerated(0.22)	benign(0.034)	15.93
chr1	TRIM45	missense_variant	deleterious(0.01)	possibly_damaging(0.863)	56.68
chr11	TRIM51	missense_variant	tolerated(0.11)	probably_damaging(0.934)	58.52
chr9	TRPM6	stop_gained	NA	NA	44.61
chr20	TSHZ2	stop_gained	NA	NA	22.31
chr12	TSPAN9	missense_variant	deleterious_low_confidence(0)	benign(0.019)	48.39
chr5	TTC37	missense_variant	tolerated(0.06)	benign(0.012)	53.33
chr1	TTC4	missense_variant	deleterious(0)	possibly_damaging(0.669)	45.34
chr6	TUBB2B	stop_gained	NA	NA	43.28
chr7	TYW1B	frameshift_variant	NA	NA	100
chr4	UBA6	missense_variant	tolerated(0.07)	possibly_damaging(0.598)	42
chr12	UBC	missense_variant	tolerated(0.07)	possibly_damaging(0.737)	52.69
chr2	UGGT1	missense_variant	deleterious(0.02)	benign(0.254)	51.52
chr4	UGT2A1	missense_variant	deleterious(0)	benign(0.119)	19.31
chr19	UNC13A	missense_variant	tolerated_low_confidence(0.17)	benign(0)	50
chr10	UNC5B	missense_variant	deleterious(0)	benign(0.121)	46.74

chr1	USP21	missense_variant	tolerated_low_confidence(0.14)	benign(0.242)	53.94
chr8	VPS13B	missense_variant	deleterious(0)	possibly_damaging(0.626)	16.86
chr8	VPS37A	missense_variant	deleterious(0.01)	benign(0.248)	100
chr10	WAC	missense_variant	tolerated(0.1)	benign(0.023)	45.83
chr10	WASHC2A	missense_variant	tolerated(0.12)	benign(0.332)	100
chr10	WASHC2C	missense_variant	deleterious(0)	possibly_damaging(0.888)	40.43
chr12	WASHC4	missense_variant	deleterious(0)	probably_damaging(0.992)	51.19
chr1	XPR1	missense_variant	deleterious(0.04)	benign(0.044)	45.18
chr12	YEATS4	missense_variant&splice_region_variant	deleterious(0.02)	probably_damaging(1)	44.58
chr1	ZFYVE9	missense_variant	deleterious_low_confidence(0.03)	benign(0.328)	50.42
chrX	ZMAT1	missense_variant	tolerated(0.17)	benign(0.086)	53.76
chr5	ZNF131	missense_variant	tolerated_low_confidence(0.66)	benign(0)	48.62
chr19	ZNF211	missense_variant	tolerated(0.53)	probably_damaging(0.927)	19.87
chr19	ZNF211	missense_variant	deleterious(0)	benign(0.143)	19.87
chr22	ZNF280B	missense_variant	deleterious(0.03)	probably_damaging(0.989)	48.47
chr19	ZNF296	missense_variant	deleterious(0)	benign(0.363)	45.91
chr19	ZNF493	missense_variant	deleterious(0)	probably_damaging(0.955)	27.27
chr20	ZNF512B	missense_variant	tolerated(0.11)	benign(0.191)	17.3
chr19	ZNF534	missense_variant	deleterious(0)	probably_damaging(0.986)	49
chrX	ZNF630	missense_variant	tolerated(0.36)	benign(0.007)	51.65
chr1	ZNF669	missense_variant	deleterious(0.01)	benign(0.022)	56.06
chr7	ZNF716	missense_variant	deleterious(0.03)	benign(0.011)	43.35
chr16	ZNF720	missense_variant	deleterious(0.04)	probably_damaging(0.986)	49.01
chr17	ZNF750	missense_variant	tolerated(0.06)	possibly_damaging(0.582)	30.91
chr16	ZSCAN10	missense_variant	deleterious(0.01)	probably_damaging(0.925)	93.87
chr1		missense_variant	NA	unknown(0)	47.37
chr2		missense_variant	deleterious(0)	probably_damaging(0.947)	46.15
chr13		inframe_insertion	NA	NA	100
chr17		missense_variant&NMD_transcript_variant	deleterious_low_confidence(0)	possibly_damaging(0.499)	99.26

11 References

1. Keum N, Giovannucci E. Global burden of colorectal cancer: emerging trends, risk factors and prevention strategies. Nat Rev Gastroenterol Hepatol. 2019;16(12):713-32.
2. Globocan 2022: Cancer Fact Sheets — Colorectal Cancer: International Agency for Research on Cancer; 2022 [Available from: https://gco.iarc.who.int/media/globocan/factsheets/cancers/41-colorectum-fact-sheet.pdf.
3. Globocan 2022: Cancer Today — Heatmap — Colorectal Cancer: International Agency for Research on Cancer; 2022 [Available from: https://gco.iarc.fr/today/en/dataviz/maps-heatmap?mode=population.
4. Aran V, Victorino AP, Thuler LC, Ferreira CG. Colorectal Cancer: Epidemiology, Disease Mechanisms and Interventions to Reduce Onset and Mortality. Clin Colorectal Cancer. 2016;15(3):195-203.
5. Kuipers EJ, Grady WM, Lieberman D, Seufferlein T, Sung JJ, Boelens PG, et al. Colorectal cancer. Nature Reviews Disease Primers. 2015;1(1):15065.
6. Yamagishi H, Kuroda H, Imai Y, Hiraishi H. Molecular pathogenesis of sporadic colorectal cancers. Chin J Cancer. 2016;35:4.
7. Kasi A, Handa S, Bhatti S, Umar S, Bansal A, Sun W. Molecular Pathogenesis and Classification of Colorectal Carcinoma. Curr Colorectal Cancer Rep. 2020;16(5):97-106.
8. Fearon ER, Vogelstein B. A genetic model for colorectal tumorigenesis. Cell. 1990;61(5):759-67.
9. Narayan S, Roy D. Role of APC and DNA mismatch repair genes in the development of colorectal cancers. Mol Cancer. 2003;2:41.
10. Zhu G, Pei L, Xia H, Tang Q, Bi F. Role of oncogenic KRAS in the prognosis, diagnosis and treatment of colorectal cancer. Mol Cancer. 2021;20(1):143.
11. Shan H, Tian G, Zhang Y, Qiu Z. Exploring the molecular mechanisms and therapeutic potential of SMAD4 in colorectal cancer. Cancer Biol Ther. 2024;25(1):2392341.
12. Michel M, Kaps L, Maderer A, Galle PR, Moehler M. The Role of p53 Dysfunction in Colorectal Cancer and Its Implication for Therapy. Cancers (Basel). 2021;13(10).
13. Aiderus A, Barker N, Tergaonkar V. Serrated colorectal cancer: preclinical models and molecular pathways. Trends Cancer. 2024;10(1):76-91.
14. Yan HHN, Lai JCW, Ho SL, Leung WK, Law WL, Lee JFY, et al. RNF43 germline and somatic mutation in serrated neoplasia pathway and its association with BRAF mutation. Gut. 2017;66(9):1645-56.
15. Caputo F, Santini C, Bardasi C, Cerma K, Casadei-Gardini A, Spallanzani A, et al. BRAF-Mutated Colorectal Cancer: Clinical and Molecular Insights. Int J Mol Sci. 2019;20(21).
16. Nazemalhosseini Mojarad E, Kuppen PJ, Aghdaei HA, Zali MR. The CpG island methylator phenotype (CIMP) in colorectal cancer. Gastroenterol Hepatol Bed Bench. 2013;6(3):120-8.
17. Chang SC, Li AF, Lin PC, Lin CC, Lin HH, Huang SC, et al. Clinicopathological and Molecular Profiles of Sporadic Microsatellite Unstable Colorectal Cancer with or without the CpG Island Methylator Phenotype (CIMP). Cancers (Basel). 2020;12(11).
18. Nojadeh JN, Behrouz Sharif S, Sakhinia E. Microsatellite instability in colorectal cancer. EXCLI J. 2018;17:159-68.
19. Flecchia C, Zaanan A, Lahlou W, Basile D, Broudin C, Gallois C, et al. MSI colorectal cancer, all you need to know. Clin Res Hepatol Gastroenterol. 2022;46(9):101983.
20. Yamane L, Scapulatempo-Neto C, Reis RM, Guimaraes DP. Serrated pathway in colorectal carcinogenesis. World J Gastroenterol. 2014;20(10):2634-40.

21. Kane MF, Loda M, Gaida GM, Lipman J, Mishra R, Goldman H, et al. Methylation of the hMLH1 promoter correlates with lack of expression of hMLH1 in sporadic colon tumors and mismatch repair-defective human tumor cell lines. Cancer Res. 1997;57(5):808-11.
22. Lepore Signorile M, Disciglio V, Di Carlo G, Pisani A, Simone C, Ingravallo G. From Genetics to Histomolecular Characterization: An Insight into Colorectal Carcinogenesis in Lynch Syndrome. Int J Mol Sci. 2021;22(13).
23. Kawakami H, Zaanan A, Sinicrope FA. Microsatellite instability testing and its role in the management of colorectal cancer. Curr Treat Options Oncol. 2015;16(7):30.
24. Jass JR, Young J, Leggett BA. Biological significance of microsatellite instability-low (MSI-L) status in colorectal tumors. Am J Pathol. 2001;158(2):779-81.
25. Survival for Bowel Cancer: Cancer Research UK 2020 [Available from: https://www.cancerresearchuk.org/about-cancer/bowel-cancer/survival.
26. Taieb J, Gallois C. Adjuvant Chemotherapy for Stage III Colon Cancer. Cancers (Basel). 2020;12(9).
27. Moertel CG, Fleming TR, Macdonald JS, Haller DG, Laurie JA, Goodman PJ, et al. Levamisole and fluorouracil for adjuvant therapy of resected colon carcinoma. N Engl J Med. 1990;322(6):352-8.
28. Hernandez Dominguez O, Yilmaz S, Steele SR. Stage IV Colorectal Cancer Management and Treatment. J Clin Med. 2023;12(5).
29. Proportion of Cancer Cases by Stage at Diagnosis (2020) - Coloerectal Cancer Cancer Research UK; 2020 [Available from: https://crukcancerintelligence.shinyapps.io/EarlyDiagnosis/.
30. Dunn GP, Bruce AT, Ikeda H, Old LJ, Schreiber RD. Cancer immunoediting: from immunosurveillance to tumor escape. Nat Immunol. 2002;3(11):991-8.
31. Davidson WF, Giese T, Fredrickson TN. Spontaneous development of plasmacytoid tumors in mice with defective Fas-Fas ligand interactions. J Exp Med. 1998;187(11):1825-38.
32. Shankaran V, Ikeda H, Bruce AT, White JM, Swanson PE, Old LJ, et al. IFNgamma and lymphocytes prevent primary tumour development and shape tumour immunogenicity. Nature. 2001;410(6832):1107-11.
33. Takeda K, Smyth MJ, Cretney E, Hayakawa Y, Kayagaki N, Yagita H, et al. Critical role for tumor necrosis factor-related apoptosis-inducing ligand in immune surveillance against tumor development. J Exp Med. 2002;195(2):161-9.
34. Smyth MJ, Crowe NY, Godfrey DI. NK cells and NKT cells collaborate in host protection from methylcholanthrene-induced fibrosarcoma. Int Immunol. 2001;13(4):459-63.
35. E OR, Tirincsi A, Logue SE, Szegezdi E. The Janus Face of Death Receptor Signaling during Tumor Immunoediting. Front Immunol. 2016;7:446.
36. Raskov H, Orhan A, Christensen JP, Gogenur I. Cytotoxic CD8(+) T cells in cancer and cancer immunotherapy. Br J Cancer. 2021;124(2):359-67.
37. Wolf NK, Kissiov DU, Raulet DH. Roles of natural killer cells in immunity to cancer, and applications to immunotherapy. Nat Rev Immunol. 2023;23(2):90-105.
38. Gupta I, Hussein O, Sastry KS, Bougarn S, Gopinath N, Chin-Smith E, et al. Deciphering the complexities of cancer cell immune evasion: Mechanisms and therapeutic implications. Advances in Cancer Biology - Metastasis. 2023;8:100107.
39. Bruni S, Mercogliano MF, Mauro FL, Cordo Russo RI, Schillaci R. Cancer immune exclusion: breaking the barricade for a successful immunotherapy. Front Oncol. 2023;13:1135456.

40. Spranger S, Gajewski TF. Mechanisms of Tumor Cell–Intrinsic Immune Evasion. Annual Review of Cancer Biology 2018;2:213-28.
41. Chang CH, Qiu J, O'Sullivan D, Buck MD, Noguchi T, Curtis JD, et al. Metabolic Competition in the Tumor Microenvironment Is a Driver of Cancer Progression. Cell. 2015;162(6):1229-41.
42. Castillo-Rodriguez RA, Trejo-Solis C, Cabrera-Cano A, Gomez-Manzo S, Davila-Borja VM. Hypoxia as a Modulator of Inflammation and Immune Response in Cancer. Cancers (Basel). 2022;14(9).
43. Waldman AD, Fritz JM, Lenardo MJ. A guide to cancer immunotherapy: from T cell basic science to clinical practice. Nat Rev Immunol. 2020;20(11):651-68.
44. Diaz LA, Jr., Shiu KK, Kim TW, Jensen BV, Jensen LH, Punt C, et al. Pembrolizumab versus chemotherapy for microsatellite instability-high or mismatch repair-deficient metastatic colorectal cancer (KEYNOTE-177): final analysis of a randomised, open-label, phase 3 study. Lancet Oncol. 2022;23(5):659-70.
45. Le DT, Uram JN, Wang H, Bartlett BR, Kemberling H, Eyring AD, et al. PD-1 Blockade in Tumors with Mismatch-Repair Deficiency. N Engl J Med. 2015;372(26):2509-20.
46. Overman MJ, McDermott R, Leach JL, Lonardi S, Lenz HJ, Morse MA, et al. Nivolumab in patients with metastatic DNA mismatch repair-deficient or microsatellite instability-high colorectal cancer (CheckMate 142): an open-label, multicentre, phase 2 study. Lancet Oncol. 2017;18(9):1182-91.
47. Andre T, Lonardi S, Wong KYM, Lenz HJ, Gelsomino F, Aglietta M, et al. Nivolumab plus low-dose ipilimumab in previously treated patients with microsatellite instability-high/mismatch repair-deficient metastatic colorectal cancer: 4-year follow-up from CheckMate 142. Ann Oncol. 2022;33(10):1052-60.
48. Ganesh K, Stadler ZK, Cercek A, Mendelsohn RB, Shia J, Segal NH, et al. Immunotherapy in colorectal cancer: rationale, challenges and potential. Nat Rev Gastroenterol Hepatol. 2019;16(6):361-75.
49. Dolcetti R, Viel A, Doglioni C, Russo A, Guidoboni M, Capozzi E, et al. High prevalence of activated intraepithelial cytotoxic T lymphocytes and increased neoplastic cell apoptosis in colorectal carcinomas with microsatellite instability. Am J Pathol. 1999;154(6):1805-13.
50. Nusslein-Volhard C, Wieschaus E. Mutations affecting segment number and polarity in Drosophila. Nature. 1980;287(5785):795-801.
51. Pathi S, Pagan-Westphal S, Baker DP, Garber EA, Rayhorn P, Bumcrot D, et al. Comparative biological responses to human Sonic, Indian, and Desert hedgehog. Mech Dev. 2001;106(1-2):107-17.
52. Burglin TR. The Hedgehog protein family. Genome Biol. 2008;9(11):241.
53. Ohba S. Hedgehog Signaling in Skeletal Development: Roles of Indian Hedgehog and the Mode of Its Action. Int J Mol Sci. 2020;21(18).
54. Bitgood MJ, Shen L, McMahon AP. Sertoli cell signaling by Desert hedgehog regulates the male germline. Curr Biol. 1996;6(3):298-304.
55. Zhang Y, Beachy PA. Cellular and molecular mechanisms of Hedgehog signalling. Nat Rev Mol Cell Biol. 2023;24(9):668-87.
56. Hall TM, Porter JA, Young KE, Koonin EV, Beachy PA, Leahy DJ. Crystal structure of a Hedgehog autoprocessing domain: homology between Hedgehog and self-splicing proteins. Cell. 1997;91(1):85-97.

57. Pepinsky RB, Zeng C, Wen D, Rayhorn P, Baker DP, Williams KP, et al. Identification of a palmitic acid-modified form of human Sonic hedgehog. J Biol Chem. 1998;273(22):14037-45.
58. Jiang Y, Benz TL, Long SB. Substrate and product complexes reveal mechanisms of Hedgehog acylation by HHAT. Science. 2021;372(6547):1215-9.
59. Bangs F, Anderson KV. Primary Cilia and Mammalian Hedgehog Signaling. Cold Spring Harb Perspect Biol. 2017;9(5).
60. Zhang Y, Bulkley DP, Xin Y, Roberts KJ, Asarnow DE, Sharma A, et al. Structural Basis for Cholesterol Transport-like Activity of the Hedgehog Receptor Patched. Cell. 2018;175(5):1352-64 e14.
61. Kinnebrew M, Luchetti G, Sircar R, Frigui S, Viti LV, Naito T, et al. Patched 1 reduces the accessibility of cholesterol in the outer leaflet of membranes. Elife. 2021;10.
62. Huang P, Nedelcu D, Watanabe M, Jao C, Kim Y, Liu J, et al. Cellular Cholesterol Directly Activates Smoothened in Hedgehog Signaling. Cell. 2016;166(5):1176-87 e14.
63. Luchetti G, Sircar R, Kong JH, Nachtergaele S, Sagner A, Byrne EF, et al. Cholesterol activates the G-protein coupled receptor Smoothened to promote Hedgehog signaling. Elife. 2016;5.
64. Deshpande I, Liang J, Hedeen D, Roberts KJ, Zhang Y, Ha B, et al. Smoothened stimulation by membrane sterols drives Hedgehog pathway activity. Nature. 2019;571(7764):284-8.
65. Niewiadomski P, Niedziolka SM, Markiewicz L, Uspienski T, Baran B, Chojnowska K. Gli Proteins: Regulation in Development and Cancer. Cells. 2019;8(2).
66. Briscoe J, Therond PP. The mechanisms of Hedgehog signalling and its roles in development and disease. Nat Rev Mol Cell Biol. 2013;14(7):416-29.
67. Qi X, Schmiege P, Coutavas E, Li X. Two Patched molecules engage distinct sites on Hedgehog yielding a signaling-competent complex. Science. 2018;362(6410).
68. Qi X, Schmiege P, Coutavas E, Wang J, Li X. Structures of human Patched and its complex with native palmitoylated sonic hedgehog. Nature. 2018;560(7716):128-32.
69. Qian H, Cao P, Hu M, Gao S, Yan N, Gong X. Inhibition of tetrameric Patched1 by Sonic Hedgehog through an asymmetric paradigm. Nat Commun. 2019;10(1):2320.
70. Kinnebrew M, Woolley RE, Ansell TB, Byrne EFX, Frigui S, Luchetti G, et al. Patched 1 regulates Smoothened by controlling sterol binding to its extracellular cysteine-rich domain. Sci Adv. 2022;8(22):eabm5563.
71. Happ JT, Arveseth CD, Bruystens J, Bertinetti D, Nelson IB, Olivieri C, et al. A PKA inhibitor motif within SMOOTHENED controls Hedgehog signal transduction. Nat Struct Mol Biol. 2022;29(10):990-9.
72. Carballo GB, Honorato JR, de Lopes GPF, Spohr T. A highlight on Sonic hedgehog pathway. Cell Commun Signal. 2018;16(1):11.
73. Walton KD, Gumucio DL. Hedgehog Signaling in Intestinal Development and Homeostasis. Annu Rev Physiol. 2021;83:359-80.
74. Peterson LW, Artis D. Intestinal epithelial cells: regulators of barrier function and immune homeostasis. Nat Rev Immunol. 2014;14(3):141-53.
75. Bao L, Shi B, Shi YB. Intestinal homeostasis: a communication between life and death. Cell Biosci. 2020;10:66.
76. Kosinski C, Stange DE, Xu C, Chan AS, Ho C, Yuen ST, et al. Indian hedgehog regulates intestinal stem cell fate through epithelial-mesenchymal interactions during development. Gastroenterology. 2010;139(3):893-903.

77. van Dop WA, Heijmans J, Buller NV, Snoek SA, Rosekrans SL, Wassenberg EA, et al. Loss of Indian Hedgehog activates multiple aspects of a wound healing response in the mouse intestine. Gastroenterology. 2010;139(5):1665-76, 76 e1-10.
78. Madison BB, Braunstein K, Kuizon E, Portman K, Qiao XT, Gumucio DL. Epithelial hedgehog signals pattern the intestinal crypt-villus axis. Development. 2005;132(2):279-89.
79. van den Brink GR, Bleuming SA, Hardwick JC, Schepman BL, Offerhaus GJ, Keller JJ, et al. Indian Hedgehog is an antagonist of Wnt signaling in colonic epithelial cell differentiation. Nat Genet. 2004;36(3):277-82.
80. He XC, Zhang J, Tong WG, Tawfik O, Ross J, Scoville DH, et al. BMP signaling inhibits intestinal stem cell self-renewal through suppression of Wnt-beta-catenin signaling. Nat Genet. 2004;36(10):1117-21.
81. Wu HJ, Wu E. The role of gut microbiota in immune homeostasis and autoimmunity. Gut Microbes. 2012;3(1):4-14.
82. Lees CW, Zacharias WJ, Tremelling M, Noble CL, Nimmo ER, Tenesa A, et al. Analysis of germline GLI1 variation implicates hedgehog signalling in the regulation of intestinal inflammatory pathways. PLoS Med. 2008;5(12):e239.
83. Lee JJ, Rothenberg ME, Seeley ES, Zimdahl B, Kawano S, Lu WJ, et al. Control of inflammation by stromal Hedgehog pathway activation restrains colitis. Proc Natl Acad Sci U S A. 2016;113(47):E7545-E53.
84. Westendorp BF, Buller N, Karpus ON, van Dop WA, Koster J, Versteeg R, et al. Indian Hedgehog Suppresses a Stromal Cell-Driven Intestinal Immune Response. Cell Mol Gastroenterol Hepatol. 2018;5(1):67-82 e1.
85. Yoshikawa K, Shimada M, Miyamoto H, Higashijima J, Miyatani T, Nishioka M, et al. Sonic hedgehog relates to colorectal carcinogenesis. J Gastroenterol. 2009;44(11):1113-7.
86. Varnat F, Duquet A, Malerba M, Zbinden M, Mas C, Gervaz P, et al. Human colon cancer epithelial cells harbour active HEDGEHOG-GLI signalling that is essential for tumour growth, recurrence, metastasis and stem cell survival and expansion. EMBO Mol Med. 2009;1(6-7):338-51.
87. Zhang X, Zhang SS, Wei GJ, Deng ZM, Hu Y. Dysregulation of hedgehog signaling pathway related components in the evolution of colonic carcinogenesis. Int J Clin Exp Med. 2015;8(11):21379-85.
88. Qualtrough D, Rees P, Speight B, Williams AC, Paraskeva C. The Hedgehog Inhibitor Cyclopamine Reduces beta-Catenin-Tcf Transcriptional Activity, Induces E-Cadherin Expression, and Reduces Invasion in Colorectal Cancer Cells. Cancers (Basel). 2015;7(3):1885-99.
89. Zhou H, Xiong Y, Peng L, Wang R, Zhang H, Fu Z. LncRNA-cCSC1 modulates cancer stem cell properties in colorectal cancer via activation of the Hedgehog signaling pathway. J Cell Biochem. 2020;121(3):2510-24.
90. Batsaikhan BE, Yoshikawa K, Kurita N, Iwata T, Takasu C, Kashihara H, et al. Cyclopamine decreased the expression of Sonic Hedgehog and its downstream genes in colon cancer stem cells. Anticancer Res. 2014;34(11):6339-44.
91. Fu X, Shi L, Zhang W, Zhang X, Peng Y, Chen X, et al. Expression of Indian hedgehog is negatively correlated with APC gene mutation in colorectal tumors. Int J Clin Exp Med. 2014;7(8):2150-5.
92. Chen S, Saeed A, Liu Q, Jiang Q, Xu H, Xiao GG, et al. Macrophages in immunoregulation and therapeutics. Signal Transduct Target Ther. 2023;8(1):207.

93. Yang Q, Guo N, Zhou Y, Chen J, Wei Q, Han M. The role of tumor-associated macrophages (TAMs) in tumor progression and relevant advance in targeted therapy. Acta Pharm Sin B. 2020;10(11):2156-70.
94. Xue T, Yan K, Cai Y, Sun J, Chen Z, Chen X, et al. Prognostic significance of CD163+ tumor-associated macrophages in colorectal cancer. World J Surg Oncol. 2021;19(1):186.
95. Hanna A, Metge BJ, Bailey SK, Chen D, Chandrashekar DS, Varambally S, et al. Inhibition of Hedgehog signaling reprograms the dysfunctional immune microenvironment in breast cancer. Oncoimmunology. 2019;8(3):1548241.
96. Petty AJ, Li A, Wang X, Dai R, Heyman B, Hsu D, et al. Hedgehog signaling promotes tumor-associated macrophage polarization to suppress intratumoral CD8+ T cell recruitment. J Clin Invest. 2019;129(12):5151-62.
97. Yamaguchi H, Hsu JM, Yang WH, Hung MC. Mechanisms regulating PD-L1 expression in cancers and associated opportunities for novel small-molecule therapeutics. Nat Rev Clin Oncol. 2022;19(5):287-305.
98. Brahmer JR, Drake CG, Wollner I, Powderly JD, Picus J, Sharfman WH, et al. Phase I Study of Single-Agent Anti-Programmed Death-1 (MDX-1106) in Refractory Solid Tumors: Safety, Clinical Activity, Pharmacodynamics, and Immunologic Correlates. J Clin Oncol. 2023;41(4):715-23.
99. Topalian SL, Hodi FS, Brahmer JR, Gettinger SN, Smith DC, McDermott DF, et al. Safety, activity, and immune correlates of anti-PD-1 antibody in cancer. N Engl J Med. 2012;366(26):2443-54.
100. Taube JM, Klein A, Brahmer JR, Xu H, Pan X, Kim JH, et al. Association of PD-1, PD-1 ligands, and other features of the tumor immune microenvironment with response to anti-PD-1 therapy. Clin Cancer Res. 2014;20(19):5064-74.
101. Onishi H, Fujimura A, Oyama Y, Yamasaki A, Imaizumi A, Kawamoto M, et al. Hedgehog signaling regulates PDL-1 expression in cancer cells to induce anti-tumor activity by activated lymphocytes. Cell Immunol. 2016;310:199-204.
102. Petty AJ, Dai R, Lapalombella R, Baiocchi RA, Benson DM, Li Z, et al. Hedgehog-induced PD-L1 on tumor-associated macrophages is critical for suppression of tumor-infiltrating CD8+ T cell function. JCI Insight. 2021;6(6).
103. Jiang J, Ding Y, Chen Y, Lu J, Chen Y, Wu G, et al. Pan-cancer analyses reveal that increased Hedgehog activity correlates with tumor immunosuppression and resistance to immune checkpoint inhibitors. Cancer Med. 2022;11(3):847-63.
104. Veglia F, Sanseviero E, Gabrilovich DI. Myeloid-derived suppressor cells in the era of increasing myeloid cell diversity. Nat Rev Immunol. 2021;21(8):485-98.
105. Tada K, Kitano S, Shoji H, Nishimura T, Shimada Y, Nagashima K, et al. Pretreatment Immune Status Correlates with Progression-Free Survival in Chemotherapy-Treated Metastatic Colorectal Cancer Patients. Cancer Immunol Res. 2016;4(7):592-9.
106. Fan Q, Gu D, Liu H, Yang L, Zhang X, Yoder MC, et al. Defective TGF-beta signaling in bone marrow-derived cells prevents hedgehog-induced skin tumors. Cancer Res. 2014;74(2):471-83.
107. Grund-Groschke S, Ortner D, Szenes-Nagy AB, Zaborsky N, Weiss R, Neureiter D, et al. Epidermal activation of Hedgehog signaling establishes an immunosuppressive microenvironment in basal cell carcinoma by modulating skin immunity. Mol Oncol. 2020;14(9):1930-46.
108. Togashi Y, Shitara K, Nishikawa H. Regulatory T cells in cancer immunosuppression - implications for anticancer therapy. Nat Rev Clin Oncol. 2019;16(6):356-71.

109. Zhu J, Yamane H, Paul WE. Differentiation of effector CD4 T cell populations (*). Annu Rev Immunol. 2010;28:445-89.
110. Hinshaw DC, Benavides GA, Metge BJ, Swain CA, Kammerud SC, Alsheikh HA, et al. Hedgehog Signaling Regulates Treg to Th17 Conversion Through Metabolic Rewiring in Breast Cancer. Cancer Immunol Res. 2023;11(5):687-702.
111. Mayes PA, Hance KW, Hoos A. The promise and challenges of immune agonist antibody development in cancer. Nat Rev Drug Discov. 2018;17(7):509-27.
112. Hay ZLZ, Slansky JE. Granzymes: The Molecular Executors of Immune-Mediated Cytotoxicity. Int J Mol Sci. 2022;23(3).
113. Tokunaga R, Zhang W, Naseem M, Puccini A, Berger MD, Soni S, et al. CXCL9, CXCL10, CXCL11/CXCR3 axis for immune activation - A target for novel cancer therapy. Cancer Treat Rev. 2018;63:40-7.
114. Gao SH, Liu SZ, Wang GZ, Zhou GB. CXCL13 in Cancer and Other Diseases: Biological Functions, Clinical Significance, and Therapeutic Opportunities. Life (Basel). 2021;11(12).
115. Mukaida N, Sasaki SI, Baba T. CCL4 Signaling in the Tumor Microenvironment. Adv Exp Med Biol. 2020;1231:23-32.
116. Single Cell Portal - Human Colon Cancer Atlas (c295) 2021 [Available from: https://singlecell.broadinstitute.org/single_cell/study/SCP1162/human-colon-cancer-atlas-c295#study-visualize.
117. The Dependency Map (DepMap) Portal 2024 [Available from: https://depmap.org/portal/.
118. Chan DKH, Collins SD, Buczacki SJA. Generation and immunofluorescent validation of gene knockouts in adult human colonic organoids using multi-guide RNA CRISPR-Cas9. STAR Protoc. 2023;4(1):101978.
119. Drost J, Clevers H. Organoids in cancer research. Nat Rev Cancer. 2018;18(7):407-18.
120. Yang C, Xiao W, Wang R, Hu Y, Yi K, Sun X, et al. Tumor organoid model of colorectal cancer (Review). Oncol Lett. 2023;26(2):328.
121. Wang H, Liu B, Wei J. Beta2-microglobulin(B2M) in cancer immunotherapies: Biological function, resistance and remedy. Cancer Lett. 2021;517:96-104.
122. Cirella A, Olivera I, Luri-Rey C, Bolanos E, Berraondo P, Melero I. Interleukin-18 in cancer immunology and immunotherapy. Expert Opin Ther Targets. 2023;27(11):1035-42.
123. Gilson RC, Gunasinghe SD, Johannes L, Gaus K. Galectin-3 modulation of T-cell activation: mechanisms of membrane remodelling. Prog Lipid Res. 2019;76:101010.
124. Dunkelberger JR, Song WC. Complement and its role in innate and adaptive immune responses. Cell Res. 2010;20(1):34-50.
125. Hinshaw DC, Hanna A, Lama-Sherpa T, Metge B, Kammerud SC, Benavides GA, et al. Hedgehog Signaling Regulates Metabolism and Polarization of Mammary Tumor-Associated Macrophages. Cancer Res. 2021;81(21):5425-37.
126. Zacharias WJ, Li X, Madison BB, Kretovich K, Kao JY, Merchant JL, et al. Hedgehog is an anti-inflammatory epithelial signal for the intestinal lamina propria. Gastroenterology. 2010;138(7):2368-77, 77 e1-4.
127. Lauth M, Bergstrom A, Shimokawa T, Toftgard R. Inhibition of GLI-mediated transcription and tumor cell growth by small-molecule antagonists. Proc Natl Acad Sci U S A. 2007;104(20):8455-60.
128. Driessens G, Kline J, Gajewski TF. Costimulatory and coinhibitory receptors in anti-tumor immunity. Immunol Rev. 2009;229(1):126-44.

129. Zollinger AJ, Smith ML. Fibronectin, the extracellular glue. Matrix Biol. 2017;60-61:27-37.
130. Hirayama D, Iida T, Nakase H. The Phagocytic Function of Macrophage-Enforcing Innate Immunity and Tissue Homeostasis. Int J Mol Sci. 2017;19(1).
131. Korbecki J, Olbromski M, Dziegiel P. CCL18 in the Progression of Cancer. Int J Mol Sci. 2020;21(21).
132. Saraiva M, Vieira P, O'Garra A. Biology and therapeutic potential of interleukin-10. J Exp Med. 2020;217(1).
133. Gharavi AT, Hanjani NA, Movahed E, Doroudian M. The role of macrophage subtypes and exosomes in immunomodulation. Cell Mol Biol Lett. 2022;27(1):83.
134. Zhang Q, Sioud M. Tumor-Associated Macrophage Subsets: Shaping Polarization and Targeting. Int J Mol Sci. 2023;24(8).
135. Wang Y, Zhao M, Liu S, Guo J, Lu Y, Cheng J, et al. Macrophage-derived extracellular vesicles: diverse mediators of pathology and therapeutics in multiple diseases. Cell Death Dis. 2020;11(10):924.
136. Arpinati L, Scherz-Shouval R. From gatekeepers to providers: regulation of immune functions by cancer-associated fibroblasts. Trends Cancer. 2023;9(5):421-43.
137. Monteran L, Erez N. The Dark Side of Fibroblasts: Cancer-Associated Fibroblasts as Mediators of Immunosuppression in the Tumor Microenvironment. Front Immunol. 2019;10:1835.
138. Mao X, Xu J, Wang W, Liang C, Hua J, Liu J, et al. Crosstalk between cancer-associated fibroblasts and immune cells in the tumor microenvironment: new findings and future perspectives. Mol Cancer. 2021;20(1):131.
139. Li L, Kanemitsu K, Ohnishi K, Yamada R, Yano H, Fujiwara Y, et al. CXCL10 Expression in Human Colorectal Cancer Tissue and its Correlation With Serum Levels of CXCL10. Cancer Genomics Proteomics. 2024;21(1):54-64.
140. Zumwalt TJ, Arnold M, Goel A, Boland CR. Active secretion of CXCL10 and CCL5 from colorectal cancer microenvironments associates with GranzymeB+ CD8+ T-cell infiltration. Oncotarget. 2015;6(5):2981-91.
141. Li Y, Han S, Wu B, Zhong C, Shi Y, Lv C, et al. CXCL11 Correlates with Immune Infiltration and Impacts Patient Immunotherapy Efficacy: A Pan-Cancer Analysis. Front Immunol. 2022;13:951247.
142. Cao Y, Jiao N, Sun T, Ma Y, Zhang X, Chen H, et al. CXCL11 Correlates With Antitumor Immunity and an Improved Prognosis in Colon Cancer. Front Cell Dev Biol. 2021;9:646252.
143. Chen R, Ma L, Jiang C, Zhang S. Expression and potential role of CCL4 in CD8+T cells in NSCLC. Clin Transl Oncol. 2022;24(12):2420-31.
144. Ozga AJ, Chow MT, Luster AD. Chemokines and the immune response to cancer. Immunity. 2021;54(5):859-74.
145. Zhang XF, Zhang XL, Wang YJ, Fang Y, Li ML, Liu XY, et al. The regulatory network of the chemokine CCL5 in colorectal cancer. Ann Med. 2023;55(1):2205168.
146. Aldinucci D, Borghese C, Casagrande N. The CCL5/CCR5 Axis in Cancer Progression. Cancers (Basel). 2020;12(7).
147. Chinchilla P, Xiao L, Kazanietz MG, Riobo NA. Hedgehog proteins activate pro-angiogenic responses in endothelial cells through non-canonical signaling pathways. Cell Cycle. 2010;9(3):570-79.
148. Barnes EA, Kong M, Ollendorff V, Donoghue DJ. Patched1 interacts with cyclin B1 to regulate cell cycle progression. EMBO J. 2001;20(9):2214-23.

149. Pelullo M, Zema S, Nardozza F, Checquolo S, Screpanti I, Bellavia D. Wnt, Notch, and TGF-beta Pathways Impinge on Hedgehog Signaling Complexity: An Open Window on Cancer. Front Genet. 2019;10:711.
150. Noubissi FK, Yedjou CG, Spiegelman VS, Tchounwou PB. Cross-Talk between Wnt and Hh Signaling Pathways in the Pathology of Basal Cell Carcinoma. Int J Environ Res Public Health. 2018;15(7).
151. Kumar V, Vashishta M, Kong L, Wu X, Lu JJ, Guha C, et al. The Role of Notch, Hedgehog, and Wnt Signaling Pathways in the Resistance of Tumors to Anticancer Therapies. Front Cell Dev Biol. 2021;9:650772.